DEVELOPMENT OF A THIRD-GENERATION ELECTROCHEMICAL ENZYME-BASED BIOSENSOR FOR A SCALABLE DETECTION OF OXYGEN IN POWER GENERATION CELLS

By

Sphumelele Nomnotho Jiyane

(Reg. No: 21206838)

Submitted in fulfilment of the requirements of the degree of Master of Applied Science in Chemistry in the Faculty of Applied Sciences at the Durban University of Technology

December 2019

DECLARATION

I,Sphumelele Nomnotho Jiyane confirm that this work submitted for the degree of Master of Applied Science in Chemistry at the Durban University of Technology has not been submitted for any other degree at any other institution of learning.

This thesis set forth is my own. except where work which has formed part of cooperative authored publications has been included. I confirms that suitable credit has been offered within this dissertation where remarks has been made to the work of others.

Student name : **Sphumelele Nomnotho Jiyane**

Student signature : Date:

Supervisor name : **Professor K. Bisetty**

Supervisor signature : Date:

Co-Supervisor name : **Dr. MI Sabela**

Co-Supervisor signature : Date:

Co-Supervisor name : **Dr. S Kanchi**

Co-Supervisor signature : Date:

DEDICATION

This is for my nephew Alwande and to Mum

Colossians 1 vs 17

'He is before all things. and in him. all things hold together'

ACKNOWLEDGMENTS

My gratitude to **Jesus the Messiah** for the wisdom, strength, peace and good health enabled me to complete this research.

Thank you to my supervision team at the Durban University of Technology. I feel very blessed to have had a team of such knowledgeable and professional academics to support me. Specifically. **Prof. K. Bisetty** has been a trusted source of forthright and useful feedback and advice throughout the project. **Dr. M. Sabela** and **Dr. S. Kanchi** have provided both pertinent technical guidance and personal encouragement. particularly at times when the project became most difficult. **Mrs. Mavis Xhakaza**. and **Avy Naicker** for their help during experimental analysis.

I'm highly indebted to my second family at the **Universidade do Porto.** LAQV-REQUIMTE. Laboratório Química Aplicada. Faculdade de Farmácia da Universidade do Porto. for their guidance and supervision. especially to **Prof.Maria C. B.S. M. Montenegro. Prof Celià Gomez.** and **Prof. Alberto N. Araújo**. Many thanks to **Álvaro Torrinha**. who has extended valuable technical input on matters relating to the biosensor investigations along with his own unique brand of enthusiasm.

The research has been carried out with financial assistance from **CSIR** and **AESOP+** I appreciate the initiative to support my dreams.

Thank you to my study colleagues in the CMBAC. both past and present. namely. **Matshidiso Lephalala. Senzi Majola. Lyndon Naidoo. and Sharlott Qwane**. They have provided essential encouragement and conversation during the duration of the project. Thank you also to **Benni Hloma** for his kind and patient technical pieces of advice.

I want to express my gratitude to my family especially my mum. who is always by my side. who served as my inspiration to pursue this journey **Mrs. T.C Jiyane;** to my beloved and supportive sisters both Mbonambi's (**Sbongile, Buhle, Mbali** and **Sthabile**) and Jiyane's (**Nolwazi, Celiwe** and **Sthembile**) for their encouragement and motivation to finish this research. I would like to give my deepest sense of gratitude for constant understanding and support throughout this journey to **Siza Nkonyane** and **Londiwe Myeza**. I would also like to express my sincere gratitude to my brother **Ayanda Manqele**.

To **Sandile** a huge thanks for the invaluable support from the distance.

ABSTRACT

Pencil graphite electrodes (PGEs) are another form of carbon electrodes with good mechanical strength and comparable electrical properties. Moreover. their low cost makes them an excellent alternative to more conventional electrodes. especially in disposable applications. In this study. the PGEs were constructed with a 2 mm diameter pencil graphite with hardness 4H. HB. and 4B. The electrodes were cleaned and modified with 1 mg/ml of graphene oxide (GO) to enhance the surface area of the electrodes. The PGE-GO was further reduced electrochemically using $Na_2S_2O_4$ from -1.2 V to 0.8 V at 50 mV/s for 50 cyclic voltammetry scans in the presence of oxygen. using $K_3Fe(CN)_6$ / $K_4Fe(CN)_6$ as a redox couple. The performance of the PGE was evaluated with multi-walled carbon nanotubes and nanomaterials with various linking agents. A further evaluation was conducted with multi-copper oxidase (MCO) enzymes (Bilirubin oxidase (BOx) and Laccase oxidase) applied for the bio-catalytic reduction of oxygen.

The outcome of this study showed that the modification with GO revealed redox peaks 3.6 times higher than the bare PGE. The immobilization of MCO was confirmed by cyclic voltammetry in the presence of a phosphate buffer. Furthermore. the amperometric measurements of O_2 at a reducing potential of +0.34 V. showed linearity up to 0.36 mM and sensitivity of 520 μA/(mM.cm^2) to O_2.

Furthermore. computational adsorption studies were performed for the layer-by-layer electrode modification steps. The adsorption simulations revealed a lowering of the energy favored between the designed electrode layers. suggesting a most favorable interaction for the GO/MWCNTs/PBSE/BOx layer. Overall the computational data correlated well with experimental work. Notably. the layer-by-layer adsorption of the GO/MWCNTs/PBSE/BOx showed excellent affinity 11.4 M^{-1} between PBSE and the enzyme interaction. The direct electron transfer (DET) of the enzymatic reaction integrated with nanotechnology. has led to a small. portable and renewable power generating device. Thus this study addresses the demand for implantable medical devices. in the absence of an external power source.

TABLE OF CONTENTS

LIST OF FIGURES

LIST OF TABLES

LIST OF SYMBOLS AND ACRONYMS

$[Fe(CN)_6]^{3-/4}$: .....ferric ferrocyanide

AA : ..... Acrylamide

ABTS : .....2.2-Azono-bis(3ethylbenzothiazoline-6-sulphonic acid

AC : ..... Alternative current

BOx : ..... Bilirubin oxidase

CA : ..... Chronoamperometry

CdI : ..... Double layer capacitance

CdTE : ..... Cadmium Tellurium

CNT : ..... Carbon Nano tubes

CPE : ..... Constant phase element

CPs : .....Conducting polymers

CV : ..... Cyclic voltammetry

CVD : ..... Chemical vapor deposition

DEp : .....Potential separation

DET : ..... Direct electron transfer

DMF : ..... Dimethylformamide

DPV : ..... Differential pulse voltammetry

EFC : .....E fuel cell

EIS : ..... Electrochemical impedance spectroscopy

ELISA : .....Enzyme-linked immunosorbent assay

FAD : .....Flavin adenine dinucleotide

FET : .....Field effect transistor

FT-IR : ..... Fourier-transform infrared spectroscopy

GCE : .....Glassy carbon electrode

GO : .....Graphene oxide

H. B. HB : .....Hardness Blackness

HOPG : ..... Highly oriented pyrolytic graphite

I : ..... Current

ISE : .....Ion selective electrode

KBr : ..... Potassium Bromide

KCl : .....Potassium chloride

kDa : .....Kilo Dalton

LOD : .....Limit of Detection

MCO : ..... Multi copper oxidase

MET : ..... Mediator electron transfer

MPA : ..... Mercaptopropionic acid

MWCNT : .....Multi walled carbon nano tubes

NADH : .....Nicotinamide adenine dinucleotide

Nh_4^+ : .....Ammonium cation

ORR : ..... Oxygen reduction reaction

PAA : .....Poly-acrylamide

PBS : .....Phosphate buffer

PBSE : .....1-pyrenebutanoic acid. succinimidyl ester

PCA : .....Portable clinical analyzer

Pd-BPD : .....Palladium-benzoporphyrin derivatives

PEG : .....Polyethylene glycol

PGE : .....Pencil graphite electrode

POB : .....Photonic biosensor

POC : ..... Point of care

PVI : .....Poly vinylimidazole

PVL : .....Polyporus versicolor laccase

Rct : ..... Charge transfer resistance

Rs : .....Solution resistance

SCE : .....Saturated calomel electrode

SDS : ..... Safety data sheet

SEM : ..... Scanning electron microscopy

SGZ : .....Syringaldazine

SPE : .....Screen-printed electrode

TEM : ..... Transmission electron microscopy

TGA : ..... Thermogravimetric analysis

TLC : .....Thin layer chromatography

TMOS : ..... Tetramethyl orthosilicate

TVL : .....Trametes versicolor laccase

UA : ..... Uric acid

UV-Vis : ..... Ultraviolet visible spectroscopy

V : ..... Potential

W : .....Warburg impedance

LIST OF CONFERENCE PRESENTATIONS

Oral presentations

- Sphumelele Nomnotho Jiyane. "*Development of a pencil graphite electrode-Bilirubin oxidase for electro-catalytic reduction of oxygen*". 3rd Interdisciplinary Research and Innovation Conference (DUT). Durban. South Africa. 18th – 20th September 2018.
- Sphumelele Nomnotho Jiyane. "*Application of a characterized graphene PGE to the electrolytic reduction of oxygen using immobilized bilirubin oxidase*". **4th interdisciplinary Research and Innovation Conference**. held at Hilton Hotel. Durban. South Africa. 17-20 of September **2019**..

Poster Presentations

- S.N. Jiyane. **M.I. Sabela. S. Kanchi. K Bisetty and** A. Araujo**. "***Application of a characterized graphene PGE to the electrocatalytic reduction of O_2 using immobilized Trametes versicolor laccase*". SPE 2018 XXIII Meeting of the Portuguese Electrochemical Society. Porto. Portugal. 2nd - 4th May 2018.

- S.N. Jiyane. **M.I. Sabela. S. Kanchi. and K Bisetty. "***Design of an efficient pencil graphite electrode for the electrocatalytic reduction of O_2 immobilized on Bilirubin oxidase*". The Chromatography Division (Chromsa) of the South Africa Chemical Institute (SACI) and Kwa-Zulu-Natal SACI section. Durban. South Africa. 6th March 2019.

Submitted Article: Journal of Electroanalytical Chemistry

"*Restricted oriented bilirubin oxidase immobilization on disposable pencil graphite electrodes for application as oxygen biosensors and bio cathodes*". Alvaro Torrinha; Nomnotho Jiyane; Myalowenkosi Sabela; Krishna Bisetty; Maria Montenegro and Alberto Araujo.

CHAPTER 1: INTRODUCTION

This chapter describes the oxygen reduction reaction (ORR) and provides an insight into the experimental and theoretical studies on the ORR over carbon nanomaterials. The effect of carbon surface modification. like chemical wiring and the reduction of the graphene surface as well as the redox polymer application. is discussed. The electrochemical techniques to study the biosensor using bilirubin oxidase (BOx) as a catalyst. is discussed. Further. we provide the overall aim as well as the study objectives. followed by the thesis overview.

1.1 Electrochemical biosensors

A biosensor is a device uses biological molecules to gather information registered by a biological physical or chemical change. and then change the information into a measurable signal (Durand et al.. 2012). based on the interlinkage of the electrical and chemical effects. This deals with the study of chemical changes caused by the passage of electric current. The electrochemical measurements are made for numerous reasons. ranging from the thermodynamics of the reaction through to qualitative and quantitative analysis. Cyclic voltammetry (CV) is the resourceful electroanalytical technique. Its flexibility integrated with the ease of measurements. leading to considerable use in electrochemistry (Kissinger. 1983). Cyclic voltammetry parameters are characterized by the position potential axis of the forward and reverse peaks. The electron transfer reaction can be studied in inorganic and in bioinorganic systems (Tanimoto and Ichimura. 2013). Carbon modified electrodes have been used for the detection of various molecules because of their advantageous properties (Yang et al.. 2015).

1.2 Miniaturized sensing technologies in energy generation.

Biosensor electrodes are widely used in biofuel cells due to high turnover rates associated with enzymes. thereby leading to high bio-catalysis. These biosensors use enzymes to catalyse the electrochemical reaction. and they can produce electric energy using naturally existing biochemical substrate as the oxidant and fuel. These

biosensors have the potential to address the power demand in applications such as implantable medical devices. in a situation where the power sources are inaccessible. or in cases where battery replacement is a big concern (Lopez and Atanassov. 2014b). However. despite continued research and on-going advancements in bio-catalysis. enzyme electrodes continue to present some drawbacks such as low catalyst stability (e.g. decreasing enzyme activity) or the low current density. when compared with traditional fuel cells. These factors are impeditive for a widespread application of EFCs (Cristina Gutierrez-Sanchez et al.. 2015).

An essential use of biosensor would be in the quality improvement of the oxygen determination for *in vitro* and *ex vivo* biomedical studies. by accomplishing detections of low amounts and covering a broader concentration range. Another envisaged advancement of this project would be the integration into micro-analytical devices with self-powered by non-requested sample analytes.

This study is therefore aimed at developing a highly sensitive and selective electrochemical biosensor for the detection and quantification of low levels of oxygen in power generation cells by means of oxygen reduction reaction (ORR). The method will involve the use of disposable pencil graphite electrodes (PGEs) (Akanda et al.. 2016) as a reduced graphene film platform for the immobilization of the enzymes with high bio-electro catalytical activity. such as bilirubin oxidase (BOx) or laccase (Cadet et al.. 2013b) fabricated with carbon nanoparticles. These nanomaterials have excellent electrochemical enhancing properties. The selection of PGEs will be made according to the labelled hardness. which is based on the intended electrochemical properties. and further modified with a highly conductive and reduced graphene film (Akanda et al.. 2016). Therefore. the surface immobilization of the enzymes with a redox polymer in addition to the nanocomposite will provide direct access to the catalytic centres of the enzymes. resulting in a scalable 3rd generation biosensor with some optimized signal-to-noise ratios(Cadet et al.. 2013b). Cyclic voltammetry will be used as a qualitative method to investigate the electrochemical behaviour of the biosensor on the surface of the graphene film modified with nanocomposites. Chronoamperometry will be used to quantify the presence of oxygen generated.

In general. pencil graphite is composed of graphite and clay. The more graphite content makes a softer pencil. and the more clay content makes a harder pencil. Depends on the hardness. a pencil was graded in 9 degrees from 8B (softest) and 9H

(hardest). Up to now various types of pencil mines of different hardness like B. 2B. 3B. 4B. 6B. 3H. 2H. 4H. 6H. HB have been used as working electrodes in electroanalysis.

In a previous study. Wang and Kawde used different types of pencil leads (B. HB.4H. and 6H) (Akanda et al.. 2016) for transducing the hybridization event in label-free electrochemical detection of DNA. They showed that 6H pencil lead displaying the most favorable signal-to-background characteristics (Wang and Kawde. 2001). The advantages of PGE have been exploited by numerous researchers in electroanalytical technical applications. including complex biological matrices. In a study performed by Özcan and Şahin. electrochemically treated PGEs were successfully used to determine the uric acid concentrations in blood serum. The method was selective and sensitive to uric acid over ascorbic acid and dopamine using (differential pulse voltammetry) DPV at optimal pH 2. The LOD of 1.5 nM and recovery result of different uric acid (UA) varied between 98.6 and 106.4% from human serum was achieved (Özcan and Şahin. 2010). In 2012. Alipour et al. performed a comparative study for electrochemically treated PGE for the detection and determination of morphine. Electrochemically treated PGE showed well defined two anodic peaks at about 0.35 V and 0.8 V respectively and was only one peak at 0.5V with untreated PGE. The detection limit with treated PGE was 0.26 mM superior to untreated (Alipour and Gasemlou. 2012) (Akanda et al.. 2016).

In the present work. B-grade pencils generated a favorable signal response amongst the tested H. HB and B for a bare electrode cyclic voltammetry. due to greater carbon content. This result correlates with a high peak current. more sensitivity. and greater sensitivity for voltammetry analysis.

1.3 Aims and Objectives

This study is aimed at devising a protocol for the development of a high-current density O_2 biosensor. providing scalability for applications requiring miniaturized sensing technologies or in energy generation.

Objectives:

- To evaluate the usefulness of pencil graphite electrodes in the electrochemical behaviour of BOx.
- Fabrication of PGEs surface using various pencil graphite material.
- To determine the size variation of the synthesized nanostructures by Field-Flow Fractionation technique.
- To enhance the performance of the electrode by modifying with carbon nanomaterials.
- To study the effect of the immobilization procedure using laccase and bilirubin oxidase for the oxygen reduction reaction.
- To characterize the biosensor by electrochemical techniques.
- To use a redox polymer for direct wiring of the enzyme.

1.4 Thesis Outline

This thesis is divided into six chapters. Following the introduction. further chapters in this thesis are divided as follows:

Chapter 2-Literature Review

The chapter describes the literature reviews of the study including an insightful understanding of electrochemical biosensors. oxygen reduction reactions. Additionally. the *state-of-the-art* electrochemical biosensor applications in a generation are presented.

Chapter 3-Theoretical Principles

This chapter deals with the theoretical principles underlying the electrochemical oxygen biosensors. Specifically. it focuses on the equations and rigorous foundation of theoretical studies in relation to electrochemistry.

Chapter 4-Materials and Methods

A description of the materials and methods used in the design of the experimental works is presented in this chapter. The experimental study including fabrication of modified electrode. characterization studies are presented here.

Chapter 5-Results and Discussion

A discussion of the results obtained from the experimental methods are presented here. The synergy between experimental and computational studies is discussed as well.

Chapter 6-Conclusions

A summary of the overall conclusions is presented in this chapter. This also deals with future perspectives.

References

This chapter comprises of a list of references cited throughout this thesis

CHAPTER 2: LITERATURE REVIEW

The chapter describes the literature survey of the study including an insightful understanding of electrochemical biosensors. It gives a brief overview of the use of pencil graphite electrodes. with world wide applications as a carbon electrode. A review of the anchoring nanomaterials such as carbon nanotubes and graphene oxides to construct a biosensor for oxygen. Additionally. the *state-of-the-art* electrochemical miniaturization of biosensor electrodes are presented. Additionally. electrode surface modification utilizing nanomaterials to construct biosensors. for gases (including graphene. carbon nanotubes. graphene oxide and MWCNTs). The focus of review is aimed at novel applications of wiring agents such as PBSE. ABTS. TMOS in the application of a biosensor for the detection of oxygen.

2.1 Pencil Graphite Electrodes

Graphite. the main composition of PGEs. is a crystalline allotrope in the form of coal. ore and other natural minerals. It is regarded as the most stable form of carbon under standard conditions. Graphite has a layered planar structure. and the carbon atoms are arranged in a honeycomb lattice and also covalently bonded. with only three bonding sites (sp^2 hybridized) (Akanda et al. 2016). The fourth electron is free to migrate in the plane. which allows the graphite to be electrochemically conductive (Akanda et al.2016).

The pencil graphite leads are composite materials containing graphite (~ 65%). clay (~ 30%). and a binder (wax. resins. or high polymer). According to (Chehreh Chelgani et al. 2016). 4% of the world graphite catalyzed to produce pencils consisting of fine graphite powder in an inorganic (resin) or organic matrix (clay or a high polymer. e.g.cellulose).

Up to now various types of pencil lead of different hardness like B. 2B.3B. 4B. 6B. 3H. 2H. 4H. 6H. HB have been used as working electrodes in electroanalysis. According to the Letter Scale. graphite pencils are marked with letters H (hardness) and B (blackness) and numbers indicating the degree of hardness or blackness from 9H (the

hardest) to 9B (the softest). B type leads contain more graphite and is softer. and the harder H-type lead has greater lead content. whereas HB type pencil leads contain closely equal portions of graphite and clay (Sakač et al. 2016. Akanda et al.2016). Levent has used the PGE for the electrochemical oxidation of nicotine was studied in aqueous as well as micellar media at a pencil graphite electrode using cyclic. differential pulse and square-wave voltammetry techniques (Levent et al. 2009).

The feature of renewable and exchangeable writing pencils where lead can be used to any desired length from the holder is very well utilized in GPEs. After each electrochemical measurement. the used surface of GPE can be easily renewed by replacing the pencil by a new clean surface. From the green chemistry perspective. the only small material is used as an electrode. no hazard to the health of the user and the environment and can be readily disposed of after using it (Akanda et al.2016).

GPE is a subtype of the graphitic electrodes that have specific characteristics of the high surface area. good conductivity. and ease to use. However. the uniqueness of GPE is credited to some of its specific properties like it is cheap. commercially available and easily disposable. Moreover. GPEs are mechanically rigid. easy to modify and miniaturize. They have mostly used electrodes because they offer a simple and faster surface renewal compared to other commercially used electrodes which involve monochrome surface polishing procedures. Because of renewable surfaces. they are expected to give reproducible results. Additionally. GPEs show strong adsorption properties. low background current. and wide potential window (Prasad et al.. 2010. Akanda et al.. 2016).

Graphite has both metallic and nonmetallic properties being thus useful as electrode material. Moreover. most pencil leads. independent of the producer and hardness. have electrical resistance lower than 5 ohms. being thus suitable as electrode material.

The voltammograms of various lead pencils were analyzed by cyclic voltammetry. The nature of the pencil lead type influenced the voltammetric response of the $[Fe(CN)_6]^{3-/4-}$ redox couple recorded. There was a difference between the voltammograms: H type harder lead pencils presented lower voltammetric signal but provided better reversibility which is ideal for qualitative analysis (Sakač et al.. 2016). The soft B type pencil lead showed the highest signal this is due to the large diameter which enables an easy electron transfer and also. higher conductivity because of higher carbon

content. whereas HB pencils were chosen because of no background current and no noise on the voltammograms peak.

The fabrication of stable and reproducible electrodes is a key issue for the development of electrochemical devices and their implementation in our society. Modern biosensors can be miniaturized. mass-produced and easily transported. Biosensors can also measure analytes in real-time which is extremely useful for monitoring rapid changes in biological fluids.

2.2 **Application of carbon nanomaterials**

Carbon base nano-material are attached for electro-analysis when nanoparticles are embedded to the electrode surface enabling different response properties. This is due to its favorable and chemical and physical characteristics with desirable catalytic properties (high surface area. conductivity. chemical stability. good mechanical strength (Pingarrón et al.. 2008). The transducer's characteristics combined with the nanoparticle's large surface area to volume ratios. make it a perfect biosensor for particular determination.

Graphene-based electrodes have been used for several applications. such as biosensing or as support for further immobilization of enzymes (Rao et al. 2010). Recently. the electrodeposition of graphene oxide and its simultaneous electrochemical reduction on the electrode surface has been proposed as a reproducible method for the fabrication of stable and high surface area electrodes (Pumera et al. 2010. Hilder et al. 2011). Manufacturing graphene-based electrodes have overcome the low reproducibility of the current fabrication methods. i.e. drop-casting. brushing or spraying (Kashyap et al.. 2014). Graphene is produced in numerous routes; mechanical exfoliation of highly oriented pyrolytic graphite (HOPG). thermal decomposition of SiC wafers. chemical vapor deposition (CVD) on metal substrates. substrate-free CVD or reduction of graphene oxide (GO) by chemical. thermal or electrochemical means (Dreyer. 2010).

Each of these strategies provides graphene with different characteristics. Graphite oxide itself is an insulator. However. being hydrophilic. graphite oxide disperses readily in water. breaking up into macroscopic flakes. mostly one layer thick. Chemical reduction of these flakes would yield a suspension of graphene flakes (Gómez-Navarro et al.. 2007).

Graphene shows many uncommon properties. and it is the most durable material tested ever. efficiently conduct heat and electricity and display nonlinear diamagnetism. It is a crystalline allotrope of carbon with 2-D properties. Its carbon atoms are densely packed in a hexagonal pattern (Cooper et al.. 2012). Graphene's stability results in its tightly packed carbon atoms and a sp^2 orbital hybridization – a combination of orbitals s. p_x and p_y that constitute the σ-bond. The final p_z electron makes up the π-bond. The π-bonds hybridize together to form the π-band and π∗-bands. These bands are responsible for most of graphene's notable electronic properties. via the half-filled band that permits free-moving electron (Carlsson. 2007).This carbon structure has also been used in other fundamental electronic devices. such as capacitors and Field Effect Transistors (FETs). in which it can act as an atomically thin channel (Akinwande et al.. 2015. Zhong et al.. 2016).

2.3 **Oxygen reduction reactions**

Oxygen is the most abundant gaseous elements in the crust of the earth. and it is also a common oxidant for most fuel cell cathodes. This is due to the availability of oxygen in the atmosphere. and the large thermodynamic driving force of the oxygen reduction reaction (ORR). This is an essential reaction in the life process related to various disciplines such as energy conversion. material dissolution or biology.

There are two ways of reductions that can take place. Oxygen can reduce to water by direct 4-electron pathway (Equations 2.1 and 2.3) or to peroxide by two-electron pathways (Equations 2.2 and 2.4). The most desirable one is the 4-electron pathway as it results in twice the number of electron transfer occurrences per ORR and. therefore. higher current generation (Wang. 2005a). E^0 value of ORR is different at different pH values. Hence. the reaction can be written in different ways according to the medium in which the reaction is taking place. The acidic medium at pH= 0-6 $[H^+]_{(aq)}$ two different pathways of ORR can be written as follows;

$$O_2\,(g) + 4\,H^+(aq) + 4e \rightarrow 2\,H_2O\,(l) \qquad E^0 = +\,1.229\ V \qquad \text{(eq 2.1)}$$

$$O_2(g) + 2\,H^+(aq) + 2e \rightarrow H_2O_2\,(l) \qquad E^0 = +\,0.670\ V \qquad \text{(eq 2.2)}$$

In the alkaline medium pH= 7-14. $[OH^-]_{(aq)}$ reactions are represented as Equation 2.3 and 2.4. indicating the number of electron transfer. The resultant hydroxide ion (Lopez and Atanassov. 2014a).

$O_2(g) + 2\ H_2O\ (aq) + 4e^- \rightarrow 4\ OH^-\ (l)$ $E^0 = +\ 0.401\ V$ (eq 2.3)

$O_2(g) + H_2O\ (aq) + 2e^- \rightarrow HO_2^-\ (l) + OH^-$ $E^0 = -0.065\ V$ (eq 2.4)

The clean energy conversion allows making a self-contained device which uses biological elements that are specific for the reduction of oxygen. ORR is the slowest reaction in any condition of the fuel cells. There are several reasons associated with this case. One of them is the higher bond energy of the oxygen molecule shown by (Equation 2.5).

$O{=}O\ (g) \rightarrow 2\ O\ (g)$ $H° = +\ 498\ kJ\ mol^{-1}$ (eq 2.5)

This biological substrate acts as a catalyst for quicker energy conversion. There has been a classified requirement for an ORR catalyst includes the high catalytic activity towards ORR. high electrical conductivity. high electrical and chemical stability (should not be oxidized by proton. oxygen or high electrode potential) not soluble in high electrolyte interaction between the catalyst particle and the support surface high catalytic stability (Lopez and Atanassov. 2014a).

2.4 **Multi copper oxidase**

The blue multi-copper oxidase bilirubin oxidase (BOx) from the ascomycete plant pathogen Myrothecium verrucaria (Mv) efficiently catalyzes the oxidation of bilirubin to biliverdin. with the auxiliary reduction of O_2 to water as shown in (Equations 2.6 and 2.7) (Tasca et al.. 2015. Shoham et al. 1995). The blue multicopper oxidase enzyme bilirubin oxidase has been highlighted as one of the highly active and efficient for ORR. This has been classified as a cathode catalyst. and this produces electricity directly from the reaction of an oxidant with reaction catalyzed by a BOx enzyme (Tasca et al. 2015).

$$\text{Bilirubin} + O_2 \rightarrow \text{Biliverdin} + H_2O_2 \quad \text{(eq 2.6)}$$

$$\text{Bilirubin} + \frac{1}{2} O_2 \rightarrow \text{Biliverdin} + H_2O \quad \text{(eq 2.7)}$$

Bilirubin shown in Figure 2.1. is a substrate of a monomeric enzyme with a molecular mass of 66 kDa bilirubin oxidase (BOx) which form a part of the multicopper oxidase (MCO) family. Multi-copper oxidase is an enzyme that couples the oxidation on an aromatic substrate to the reduction of diatomic oxygen (So et al. 2016).

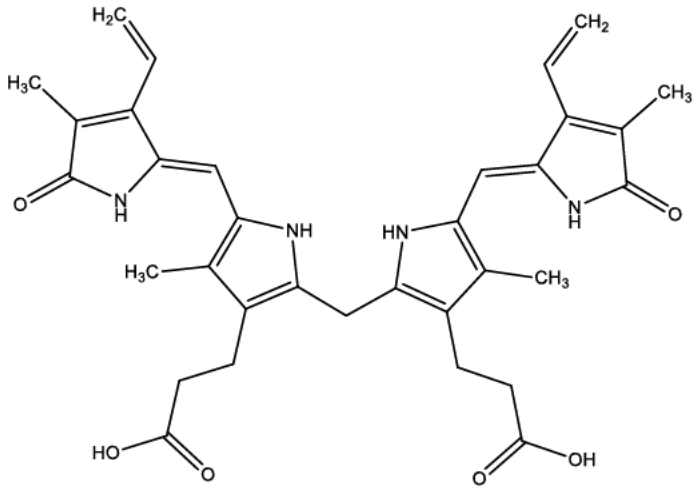

Figure 2-1: Bilirubin molecular structure

These enzymes are essential for the oxygen reduction reaction at the electrochemical potential. They have been identified as useful cathode catalysts (Wang. 2005a. Atalah et al.. 2018). This reduction reaction of considerable interest because they occur at near-neutral pH. low-temperature with minimal over potential biofuel cell applications (Cracknell et al.. 2011).The redox-active center of an MCO has four copper co-ordinates atoms: type 1T (I). this site is close to the substrate-binding pocket of the enzyme. This is a primary electron acceptor which then passes the electrons to the tri-nuclear copper center T (II) and T(III) where oxygen is converted to water (Ramaraja P.Ramasamy et al.. 2010).

Hence BOx and laccase have been used in the cathode of biofuel cells. Their redox potential is depended on the source of the enzyme vs a reference electrode (Ag/AgCl). BOx on modified electrodes has been studied numerously using various electrodes and few metallic films in the preparation of the bio-cathodes (Salaj-Kosla et al.2012).The MCO allows a direct electron transfer (DET) between the immobilized enzyme and a particular electrode. The electron transfer is governed by the potential difference and the distance between the active center of the enzyme and the electrode surface. There are advantages such as simple fabrication. easy energy conversion and active enzyme center (Xia et al.. 2016). Most DET reaction performance is achieved by the addition of nanoparticles. This is for specific surface area and conductivity; carbon is widely used because it shows all the ideal properties. The DET-type BOx based bio-cathodes has been constructed for the development of biofuel cells.

2.5 Biofuel cells

An amperometric electrochemical biosensor takes advantage of the specificity and selectivity of the enzymatic process. These devices produce electricity directly from the reaction of a fuel and an oxidant. with one or more reactions catalyzed by an enzyme (Pita et al. 2013).

Enzymatic biofuels cells use a clean energy conversion system where the enzyme is oxidized at a bio-cathode. This can operate at mild and environmentally friendly conditions/ non-hazardous conditions. which includes neutral pH. ambient temperature at atmospheric pressure (So et al. 2016).

These biofuel cells have been used micro-power devices for energy conversion from biological source to visible electrical signals. and this has been can be applicable for implantable biomedical devices. An important advance biosensor would be developing O_2 biosensor that is easy to use. small portable devices with renewable power generation (Lopez and Atanassov. 2014a). There are various systems that are used to construct effective bio-cathodes.

2.6 Biosensors

A biosensor is an analytical device. a sensor which integrates the biological elements with the physiochemical transducer to produce an electronic signal. The signal response is proportional to a single analyte and which is produced by a detector.

2.6.1 General consideration of biosensors

The biosensor is used to detect the analyte. so the biosensor is an analytical device. and it gathers the biological components with a physicochemical detector. The sensors use biological elements and biometric components which interact with the recognition elements. The biorecognition elements that could be used are tissue. microorganisms. antibodies. and nucleic acids. The biological recognition elements can also generate by biological engineering. The detector elements transform the signals from the interface of an analyte with the biochemical elements into other signals like transducer. and it can be measured more easily and qualified. The biosensor devices are associated with the electronics and the signal processors. They are generally responsible for the display of the results. and they are user-friendly. The

biosensor research has a significant role in the development of modern electronics (Jenie et al.. 2015).

2.7 Biosensor components

2.7.1 Transducer

The physiochemical transducer converts the bio-recognition event into a measurable signal and may have purely physical components (e.g. electrodes) or include a chemical infrastructure linking the bio-recognition element to the physical base. The biosensor is most commonly constructed upon the working electrode (common materials used are gold and carbon) of a three-electrode system. completed by a counter and/or reference electrode (Pike. 2014) (Shukla et al.. 2015).The former refers to just the complete three-electrode system used to convert the biochemical event to a measurable signal (i.e. excluding any chemical linking infrastructure). while the latter refers specifically to the electrode upon which the biosensor is constructed (i.e. the working electrode) (Wisniewski and Reichert. 2000).

A range of different methods of transduction is used for research biosensors. with the selected method typically being the most appropriate to the analyte-bioreceptor binding mechanism (this point is considered further in the section below 3.3). The method of transduction is one common approach to categorizing biosensor type: Electrochemical biosensors are a simple device to measures electronic current. ionic or by conductance changes carried by bio-electrodes (Pike. 2014) (Pingarrón et al.. 2008)

i. An optical biosensor is a device. that utilizes the principle of optical measurements like fluorescence and absorbance. They are used in fibre optics and optoelectronic transducers. These biosensors are safer non-electrical remote sensing materials. In the transducer elements are primarily dependent on light scattering techniques. Usually. the biosensors do not require any reference sensors and the comparative signals are generated by using the sampling sensor (Goral et al. 2011).
ii. Piezoelectric: The principle of the piezoelectric biosensor is used in sound vibrations; hence. it is called acoustic biosensors. The piezoelectric crystals form the basis of the biosensors. and the characteristic frequencies are

trembling with the crystals of positive and negative charge. By using the electronic devices. we can measure the certain molecules on the crystal surface and alters the response frequencies using these crystals. we can attach the inhibitors. The biosensors for cocaine in the gas phase involves attaching the antibodies of cocaine to the crystal surface. Sankaran et al. (2011).

This project is concerned with the development of a specific type of electrochemical biosensor.

2.7.2 Processing unit

The signal processing unit converts the transducer signal to digital data suitable for the analysis and understood by the user. The unit can be integral to. in handheld point-of-care (POC) medical biosensor units (e.g. glucose biosensor (Shukla et al. 2015), Newman and Turner 2005).

2.7.3 Bio-recognition element response

The preceding sub-section described how biosensors could be categorized by the method of transduction used to convert the bio-recognition event of a biosensor into a measurable signal. Biosensors are mostly classified according to the transduction method they use. This wide field of biosensors can be categorized according to the physical process in which the device translates the adsorption of the analyte into the measurable signal. There are predominant categories of sensors: electrical. optical. chemical. magnetic. mechanical biosensor. The sensing technology may be further divided between the analyte/targeting species in order to amplify the interaction with the devices and those that interact and detect directly with the sensor.

2.7.4 Electrochemical biosensors

The electrochemical biosensor utilizes an electrical circuit response to the interaction between the bio-recognition element of the sensor and the target analyte. Different aspects of this electrical circuit response can be investigated. and the method of electrochemical investigation employed is commonly used as one method of electrochemical biosensor classification. The most common electrochemical research biosensors are classified by the type of electrochemical measurement. Before outlining the differences between these types of the electrochemical biosensors;

however. it is useful to first describe the electrode configurations that allow for biosensor interrogation (Pike. 2014).

Except for potentiometric biosensors (the nature of this exception will be described below). a three-electrode system is typically used for the electrochemical biosensor types listed above. This system is an electrical circuit comprised of a working electrode. a counter electrode. and a reference electrode (Wisniewski and Reichert. 2000) (Wisniewski and Reichert. 2000. Pike. 2014). The biosensor is constructed upon the working electrode of the three-electrode system. and therefore the measurable biosensor-analyte reaction or interaction takes place at the surface of this electrode. The primary purpose of the counter electrode in a three-electrode electrochemical system is to complete the circuit between itself and the working electrode. for which the flow of current can be measured (Say et al.. 2000. Pike. 2014). The reference electrode utilizes materials which provide an established stable electrode potential (Table 1 below) and operates as a half-cell with the working electrode. The fixed stable potential of the reference electrode. therefore. allows for the control of a fixed potential. or range of potentials. as applied at the working electrode.

Table 1: The commonly used three working electrode system

Electrode	Commonly used materials	Essential material
Working	Glassy carbon. Silver. Platinum. Gold	chemical structure properties specific to a biosensor chemical and biological binding Chemically inert.
Auxiliary	Carbon Platinum. Gold	Chemically inert
Reference:	Silver/silver chloride. Saturated calomel electrode (SCE)	Provide stable electrode potential

The analysis of an amperometric. voltammetric or impedimetric biosensor is typically conducted by using a potentiostat to control an applied potential (V). between the working electrode (upon which a biosensor has been constructed) and the reference electrode of a three-electrode system as shown in Figure 2.2. The resultant current (A). that subsequently flows between the working and the counter electrodes is measured. and thereafter and a relationship between the electrical circuit response and biosensor-analyte interaction is investigated using the output data.

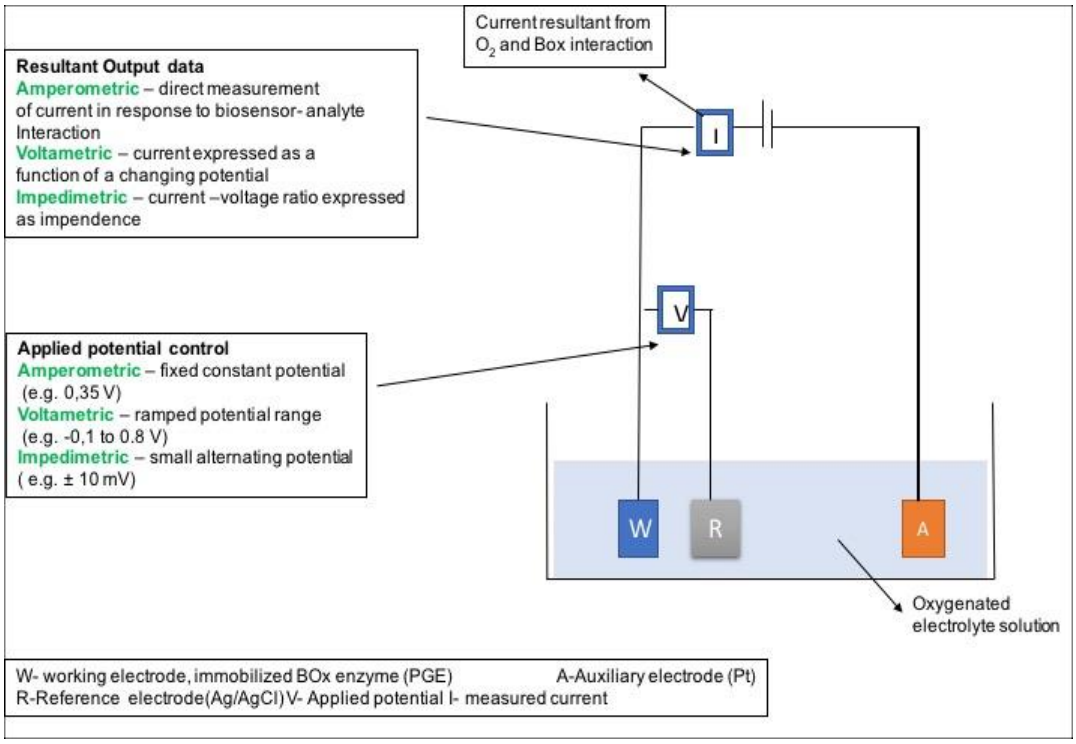

Figure 2-2: The electrochemical cell and three-electrode system in the electrolyte

The differences between biosensors employing amperometric. voltammetric and impedimetric methodology relate to how the application of potential is controlled with

respect to the electrical circuit of the three-electrode system. and how the output data obtained from the current flow response is manipulated. For voltammetric biosensors. a ramped voltage range is applied. and the current results from the biosensor-analyte interaction are expressed as a function of the changing potential (Harper and Anderson. 2010. Pike. 2014). Standard methods of voltammetry include linear sweep voltammetry where the potential is simply ramped linearly from a minimum to a maximum value (e.g. -0.4 V to 0.4 V) and cyclic voltammetry where an initial sweep between a minimum and maximum potential is made. However. a reverse sweep is also conducted from the maximum potential to the minimum potential. For Amperometric biosensors there is no ramping of the potential. a fixed potential only is applied. and the resultant change in current is typically expressed as a function of time.

2.7.5 Impedimetric biosensors

Impedimetric biosensors utilize the change in impedance resultant from the interaction between the biosensor's bio-recognition element and the target analyte. In this case. a small alternating potential is applied between the working and reference electrodes (e.g. ±10 mV). Impedance is a complex property that describes the opposition that an electrical circuit provides when a potential is applied (Guan et al. 2004. Conroy et al.2010). The basis of impedance measurements is the ratio between the current results from the biosensor-analyte interaction and the applied voltage. An analysis is typically conducted through electrochemical impedance spectroscopy (EIS) (Rushworth et al. 2014).

2.7.6 Amperometric biosensors

These biosensors are based on the electron movement; the electronic current is probed by an enzyme catalysed reaction. The presence of a mediator allows for communication between the electrode and the enzymes. Generally. a standard contact potential passes through the electrodes to analyse. An enzymatic reaction can produce either a substrate or product can transfer the electrons with the surface of the electrodes to be reduced. Henceforth a result is a measurable alternate current flow. The substrate concentration is directly proportional to the magnitude of the current.

The reduction of oxygen is obtained through the oxygen electrode. and this is a simple way to form an Amperometric biosensor (Şenel et al. 2010).

Amperometric enzyme biosensor is commonly classified into three primary generations depending on the electron transfer method used for the measurement of the biochemical reaction. Some examples of these biosensors are shown in Table 2. In all cases. the presence of an enzyme requires optimised different parameters. such as pH. buffer and temperature. impacting on the sensor's performance.

Table 2; Examples of first generation biosensors based on the use of oxidase enzymes used in amperometric biosensor.

Enzyme	Source	Substrate	Reference
Lactate oxidase	*Pedi coccus sp. Aero coccus viridians*	L-lactate	(Hernández-Ibáñez et al.. 2016)
Laccase oxidase	*Trametes versicolor*	polyphenols	(Gonzalez-Rivera and Osma. 2015)
Cholesterol oxidase	*Streptomyces sp.*	cholesterol	(Shukla et al.. 2015)
Glucose oxidase	*Aspergillus niger*	β-D-Glucose	(Devasenathipathy et al.. 2015)

The description is about the first-generation biosensors shown in Table 2. This relies on the use of enzymes that belong to two main categories: oxidase and dehydrogenases. Both oxidase and dehydrogenases require coenzymes during the catalysis e.g. (NAD^+. $NADP^+$. NADH. NADPH) which needs to be regenerated in order to allow the enzyme to catalyse the following reactions. For example. when oxidase enzymes are involved. the reactions in Equations 2.8 and 2.9 can be expected to occur.

$$S + E - FAD \rightarrow E - FAD - S \rightarrow E - FADH_2 + P \quad \text{(eq 2.8)}$$

$$E - FADH_2 + O_2 \rightarrow E + FAD + H_2O_2 \quad \text{(eq 2.9)}$$

Where S and E are for enzyme and substrate. The common co-factor in enzyme oxidase is flavin adenine dinucleotide (FAD).which is not covalently bonded into the enzyme (Harper and Anderson. 2010). The oxidase biosensor can either monitor the production of hydrogen peroxide (H_2O_2) by applying a fixed anodic/oxidizing potential against a reference electrode Ag/AgCl or oxygen O_2 consumption by applying fixed cathodic /reducing potential -0.7 V against Ag/AgCl.

Table 3; second generation biosensors based on the use of dehydrogenase enzymes propose the following reaction scheme

Enzyme	Source	Substrate	Reference
Lactate dehygenase	Rabbit muscles	L-Lactate	(Jenie et al.. 2015)
Glucose dehygenase	*Escherichia coli*	glucose	(Liang et al.. 2013. Kim et al.. 2013)
Glutamate dehydrogenase	Bovine liver	L-glutamate	(Liang et al.. 2015)
Alcohol dehygenase	*Saccharomyces cerevisiae*	ethanol	(Gómez-Anquela et al.. 2015)

$$S + E + NAD^{+} \rightarrow S - E - NAD^{+} \rightarrow E + P + NADH + H^{+} \quad \text{(eq 2.10)}$$

$$NADH \rightarrow NAD^{\bullet} + H^{\bullet} + 2e^{-} \quad \text{(eq 2.11)}$$

This type of biosensor the (nicotinamide adenine dinucleotide) NADH concentration is directly proportional to the concentration of the monitored analyte. NADH must be in the matrix in order to produce a signal. Resultant chemical reaction shown in Equations 2.10 and 2.11 above. A second-generation biosensor is known as a mediator amperometric biosensor. The mediators are oxidizing agents. to act as electron carriers. This approach makes it possible to work at low potentials. hence eliminate the interferences from other molecules and avoiding O_2 dependence (Liang et al.. 2013).

There are well-known mediators which have been used. including ferricyanide and ferrocene (Deng et al.. 2006). The improvements are obtained by replacing O_2 with an electron acceptor capable to carry electrons from the redox center of the enzyme (E) to the electrode (Rocchitta et al.. 2016) and co-workers reported reaction scheme below:

$$S + E\,(ox) \rightarrow P + E\,(red) \quad \text{(eq 2.12)}$$

$$E\,(red) + 2M_{OX} \rightarrow E(ox) + 2M_{RED} + 2H^{+} \quad \text{(eq 2.13)}$$

$$2M_{RED} \rightarrow 2M_{OX} + 2e^{-} \quad \text{(eq 2.14)}$$

Where M_{OX} and M_{RED} are the redox form of the mediator. M_{RED} is oxidized at the electrode surface. producing a current signal proportional to the detected analyte concentration. A mediator can either be added onto the sample or immobilized on the electrode surface (Rocchitta et al.. 2016). For immobilized mediators. the mediators must be entrapped very close to the enzyme so that the mediator is not lost. Suitable mediators are stable during the reaction under the working conditions and are only involved in the electron transfer (Jenie et al.. 2015). The mediator should have a lower potential than the other electroactive compounds in the sample (Chaubey and Malhotra. 2002).

The second-generation biosensor diagram and electron transfer shown by Figure 2.3 below. are less used because they generally have low stability compared to the first-generation biosensors. due to immobilized mediators.

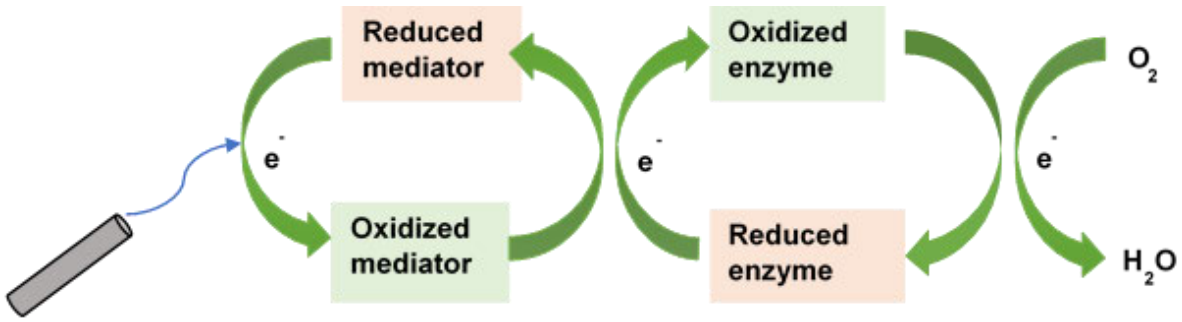

Figure 2-3: The general electron exchange for second-generation biosensor. oxidized and reduced mediator

The third-generation biosensor consists of the direct electron transfer (DET) between the enzyme and the electrode. which mostly relies on the bio-electrocatalysis properties of the enzyme (Xia et al.. 2016). Figure 2.4 shows a third-generation biosensor diagram with three elements: a bio-recognition element (enzyme). redox polymer or nanoscale wiring agent to ensure the signal reproducibility and the electrode surface to enhance the performance (Filip and Tkac. 2014).

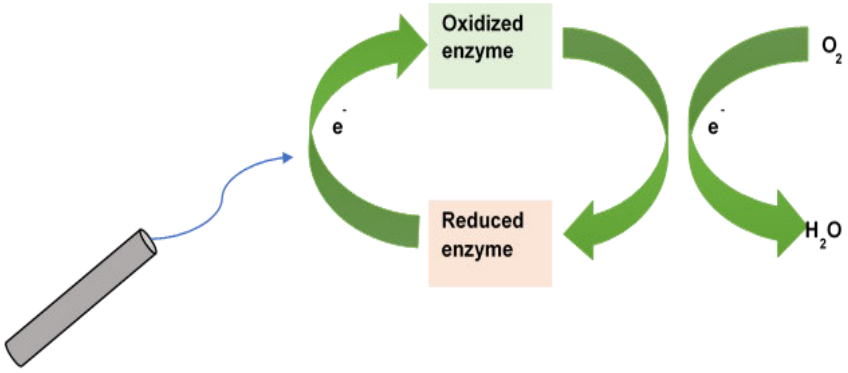

Figure 2-4;The direct electron transfer exchange between the enzyme and the transducer.

This third-generation biosensor is still a new development and have not been used widely. However. the combination of nanotechnology and polymer science makes the third-generation biosensor promising and feasible for application. Hence. this study aimed at developing a third-generation biosensor for the detection of Oxygen.

2.7.7 Types of biosensor

In generally. potentiometric biosensors typically use a three-electrode system which comprises of an ion selective electrode (ISE). the working electrode) and a reference electrode. Most usually the ISE operates by sensing either H^+ or NH_4^+ ions (Schaller et al.. 1994). The sensor specificity is conferred by an immobilized enzyme where action on the analyte generates one of these two ions. The current that flows through the working electrode is very low. and often zero. The other difference. when compared to the other three electrochemical biosensor types described below. is that the measured output is the potential (V) (Koncki. 2007). Ultimately. the operation of a biosensor will be determined by the biochemical interaction between the bio-recognition element of the biosensor and the target analyte.

Amperometric methods are typically used where the bio-receptor of the biosensor (e.g. an enzyme) produces an electroactive species in response to a target analyte. The measured current is generated by the oxidation or reduction of an electroactive species as an appropriate potential is applied to the system. because impedimetric

biosensors measure the change in impedance caused by a binding event at the biosensor surface. and an electrochemical reaction is not required (Lau et al.. 2015).

For all of the electrochemical biosensor types considered above. the practical operation of the biosensor relies upon the identification of a demonstrable and calibrated relationship between the analyte concentration and the appropriate signal output (e.g. impedance in the case of impedimetric biosensors).

Table 4 below summarizes the attributes and considers the operational advantages/disadvantages of each type of electrochemical biosensor

Table 4; Types of an electrochemical biosensor used for different applications

Electrochemical biosensor	Operational defining characteristics	Operational advantage	disadvantage	Reference
Voltammetric	Three electrode system. 2. Application of ramped potential. 3. Electroactive species produced from the analyte-sensor interaction. 4. Resultant change in current is measured	1) Rapid response signal measurement. 2) High sensitivity to changing analyte concentrations	1) Species detection selectivity dependent on operating potential. 2) Limited range of measurable analytes	(Goyal et al.. 2010)
Amperometric	Three electrode system. 2) Application of ramped potential. 3) Electroactive species produced from the analyte-sensor interaction. 4) Resultant change in current is measured. 5) Application of fixed potential.	1) Rapid response signal measurement. 2) High sensitivity to changing analyte concentrations	1) Species detection selectivity dependent on operating potential. 2) Limited range of measurable analytes	(Habermüller et al.. 2000) (Wang. 2005b)
Impedimetric	Three electrode system. 1) Application of alternating potential. 2) Change in impedance resulting from the analyte-biosensor interaction measured	1) A greater range of measurable analytes than for amperometric or voltammetric biosensors (no need for electroactive species)	1) Reproducibility issues. 2) High detection limits. and. 3) non-specific binding in some cases (discussed in Chapters 5	(Guan et al.. 2004) (Bonanni et al.. 2012)
Potentiometric	Three electrode system. 2) Application of ramped potential. 3) Electroactive species produced from the analyte-sensor interaction.	1) High portability. 2) High selectivity for target analytes. 3) Low cost. 4) Large dynamic range	1) Relatively longer response time (than other biosensor types). 2) low sensitivity to changing analyte concentrations	(Tombelli. 2012) (Koncki. 2007)

2.7.7.1 Biosensor application

The biosensor holds a potential to address the power demand for application in an implantable medical device where the traditional sources are hardly accessible or zinc battery replacements. The improved usage of micro to nanotechnology and electrical power storage has led to high demand for a small. portable and self-powered devices. This device will not rely on expensive or rare metal catalysts. Resulting to a new promising fuel cell as it is catalysed by enzymes. mostly the multi copper oxidase (MCO) family (Lopez and Atanassov. 2014a).

2.7.7.2 Successful biosensor commercialization

A significant proportion of biosensor development research has been focused upon medical applications. driven by a desire to reduce diagnosis costs and times. particularly in the developing world. Therefore. it is not particularly surprising that the main success in biosensor point-of-use (point of- care) POC deployment and commercialization have been investigated in this area.

The most commercially successful. and most well-known. biosensor is the blood glucose biosensor (of which many variations are now available). utilized across the world by people with diabetes management (Devasenathipathy et al.. 2015). The commercial success of this sensor is at least in part related to the successful integration into a compact and mobile analytical device. making it suitable for home as well as professional clinical use. Additionally. the perimetrically analyzed the enzymatic reaction of this biosensor is very stable and reproducible.

The i-STAT Portable Clinical Analyzer (PCA) is one further example where biosensors have been integrated with a fluid control system. and signal processing capability to provide a portable medical diagnostic tool (Gallagher et al.. 2010). This system has been used in healthcare applications for a number of years. specifically for the measurement of chemical diagnostic indicators (e.g. sodium. chloride. and urea nitrogen). haematological indicators (haematocrit and haemoglobin) and blood gases. Several removable self-contained cartridges. each capable of analyzing a different range of indicators. are available for incorporation into the PCA (Rushworth and Hirst. 2013).

These commercially successful examples demonstrate the potential for the integration of biosensors into portable hand-held devices. and for which the fluid sample is applied manually. Such applications for environmental monitoring would be welcome. although no successfully commercialized examples were identified as part of this literature review. However. (Roth and Rotabakk. 2012). was a rare example of where a biosensor array was operationally demonstrated as part of a 'portable' analysis system but. in environmental monitoring terms. this system had its limitations concerning not being genuinely automated and not remotely controlled and was not truly portable when compared to the medical application examples given above (Vasylieva et al.. 2011).

2.7.7.3 Barriers to commercialization

The limited number of successful instances of biosensor integration into deployable analytical systems is in itself an indication of the presence of barriers limiting such transitions. Furthermore. the limited commercial opportunities provide an indication that challenges remain in the successful integration of biosensors with fluid control and signal processing systems.

Some of these barriers and challenges are not necessarily specifically expressed in the literature. However. the focus of published material can in itself highlight an ongoing problem or challenge that is not easy to resolve. The reproducibility of electrode biosensor substrates is one such area. relating to gold electrode preparation for self-assembled monolayer construction. and for the regeneration of electrode surfaces following biosensor construction.

Other methods of immobilizing the bio-recognition element of a biosensor are employed besides binding to SAM's. These include bio-affinity bonding. covalent coupling to polymeric supports. direct enzymatic (or another bio-recognition element) adsorption onto solid electrode surfaces. and entrapment within a 3-D matric such as a photopolymer. However. each of these methods has their disadvantages as well as advantages with respect to producing stable and reproducible biosensor construction (Kircher et al.. 2012. Jokerst et al.. 2012). The matching of the bio-recognition element to an ideally suitable immobilization method to the degree that will enable reliable and

reproducible biosensor performance is therefore. an important element of biosensor design.

Another challenge for integrated point-of-use biosensors. including for those deployed within environmental settings is the requirement to process or pretreat the sample to be analyzed prior to delivery to the sensor. This can afford additional complexity to the fabrication of the fluid delivery system in the process of miniaturization of the integrated biosensor-fluidic system unit (Kircher et al.. 2012).

2.7.8 Oxygen biosensor

2.7.8.1 Biosensor development and background

It is essential to integrate systems for monitoring and controlling oxygen concentration. Electrochemical oxygen sensors are self-powered or controlled by a spontaneous oxygen reduction reaction (ORR) to produce potential. These devices contain an anode. an electrolyte and cathode as well as enclosed electrode. The enclosure is sealed apart from a small capillary that controls the rate at which oxygen gas can enter the cell.

2.7.9 Electrode preparation method

There are numerous wiring agents used to enhance the electron transfer between the electrode and the enzyme. In this study different classes of biosensor are used. depending on the wiring agent. This can either be a mediator electron transfer or direct transfer of electrons.

2.7.9.1 Mediated electrode transfer (MET) – ABTS

2.2'-azino-bis 3-ethylbenzothiazoline-6-sulphonic acid (ABTS) is a chemical compound used to observe the reaction kinetics of specific enzymes. An everyday use for it is in the enzyme-linked immunosorbent assay (ELISA) to detect the binding of molecules to each other. It is commonly used as a substrate with hydrogen peroxide for a peroxidase enzyme. (horseradish peroxidase) or with blue MCO enzymes. (laccase or bilirubin oxidase). Its use allows for the reaction kinetics of peroxidases themselves to be followed. In this way. it also can be used to indirectly

follow the reaction kinetics of any hydrogen peroxide -producing enzyme or to quantify the amount of hydrogen peroxide in a sample.

The organic compound best fitting the term “redox mediator” is ABTS. Its use for the oxidation of nonphenolic lignin structures gave impetus to search for new laccase mediators. Formerly. it was thought that just the ABTS cation radical. formed by enzymatic oxidation. could oxidize nonphenolic lignin structures. However. later studies. mainly electrochemical and spectro electrochemical. showed that the process could involve another mechanism (Farneth et al.. 2005). It was shown that laccase-mediated ABTS oxidation occurred in two stages as shown in Figure 2.5 below. It is known that electrochemical oxidation of ABTS sequentially produces the ABT cation radical and the $ABTS^{2+}$ di-cation. Cyclic voltammetry studies have shown that the redox states of ABTS are stable and reversible. having formal redox potentials 0.472 V for the ABTS/ABT couple and 0.885 V for ABT /$ABTS^{2+}$ against the Ag/AgCl reference electrode (Sergey Shleeve et al.. 2005).

The formal reduction potentials for ABTS are high enough for it to act as an electron donor for the reduction of oxo species such as molecular oxygen and hydrogen peroxide. particularly at the less-extreme pH values encountered in biological catalysis. Under these conditions. the sulfonate groups are fully deprotonated. and the mediator exists as a dianion as shown if Figure 2.5 below (Suraniti et al.. 2013).

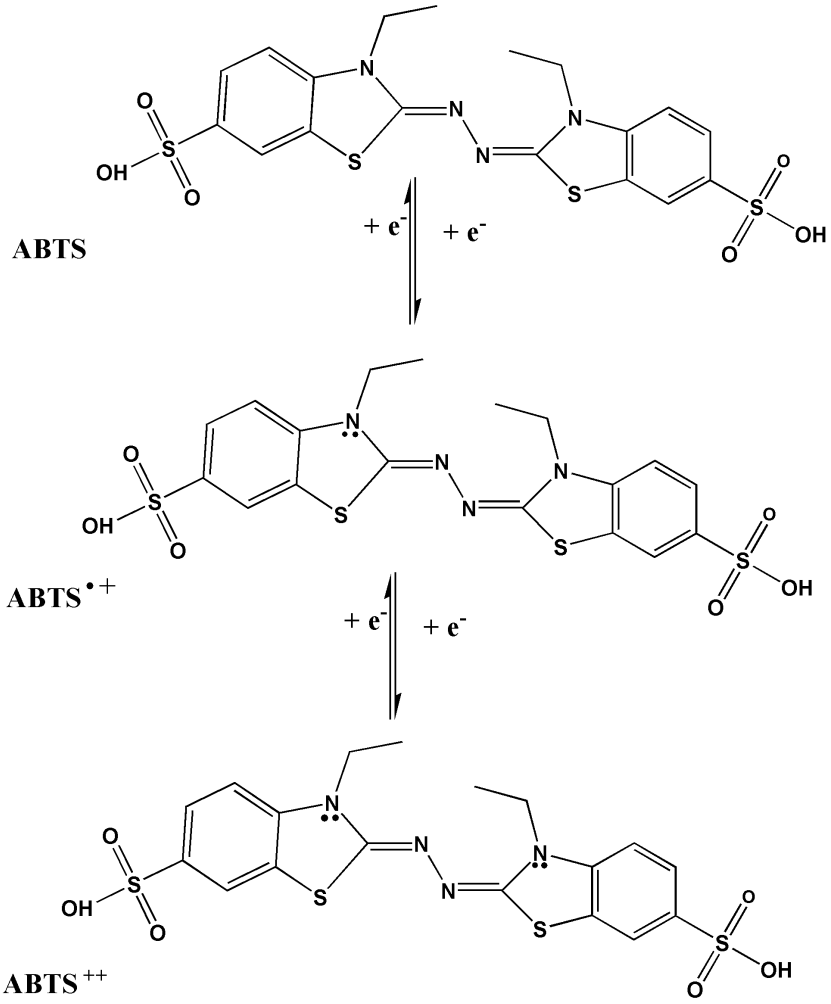

Figure 2-5;the electron exchange in $ABTS^{2+}$ radical to ABTS

$$ABTS^{-\cdot} + e^- \rightarrow ABTS^{2-} \qquad E^0 = 0.67 \text{ V vs SHE} \qquad \text{(eq 2.16)}$$

$$ABTS + e^- \rightarrow ABTS^{-\cdot} \qquad E^0 = 1.08 \text{ V vs SHE} \qquad \text{(eq 2.17)}$$

This compound is chosen because the enzyme facilitates the reaction with hydrogen peroxide. turning it into a green and soluble end-product. The chemical equation 2.16 shows the di anion ABTS reduced at 0.67 V. it is further reduced at a higher potential 1.08V shown in equation 2.17 above.

2.7.9.2 TMOS

Tetramethyl orthosilicate (TMOS) is popularly used in the sol-gel synthesis of silicates that are inorganic-organic nano-composite and in the formation of hexagonal mesoporous silica layers (Szot et al.. 2009a). It is a catalyst by nature. and they are mainly affected by pH for the reaction rate and morphology of the resulting silica bonds. During the hydrolysis or condensation of TMOS under alkaline conditions. the rate of condensation is faster compared to the hydrolysis rate. leading to a particular dense structure (Szot et al.. 2009a).

2.7.10 Direct Electron Transfer electrode preparation

The direct electron transfer (DET) with the enzyme electrode has been established using numerous methodologies. The electrons may hop between the enzyme redox centre and the electrode (Varfolomeev et al.. 1996). The DET eliminates the redox mediators in biological fuel cells and biosensor application. It electronically connects the electrode and the biocatalyst by simple physisorption or covalent linkage. entrapment of conductive polymeric films. association with metal colloids and encapsulating porous matrices that incorporate conductive nanomaterial.

2.7.10.1 PBSE

This is one of the wiring agents that has been used for the DET. The modification of CNT using 1-pyrenebutanoic acid. succinimidyl ester (PBSE) has been reported by (Devasenathipathy et al.. 2015). The aromatic pyrenyl moiety interacts with the aromatic structure of the CNT walls through irreversible pie stacking interactions on the CNT and the PBSE interface. The immersing on the PBSE solution allow the amines onto the protein surface to form covalent amide bonds that link the protein to PBSE and CNTs (Lopez and Atanassov. 2014a).

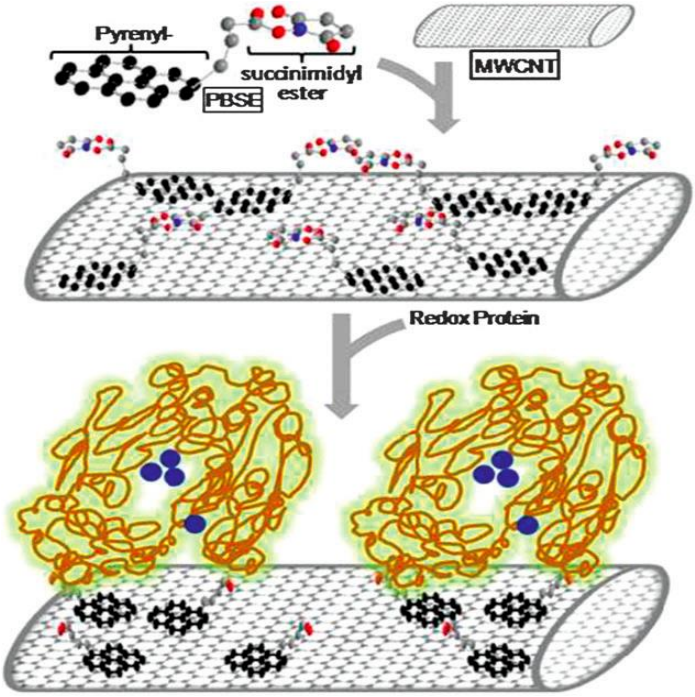

Figure 2-6;MCO immobilization using PBSE. the interaction between the protein and MWCNTs

The above Figure 2.6 shows PBSE modification of MWCNTs via π-π stacking preserves the electronic properties of MWCNT to allow efficient electron transport through the matrix. The covalent linkage between the MCO and PBSE ester will position the enzyme close to the MWCNT and reduce tunneling distance between the enzyme and the electrode. In addition. the distribution of amines on the surface of the proteins will guide orientation with the MWCNT.

2.7.10.2 REDOX polymer

Biosensors often have two main problems which are biofouling and interferences. Biofouling is the accumulation of proteins. cells and other biological materials on a surface of the sensor. Biofouling can be caused by large and small molecules as well as by cells. These affect the performance. especially for implantable devices due to the presence of a electroactive substances on the physiological complex (Wisniewski and Reichert. 2000).The functionalized conductive polymers are used to trap enzymes through ion-pair interactions and hydrogen bonds. This stabilizes the enzyme by shielding an active site from polar aqueous habitant and vanishing water activity around the protein. In order to allow the detection. the polymer selected must allow

the analyte and other co-factor to reach and diffuse out of the active site. The polymeric films act as perm selective layers.

2.7.11 Enzyme Immobilization strategies

It was vital to understand the ways to deposit the enzyme into the electrodes. Numerous strategies were used to improve the performance of the biosensors (Chaubey and Malhotra. 2002). From identifying the concentration to use. and the volume to cast onto the electrode surface. Also. to decide on the immobilization method. whether as a drop or immersing into the solutions. All the aspects were studied. The anchoring of each aspect has a direct impact on the lifespan. sensitivity and the response of the immobilized sensor. This help to improve the sensitivity. response time. storage stability as well as operational stability and reproducibility. Couple of common immobilizations were included and explained briefly (Lopez and Atanassov. 2014a).

2.7.11.1 Adsorption

Adsorption represents the most straightforward route of depositing enzymes onto the electrode surface. achieved by drop-casting onto the electrode surface or by immersing the fabricated electrode into an enzyme solution. The enzyme is deposited by dipping the electrode into the enzyme solution for a while. Adsorption is usually before the exposure to PBSE or ABTS in order to crosslink the enzyme (Ramaraja P.Ramasamy et al.. 2010). The drop-cast approach may have some downfalls. which includes the evaporation of the enzyme solution pipetted into the electrode. However. fully immersed approach covers the whole electrode surface. Hence the enzyme is deposited evenly and orderly on the electrode. as the dipping is easy and straightforward.

2.7.11.2 Sol-gel process

The process starts with the formation of a ‘sol’ which is a stable compound dispersed as colloids in a solvent. A ‘gel’ is formed by a continuous network in aqueous phase. There are several stages involved. initially being silicate solution which form a solution which then transform into a gel. High surface areas and small pore sizes characteristic

of inorganic gels are properties unattainable by conventional ceramic processing methods (Szot et al.. 2009b). These unique properties may be exploited in applications such as filtration. separation. catalysis. and chromatography.

Sol-gel enzyme immobilization method has been used for decades in enzymatic biosensor developments (Reetz et al.. 1996). It is regarded as one of the more straightforward methods for enzyme immobilization which results in a stable material. This method is performed at low temperature; hence it is compatible for use with biomolecules. This preserves the enzyme activity; thus. biosensor sensitivity is intensified. (Briones et al.. 2016).

2.7.11.3 Covalent binding

Enzymes can then be covalently bonded to the support matrices by water- insoluble linkers. An enzyme has nucleophilic groups (amino. carboxyl. hydroxyl. phenolic and thiols groups as well as sulfhydryl groups) present in the amino acids of the enzymes. These nucleophilic groups are not involved in the activity site hence are used for covalent linkage. These reactions are mostly conducted under specific conditions: low temperature. neutral pH and low ionic strength in order to eliminate the loss of the enzyme which improves the lifespan of the biosensor (Roy and Gao. 2009). Ramasamy and co-workers has reported some work where the aromatic pyrenyl moiety interacts with the aromatic-like structure of the carbon nanotubes (CNT) walls through the irreversible π-π stacking at the CNT and PBSE interface (Ramaraja P.Ramasamy et al.. 2010).

2.7.12 Polymeric films

The work on redox polymer has been recently reported by Marine Cadet. where she used PAA/PVI-Os[4.4-dichloro-(2.2-bipyridine)$_2$ Cl]$^{+/2+}$ with variable osmium concentrations which were 25. 35 and 58 mM synthesized by changing the reaction time and temperature. The polymer was then used to study the O_2 reduction current on bare glassy carbon electrode (GCE). The prepared: redox polymer. enzyme and cross-linker were at a particular ratio. The analysis was run using cyclic voltammetry under N_2 and O_2 at 50 mVs^{-1} in a 100 mM sodium phosphate buffer (Cadet et al.. 2013b).

2.7.13 Enzyme kinetic parameters

These MCO enzymes generally display a parabolic curve when the reaction rate is graphed as a function of substrate concentration. and they can be often described by an equation relating substrate concentration initial velocity V_0 known as Michaelis-Menten equation. Enzymes whose kinetics obey this equation are called Michaelis-Menten enzymes. Such graph is a plot of the substrate and V_0 (X; Y) pair. The V_0 value will increase rapidly at low substrate concentration then level off to a plateau at high substrate concentration. The plateau occurs because the enzyme is saturated (all available enzyme molecules are already tied up). This maximum rate of reaction is a characteristic of a particular enzyme at a specific concentration and is known as the maximum velocity V_{max}. V_{max} is the Y-value (initial rate of reaction value) at which the graph above the plateau. The substrate concentration that gives a rate that is halfway to V_{max} is called the K_m and is a useful measure of how quickly the reaction rate increases with substrate concentration. K_m is also a measure of enzyme affinity for (tendency to bind) its substrate. A lower K_m corresponds to higher affinity for the substrate and a higher K_m correspond to lower affinity. Unlike V_{max}. which depends on enzyme concentration. K_m is always the same for a particular enzyme characterizing a given reaction. Moreover. the binding of a substrate at one active site increases the ability of other active sites to bind and process substrate. Cooperative enzymes are more sensitive in their response to change in the substrate than the other enzymes and display a switch transition from low to high reaction rate as a substrate concentration increases. The examination of kinetic parameters is a central point of enzyme characterization (Cornish-Bowden. 2013). Linear transformation of the Michaelis-Menten equation. with the Lineweaver-Burk double reciprocal transformation is still used in this study regardless of the criticism.

2.7.13.1 Linear transformation

Linear transformations are not appropriate for accurate measurements of kinetic parameters; this is because they distort experimental errors. Using a Michaelis-Menten equation. it was observed that kinetic constant obtained after linear regression

of transformed date may vary by 150% when compared to the non-linear regression applied to the non-transformed data (Motulsky and Ransnas. 1987).

2.7.13.2 Non-linear regression

This is regarded as a more accurate method. but it is not easy to work with. This has been addressed recently. by the usage in software applications. such as Microsoft office excel. Optimization of a non-linear equation parameters is obtained after minimizing the sum of square of distance of the data from the curve (sum of square error) SSE.

$$\text{SSE} = \text{sum of } [y \text{ data} - (y \text{ curve})^2] \qquad \text{(eq 2.15)}$$

Two different processes of curve fitting can be addressed according to the to the uncertainty of dependent variable data: 1. unweighted. when all y values have equal uncertainty and 2. Weighted. when the different values of y have different uncertainties (Yildirim et al.. 2003). These reported problems and suggested solutions by Motulsky are;

Table 5;The advantages of and suggestions for non-linear regression.

	Disadvantage	Suggested solution
1	Data values are too small or too large	Consider changing the units
2	The selected equation not fitting the data	Change the equation
3	Poor initial values	Can be estimated on Linear weaver-Burk double reciprocal plot
4	Data not spanning a sufficient range	Obtain more experimental point
5	Computer calculation with sufficient significant digits	Values can be change
6	Too many parameters to bit fitted	Fix one or more as constants

2.7.13.3 Gauss Newton

The Gauss–Newton algorithm can only be used to minimize a sum of squared function values. but it has the advantage that second derivatives. which can be challenging to compute. It is used to find a minimum point of a function. It presumes that the objective function is approximately quadratic in the parameters near the optimal solution Gauss-Newton method typically converges much faster than gradient-descent methods (Cornish-Bowden. 2013).

2.7.13.4 Marquadt-Levenberg

The Levenberg-Marquardt method approaches the Gauss-Newton method. but the Levenberg-Marquardt algorithm adaptively varies the parameter updates between the gradient descent update and the Gauss-Newton update. where small values of the *damping parameter* λ result in a Gauss-Newton update. and large values of λ result in a gradient descent update. The damping parameter λ is initialized to be large so that first updates are small steps in the steepest-descent direction. If any iteration happens to result in a worse approximation ($\chi^2(\mathbf{p} + \mathbf{h}\text{lm}) > \chi^2(\mathbf{p})$). then λ is increased. Otherwise. as the solution improves. λ is decreased. and the solution typically accelerates to the local minimum (Cornish-Bowden. 2013).

2.7.13.5 Excel solver

This technique involves the generalized reduced gradient algorithm. Using the same data set. all of these methods should yield the same parameter values. As the non-linear regression is an interactive method. the program must start with an initial value for each targeted parameter. The unrealistic initial values can lead to acceptable convergence. which is often associated with impossible parameter values. (Dias et al.. 2014. Deng et al.. 2006).

2.8 Multi copper oxidase (MCO)

2.8.1 Bilirubin Oxidase

Bilirubin oxidase (Box) is an enzyme encoded by a gene in various organisms that catalyze the chemical reaction in the form:

$$2 \text{ bilirubin} + O_2 \rightarrow 2 \text{ biliverdin} + 2\ H_2O \qquad \text{(eq 2.16)}$$

Thus. the two substrates of this enzyme are bilirubin and O_2. whereas its two products are biliverdin and H_2O. This enzyme is part of oxidoreductase family. they act on the CH-CH group of a donor to oxygen as an acceptor. This enzyme is also called bilirubin oxidase M-1. BOx have attracted attention because. these enzymes have high activity at neutral pH. high thermal tolerance. and are capable of oxidizing bilirubin (Suraniti et al.. 2013). In addition to more traditional laccase substrates like 2. 2′-azino-di-[3-ethylbenzthiazoline-6-sulphonic acid] (ABTS) and syringaldazine (SGZ). BOx catalyze the oxidation of bilirubin to biliverdin (Equation 2.16). This enzyme can be used for bio-electroanalysis. as it is able to reduce oxygen molecule to form water. The oxygen reduced can be quantified in terms of sensitivity using a biosensor. This biorecognition element can be used to substitute expensive metal catalyst such as platinum.

It can also be used for detection of bilirubin is of particular importance in the medical field. making BOx attractive enzymes in that respect (Durand et al.. 2012). Bilirubin is a bile pigment. a metabolic product of heme formed from the degradation of erythrocytes by reticuloendothelial cells (Gourley. 1997).The typical biological form of bilirubin exits in serum either in free form. unconjugated bilirubin. or in conjugated form (Person et al.. 1994). The conjugated form results from the transformation of the

unconjugated bilirubin in the liver by the hepatic enzyme glucuronyl transferase. Conjugated bilirubin is known to be a better indicator of liver function and is used in the diagnosis of jaundice and hyperbilirubinemia. The detection of unconjugated bilirubin is more accurately used in new-born where the liver is not mature enough to convert the unconjugated bilirubin to conjugated bilirubin resulting in jaundice affecting ~60–80% of new-born (Johnson et al.. 2002).

2.8.2 Lacasse Oxidase

Laccases are oxidoreductases belonging to the multi-nuclear copper-containing oxidases; they catalyze the monoelectronic oxidation of substrates at the expense of molecular oxygen (Piontek et al.. 2002). Interest in these mainly 'ecofriendly' enzymes – they work with air and produce water as the only by-product – has grown significantly in recent years: their uses span from the textile to the pulp and paper industries. and from food applications to bioremediation processes (Piontek et al.. 2002). They are glycoproteins. which are ubiquitous in nature – they have been reported in higher plants and virtually every fungus that has been examined for them (Ying Liu. 2007). Laccases also have uses in organic synthesis. where their typical substrates are phenols and amines. and the reaction products are dimers and oligomers derived from the coupling of reactive radical intermediates (Sakurai and Kataoka. 2007). The reactions catalyzed by laccases proceed by the monoelectronic oxidation of a suitable substrate molecule (phenols and aromatic or aliphatic amines) to the corresponding reactive radical. The redox process takes place with the assistance of a cluster of four copper atoms that form the catalytic core of the enzyme; they also confer the typical blue color to these enzymes because of the intense electronic absorption of the Cu–Cu linkages (Sergio Riva 2006). The overall outcome of the catalytic cycle is the reduction of one molecule of oxygen to two molecules of water and the concomitant oxidation of four substrate molecules to produce four radicals. These reactive intermediates can then produce dimers. oligomers and polymers. However the poor solubility in water of most potential laccase substrates has raised interest in the behavior of these oxidases in a non-conventional reaction media with a restricted water content and dissolved in ethyl acetate. catalyzed by laccase from Polyporus versicolor dissolved in acetate buffer (Claus. 2003). The presence of solvents.

particularly those forming homogeneous phases with the buffered solutions containing the enzymes. can significantly affect the structure. the stability and the activity of the biocatalysts. through direct interactions with the protein molecules or through modification of the thermodynamic water activity (aw) (Piontek et al.. 2002).

T. Versicolor laccase (TVL) has been previously studied for oxygen reduction reaction in a biofuel cell cathode. Different strategies have been tried to maximize the electro-catalytic activity of enzyme-modified electrodes. and it has been reported that immobilization methods involving carbon-nanotubes (CNT) will create a porous conductive matrix that allows a higher number of active sites to be effectively attached to the electrode (Atalah et al.. 2018). In this case. CNT could serve as a platform to conjugate with enzymes. which provide support for enzyme stability. the enhanced surface area for enzyme loading and high electrical conductivity for signal processing. It is possible to further modify the CNT with 1-pyrenebutanoic acid succinimidyl .5 ester (PBSE) before immobilizing the enzyme on to the CNT (Ramasamy et al.. 2010).

The aromatic pyrenyl moiety in PBSE irreversibly stacks to the aromatic structure of the CNT walls via π-π interactions. and the ester group forms covalent amide bonds with the N-terminus of the enzyme structure. This yields highly electro-catalytically active enzyme-modified electrodes (Zhou et al.. 2017). Although enzyme-based biological fuel cells hold the potential to be small-power sources for various bio-electrochemical applications. their use is currently limited by their relatively short life that is caused by the susceptibility of enzymes to denaturation and loss of their activity. Thermophilic bacteria. however. have evolved to produce enzymes capable of functioning in the high- temperature environments in which they live (Hoegger et al.. 2006). Thermophilic enzymes are generally more resistant to denaturation and show overall better stability than their mesophilic counterparts. For this reason. we wanted to explore the thermophilic enzymes as electrocatalysts for oxygen reduction reaction (Lasa and Berenguer. 1993).

CHAPTER 3: THEORETICAL PRINCIPLES

This section describes in detail the techniques and methods used in this work. The relationship of the current study with those previously reported in the literature is also reported.

3.1 Comparative Validation

An electrode is a metal whose surface serves as the location where oxidation-reduction equilibrium is established between the metal and what is in the solution. The electrode can either be an anode or a cathode. An electrode has to be a good electrical conductor. so it is usually a metal. Some reactions require an inert electrode that does not participate in the reaction. An example of this would be platinum in the SHE reaction. Other reactions utilize solid and inert forms of electrodes such as graphite(carbon). platinum. gold. and rhodium and mostly. commonly used reactive (or involved) electrodes: copper. zinc. lead. and silver. All these electrochemical electrodes are made from expensive metals making them very valuable. As much as they are inert. but they require special treatment to maintain and prolonging their life span. The use of pencil graphite offer an insight to the electrode with a wide potential range and can analyze both organic and inorganic analytes.

3.1.1 Pencil graphite electrode

Graphite. the main composition of a pencil graphite electrode (PGE). found in coal. ore and other natural minerals is the most stable form of carbon. Importantly. PGEs can provide a renewable surface that is simpler and faster to reproduce than the polishing procedures commonly applied to solid-state electrodes including. GCE.

Among. these carbon electrodes and other commercial metal electrodes PGE. as a disposable electrode material. has attracted much attention in the electrochemical community due to its wide availability. low technology. low cost. good mechanical rigidity. chemical inertness. interesting electrochemical properties. low background

current. wide potential window. adsorption of analyte. ease of modification. and miniaturization.

3.1.2 Glassy Carbon Electrode

The GCE has been widely used for numerous electroanalytical analysis for both qualitative and quantitative studies. It has proven to be reliable and very reproducible. It possesses numerous advantages for many types of configuration and good cathodic potential range. Although it is mostly used in electrochemical. but suffer some disadvantage which includes quality varieties. being the most expensive carbon electrode and most fragile. The electrochemistry is affected greatly by its surface chemistry of carbon-oxygen functionalities and its cleanliness. Cleaning and storing GCE remove adsorbed impurities is ideal before every analysis. The most common method of activation is to polish the GC surface with micro-sized abrasives. Such treatment exposes the fresh new surface (Balgobind et al.. 2016). The maintenance of clean conditions during such polishing is critical. For instance. polishing on some types of abrasive containing pads can deactivate the surface. After polishing. sonication is often required to remove carbon particles and remains of polishing material.

3.1.3 Screen-printed electrode

Screen-printed electrodes (SPEs) are mass-produced. but with consistent chemical performance. Besides the need for controlling the chemical nature of the measure media. SPEs may be the most appropriate electrochemical sensors for *in situ* analysis because of their linear output. low power requirement. quick response. high sensitivity and ability to operate at room temperature. It is because of such material properties that SPEs have been successfully utilized for the rapid *in situ* analysis of environmental pollutants (Sabela et al.. 2016). Figure 3.1 exemplify the SPE and labelled components

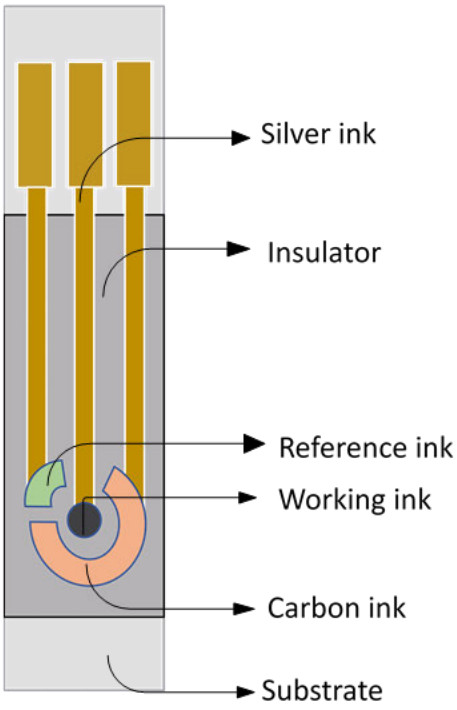

Figure 3-1;Screen-printed carbon electrode and labeled components

Many commercial sources of SPEs in different configurations exist. The formats of SPEs are changeable with respect to the requirements for a specific analyte. In addition. the surface of SPEs can be easily modified to fit multiple purposes related to different pollutants and to achieve a variety of improvements. Many kinds of modifiers of SPEs exist for environmental analysis. including noble metals. inorganic nanomaterials. enzymes. and DNA sequences (Kunene. 2018). SPEs combine ease of use and portability with simple. inexpensive analytical methods. Consequently. SPEs can be successfully applied to *in situ* environmental analysis and achieve improvements in detection. as has been shown over the past several years (Renedo et al.. 2007).

3.2 **Integration investigation methods**

This study addresses a disposable carbon electrode. with similar advantages of any globally used carbon electrode. but with other new interesting functionalities. In a recent study reported in 2019; Kristina Rivera explored the photonic biosensor (iPOB) for monitoring oxygen levels in 3D cell culture systems. A system was designed and engineered for real-time monitoring and control of oxygen concentration in 3D cell

culture. By using a continuous gas exchange of N_2 and O_2 in the medium above the 3D tissue scaffold. the oxygen concentration was precisely controlled to generate a range of normoxic and hypoxic conditions (Rivera et al.. 2019). The integrated phosphorescence-based oxygen biosensor employs the quenching of palladium-benzoporphyrin by molecular oxygen to transduce the local oxygen concentration in the 3D tissue scaffold as illustrated in Figure 3.2 below. The system was validated by testing the effects of normoxic and hypoxic culture conditions on healthy and tumorigenic breast epithelial cells. MCF-10A cells and BT474 cells. respectively (Gallagher et al.. 2010) (Rivera et al.. 2019).

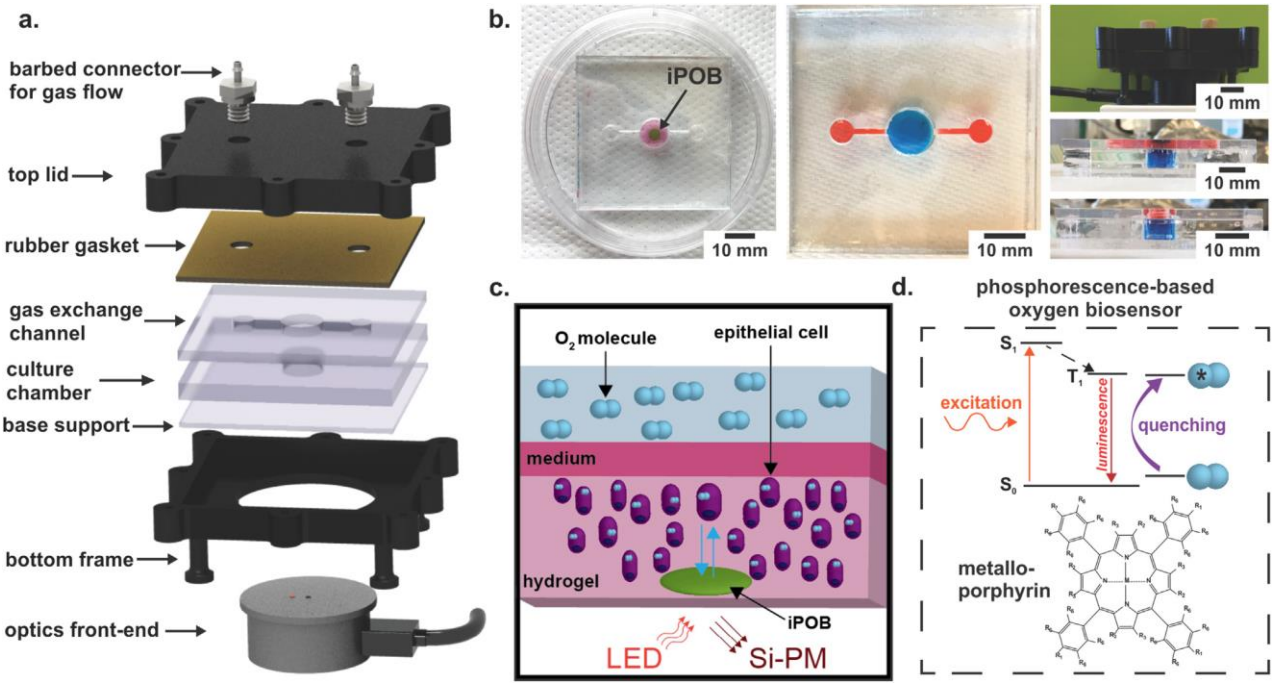

Figure 3-2; 3D Culture and Oxygen Monitoring System (Rivera et al.. 2019). (a) construction of O_2 monitoring system (b) shows the real sample analysis (c) allustrates the mobility of O_2 detection (d) chemical processes involved for O_2 detection.

3.3 Impedimetric biosensor

3.3.1 Impendence basic theory

An impedimetric biosensor. such as the uranyl biosensor developed by (Millner et al.. 2012). utilizes the opposition to the electrical current flowing from the interaction

between the biosensor's bio-recognition element and the target analyte. The concept of impedance can be understood by firstly considering Ohm's Law. which describes the relationship between the resistance to current flow (R). voltage amplitude (E). and current (I) shown by (Equation 3.1).

$$R = {}^{V}/_{I} \qquad \text{(eq 3.1)}$$

For an electrical circuit. however. only an ideal resistor is represented by this relationship. An ideal resistor does not fully represent the complexities inherent in real-world circuit components due to the following simplifying limitations:

- The relationship stated by Ohm's law should apply at all currents and voltages
- The voltage and AC current signals that pass through the ideal resistor are in phase with each other
- Variations in frequency do not impact the magnitude of resistance.

The utilization of the property of impedance instead of simple resistance in the analysis of electrochemical phenomena avoids these limitations. Before examining the method of impedance analysis. electrochemical impedance spectroscopy (EIS). It is useful to introduce the most common equivalent electrical circuit elements in an impedimetric electrochemical system:

- Solution resistance (Rs) – Describes the electrical resistance present due to the ionic solution (electrolyte) under analysis in the electrochemical cell. Specifically. it is the solution resistance between the reference and working electrodes of the electrochemical cell that is relevant here. The parameters that determine the magnitude of solution resistance are cell surface area (A). cell length (l) and solution resistivity (ρ) (Equation 3.2) (Bard et al.. 1980);

$$Rs = p.\frac{l}{A} \qquad \text{(eq 3.2)}$$

  Because the solution resistance is determined by the fluid properties and fixed cell geometry dimensions. it will not usually change during electrochemical analytical investigations of biosensor-analyte systems.

- Charge Transfer Resistance (Rct) – For a biosensor-analyte system. the charge transfer resistance describes the resistance of electron flow from the analyte solution to the electrode. An equation can be derived from the Butler-Volmer equation for the determination of charge transfer resistance (Equation 3.3) (Bard et al.. 1980);

$$Rct = \frac{RT}{nFio} \qquad \text{(eq 3.3)}$$

where R is the universal gas constant. T is temperature. n represents the number of electrons involved in the transfer reaction. F is the Faraday constant. and i_0 is the exchange current density. In a biosensor analyte system. the binding of target analyte ions to the biorecognition element of the biosensor will alter the exchange current density. and therefore; lead to an increase or decrease in charge transfer resistance.

- Double-layer Capacitance (Cdl) – A capacitance is associated with the formation of an electrical double-layer due to the adsorption of ions onto the electrode (biosensor) surface. The double-layer effectively insulates the electrode from the electrolyte (analyte-containing fluid) and behaves like a capacitor.

- Warburg Impedance (W) - Warburg impedance is a constant phase element (CPE) which describes the finite rate of unhindered diffusion of electrons from an electrolyte solution to a planar electrode. The Warburg impedance is typically independent of the analyte receptor binding activity (Rushworth et al.. 2014).

In some electrical circuits describing electrochemical systems. a constant phase element (CPE) is used instead of double-layer capacitance. This is because Cdl describes a capacitor with ideal behavior. while a constant phase element is sometimes considered more appropriate to real electrochemical systems (Huang et al.. 2011).

The equivalent circuit developed through EIS analysis is commonly described by the Randles circuit model (Figure 3.4).

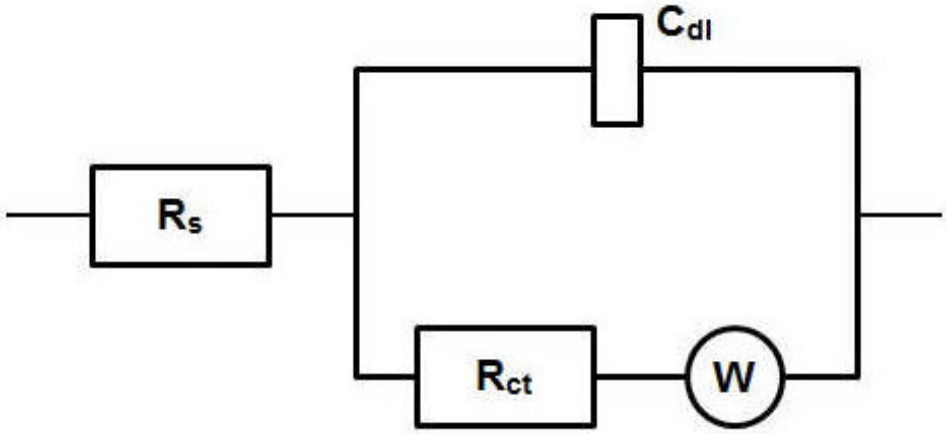

Figure 3-3;Randles equivalent circuit and essential components (redrawn from Conroy 2010)

The solution resistance (Rs) is in series with a parallel circuit consisting of double-layer capacitance (Cdl) in parallel to charge transfer resistance (Rct) and Warburg impedance (W). The Randles equivalent circuit model applies to systems for when faradaic currents are generated. These are produced as a result of an electrochemical reaction at the electrode surface. setting up a charge transfer between the analyte solution and the electrode. Distinct from these are non-faradaic currents. for which electrochemical reactions and charge transfer are not involved. Instead. charge accumulates on or near the electrode as a result of the current (Lasia. 2002).

3.4 Electrochemical Impendence Spectroscopy (EIS)

Electrochemical impedance spectroscopy is the standard method used to measure and analyze biosensor-analyte interactions. An alternating (AC) potential (V). typically consisting of a small amplitude sine wave (±10 mV) set against a background voltage (of typically 0v. giving a potential range of +10 mV to -10 mV) is applied through a potentiostat to the electrode unit containing the biosensor. The AC potential is applied across a range of selected frequencies. The biosensor unit is immersed in a solution containing the target analyte (Macdonald. 1992). Fundamentally. the change in impedance due to analyte binding at the bioreceptor of the sensor is examined by

calculating the ratio of the applied AC potential (V) to the change in current resultant from the biochemical binding. For any given frequency. the resultant current is typically also a sin wave. although it is shifted in phase with respect to the sinusoidal potential. When the amplitude of the sine wave is plotted against time. a phase angle can. therefore. be determined. Equation 3.4 describes the relationship between the impedance. phase angle and the voltage-current ratio (Macdonald. 1992).

$$Z = \frac{V\sin(\omega t)}{I\ \sin(\omega t+\theta)} = Zo\frac{\sin(\omega t)}{\sin(\omega t+\theta)} \quad \text{(eq 3.4)}$$

where Z is the total impedance of the system. V is the applied voltage. I is the resultant current. *t* is time. ω is radial frequency. θ is the phase angle of the sinusoidal current. and Z_0 is impedance magnitude. Therefore. equation 3.4 describes the impedance in terms of a magnitude and a phase shift. The radial frequency (ω) is determined from the frequency applied to the AC voltage (f). as described in equation 3.5

$$\omega = 2\pi f \quad \text{(eq 3.5)}$$

For data obtained through an electrochemical impedance spectroscopy method. it is useful to convert the polar co-ordinates generated from the application of equation 3.5 to cartesian values. The impedance in cartesian co-ordinates is presented in equation 3.6 (Macdonald. 1992).

$$Z(\omega) = Z'(\omega) + jZ''(\omega) \quad \text{(eq 3.6)}$$

where Z is the total impedance. Z' is the real component of impedance. Z'' is the imaginary component of the impedance. and j is equal to $\sqrt{-1}$. From equation 3.6. it can be seen that the impedance has been converted into real (Z') and imaginary (Z'') components. In general terms. the real component of the impedance can be regarded as representing properties of the electrochemical system similar to the resistance. while the imaginary component represents properties similar to the capacitance. When the real component of impedance (x-axis) is plotted against the imaginary component (y-axis) for a given EIS dataset. a Nyquist plot is created. A drawback of these Nyquist plots is that they do not explicitly display information on the measured frequency (Millner et al.. 2012). However. the impedance response appropriate to high

frequencies is always displayed to the left of the plot. and those appropriate to low frequencies to the right (Figure 3.5). Based on this understanding. information about the Randles equivalent circuit components associated with the analyzed biosensor can be determined (Huang et al.. 2011). The solution resistance (Rs) and the charge transfer resistance (Rct) are determined from the x-axis intercepts at high and low frequencies respectively. and the double-layer capacitance (Cdl) from the y-axis intercept of a line change initial to the top of the resultant semi-circle. The Warburg impedance element (W). if present. will always appear on such Nyquist plots as a 45^{o} straight line at low frequencies as shown Figure 3.4 below.

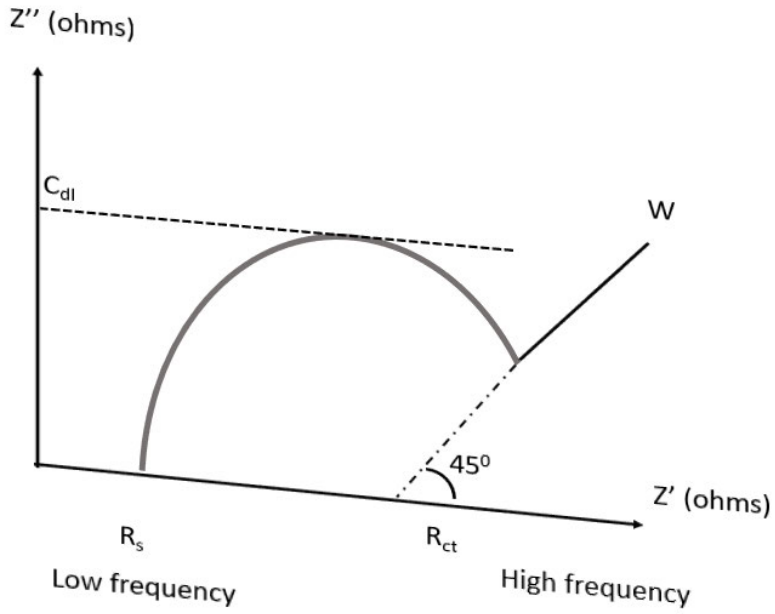

Figure 3-4: Nyquist plot for electrochemical impendence spectroscopy analysis.modified from (Rushworth and Hirst. 2013).

3.5 **Cyclic voltammetry**

Cyclic voltammetry (CV) is a commonly used analytical tool in electrochemical experiments. For biosensor investigations. it is regularly applied to the study of the effectiveness of electrode preparation (cleaning) methods. and the process of biosensor layer deposition. To conduct CV analysis. an electrode/biosensor is immersed in an electroactive species; in the presence of the ferrocyanide/ferricyanide

redox couple $Fe(CN)_6^{-3/-4}$. A potential (E) is applied between the reference and working electrodes of a three-electrode system. and the resultant current (I) is measured between the working and counter electrodes. The applied potential is ramped linearly with time through a specified scan rate (mV s^{-1}) between 1st and 2nd potential limits. and the potential is applied between the limits in both forward and reverse directions. The potential limits are chosen specifically to allow for the oxidation and subsequent reduction of the electroactive species couple used in the investigation (Tanimoto and Ichimura. 2013). For a bare electrode immersed in an electroactive species. a plot similar to that presented in Figure 3.6 will be produced. where the potentials at which an oxidation peak (anodic peak potential. E_{pa}) and reduction peak (cathodic peak potential. E_{pc}) occur are identified on a voltammogram. Additionally. by utilizing suitable baseline currents. a peak anodic current (I_{pa}) and peak cathodic current (I_{pc}) can also be determined (Kissinger. 1983).

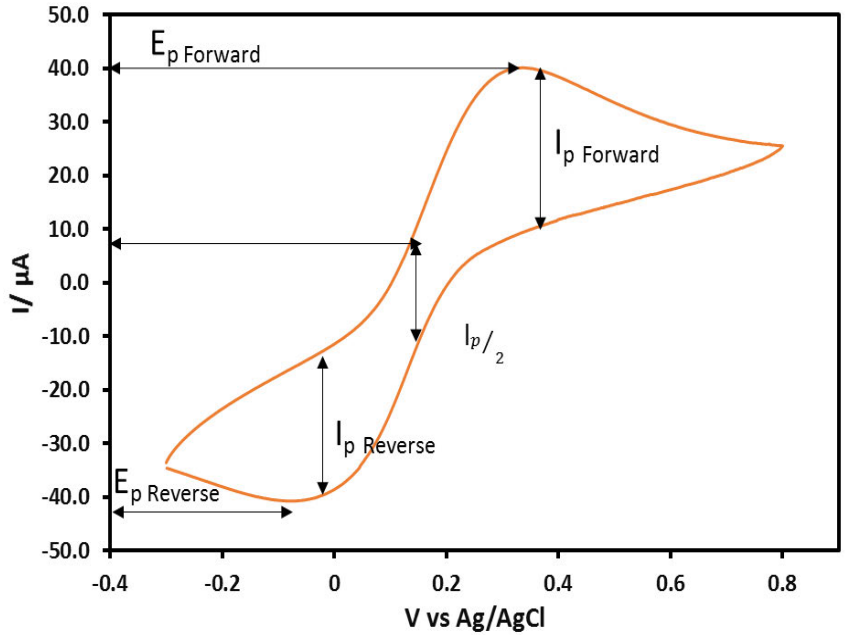

Figure 3-5;Cyclic voltammogram schematic diagram for an electroactive redox couple. E_{pa} – (oxidation) potential. E_{pc} - (reduction) potential. i_{pa} –. i_{pc} – peak cathodic current.

The mathematical determination of the peak currents is given by the Randles–Sevcik equation. Comparative examination of cyclic voltammograms before and after the application of electrode cleaning methods and following the deposition of biosensor layers on the electrode surface can be used to assess the nature of electrode surface

modification. This is typically done through relative analysis of parameters such as the peak currents and peak potentials. and the relative distance between peak potentials (i.e. $E_{pa} – E_{pc}$). Cyclic voltammetry techniques were utilized primarily in the analysis of electrode preparation methods. for electrodes upon which the biosensors were constructed.

3.6 **Biosensor emplacement**

Although research into the design and development of biosensors across a range of applications has steadily increased over the past 10-15 years. the transition to successful deployable point-of-use (POU. usually referred to as point-of-care (POC) for medical applications) systems has been very limited. This. in turn. has limited the commercial exploitation of biosensors.

Four key components are identified to enable impedimetric biosensor transition from laboratory proof of concept to point-of-use deployment:

- Impedimetric biosensor – Incorporating a physio-chemical transducer and biosensor recognition element. The basic requirements for successful lab-to-field transition are reproducible and reliable performance. such that results are comparable to both laboratory-based biosensor operation and ‘gold standard’ non-biosensor laboratory methods for the analytical process concerned.
- Fluid sample collection. delivery and processing capability –Typically. a microfluidic platform will be utilized for fluid handling capabilities. incorporated with valves and pumping systems for fluid control. Pre-treatment may be required. and the deployment system will therefore. be required to accommodate the storage and handling of buffers and reagents. The uranyl biosensor. for example. would require delivery of buffer for storage of the biosensor within the deployment system. and for regenerating the biosensor surface after analysis (Conroy 2012).
- Signal processing capability – Incorporation of a compact potentiostat to enable electrochemical analysis. For automated. remotely controlled systems. this would need to be battery operated or rechargeable (through renewable energy sources for example). Stand-alone commercial portable potentiostat products

are available (e.g. Uniscan Instruments. PG581 Potentiostat - Galvanostat 2013). and the technology could be readily adapted to allow for built-in incorporation into a fluid delivery system for example.

CHAPTER 4: MATERIALS AND METHODS

The chapter focuses on methodologies used in this study. The first subsection describes the electrochemical instrumentation. the characterization techniques that were used to confirm the Osmate redox polymer followed by the surface analysis of PGE. Afterwards there is list of chemicals that were used throughout the experimental analysis of this study. This is followed by a descriptive section for preparation of all the working standards. solution also the preparation for enzyme activity analysis. The second subsection is based on the experimental procedure including the material and conditions for the polymer synthesis used for the formation of third generation biosensor. providing a deep insight for the reaction of polymer synthesis.

4.1 Instrumentation

This section gives an overview of the instrument for this work. including the parameters. The techniques were selected to support the evident information found in this study. These techniques are for qualitative and quantitative analysis. as well as the characterization instrumentation used. All the reported results are analysed using optimised parameters.

4.1.1 Electrochemical techniques

The electrochemical measurements were used for both the qualitative and quantitative analysis carried out with two different electrochemical instruments: Autolab PG-STAT 10; Program- General purpose electrochemical systems 4.9; Eco chemic B.V. Utrecht. the Netherlands and a portable USB-powered 910 PSTAT software for cyclic voltammetry and chronoamperometry using a three-electrode system. The Pt wire and Ag/AgCl as the auxiliary electrode and

reference electrode respectively. modified PGE was the working electrode. The computer was used to control the potentiostat software. the electrochemical experiments were carried out in a biological phosphate buffer with pH 7. in an unstirred solution at ambient temperature.

4.2 Reagents and materials

Several salts were used for the preparation of the buffer solution including sodium dihydrogen phosphate (NaH_2PO_4. disodium hydrogen phosphate ($Na_2HPO_4.7H_2O$). for the fabrication of PGE. multi-walled carbon nanotubes (MWCNTs). carbon nanoparticles (CNPs). The synthesis of the redox polymer acrylamide. 1- vinylimidazole. *N.N.N.N* tetraethylenediamine. 2.2-azobis(2-methylpropionitrile. ammonium hexachloro osmiate. ethylene glycol. bilirubin oxidase. graphene oxide. 1-pyrenebutyric acid N-Hydroxysuccinimide ester (PBSE). potassium hexacyanoferrate trihydrate $K_3Fe(CN)_6$. potassium hexacyanoferrate $K_4Fe(CN)_6$. sodium sulphate ($Na_2S_2O_4$) citric acid ($C_6H_8O_7$). sodium citrate ($Na_3C_6H_5O_7$). syringaldazine. bilirubin (magnaporthe oryzae). laccase (trametes) and 2.2′-Azino-bis(3-ethylbenzothiazoline-6-sulfonic acid) diammonium salt $C_{18}H_{24}N_6O_6S_4$ (ABTS). All the reagents were purchased from Sigma Aldrich and used without further purification. Potassium chloride (KCl). Dimethylformamide $HCON(CH_3)_2$ (DMF). ethanol (C_2H_5OH) 99.9 %. hydrochloric acid (HCl) 35 % were acquired from Merck. All the used chemicals were of analytical grade. The chemicals were stored and treated according to the safety data sheet (SDS) requirements in order to prolong the life span and eliminate the chemical hazard/ prolonged exposure.

4.2.1 Preparation of working solutions

i. **Iron solution**: this was prepared from two iron salts (Fe II and Fe III) while using KCl as a supporting electrolyte. The weighed masses were 0.106 g 0.082 g followed by 0.373 g. respectively. The amounts of salts were weighed to prepare Concentrations of 5 mM 2.5 mM and 2.5 mM for Fe II and Fe III and

KCl. respectively into a single 50 mL volumetric flask. The resulting solution was coloured yellow when homogenized. This solution was freshly prepared for each day of use.

ii. **$Na_2S_2O_4$**: The 0.1 mol/L solution was prepared using $Na_2S_2O_4$ weighed accurately with the mass balance of four decimal places and weighing boat. This was transferred into a 100 mL volumetric flask. This was dissolved and made to calibration mark with de-ionized water.

iii. **Graphene oxide**: A commercial purchase graphene oxide was **used.** 4.0 mg/ml in aqueous water solution. To make 1.0 mg/mL. a 50 μL was pipetted from 4 mg/mL into a 1.0 mL Eppendorf tube. it was then diluted with 150 μL of de-ionized water and then mixed using a vortex mixer

iv. **1-pyrenebutanoic acid. succinimidyl ester (PBSE**): The spatula used for measuring was initially purged with N_2. A 10 mM (0.001 M) was prepared by weighing the powder into the 1 mL Eppendorf tube. This compound was dissolved with Dimethylformamide (DMF) as a solvent. The pipetted volume of the solvent used is mainly depended on the mass of PBSE weighed from the balance. This produced a faint yellow colour. This solution was prepared inside the fume-cupboard.

4.2.2 Preparation of buffer solutions

i. **Phosphate buffer**: The buffer was prepared from two KHP salts with a similar concentration of 0.1 M. These two (KH_2PO_4 and K_2HPO_4) monobasic and dibasic salts respectively were weighed accurately using a four-decimal balance. The salts were dissolved using de-ionized water at room temperature. into cleaned 50 mL and 100 mL volumetric flasks. The solutions were properly homogenized then made to mark and let to settle before use. The ideal pH is made by mixing different volumes of each solution to make a buffer. This is then confirmed by measuring the value using the electrode.

ii. **Citrate buffer:** This buffer was prepared using two salts a citric acid and sodium citrate both concentrations were 0.1 M. The salts were prepared individually into a 100 mL volumetric flask. A certain volume of these solutions

was then mixed into a 100 mL volumetric flask and diluted with 50 mL de-ionized water.

iii. **Tris HCl**: Tris (hydroxymethyl) aminoethane. a 0.2 M solution was prepared into a 100 mL volumetric flask. by accurately weighing a mass. The salt was then dissolved in water. homogenized well then made to calibration mark. This solution was kept while preparing a 0.2 M HCl acid. The acid volume was calculated using a Sigma-Aldrich calculator. It was then pipetted into a 100 mL volumetric flask diluted with gently pouring of water. This was then used to adjust the Tris (hydroxyethyl) amino ethane pH.

4.2.3 Preparation of enzyme solutions

i. **Laccase oxidase TV and RV**: These two enzymes are from different sources. The ideal concentration for use is 25 mg/ml. The 1 mL Eppendorf carry mass weighed using a four decimal mass balance. The pipetted volume is depended on the mass weighed. The solvent is a pH 6 phosphate buffer. The enzyme is freshly prepared each day of use.

ii. **Bilirubin oxidase**: The BOx from *M. oryzae* (25 U mg^{-1}) was store in a concentration 0. 5 mg mL^{-1} the spatula was initially purged with nitrogen to weigh the enzyme into 1 mL Eppendorf. using a four decimal mass balance. The pipetted volume was calculated depended on the mass weighed. It is then dissolved a pH 6 phosphate buffer. The enzyme is then in -20 ^{o}C. prior to use the enzyme was let to melt at ambient temperature.

4.2.4 Enzyme activity measurements

i. **Laccase Oxidase**: The enzyme activity was determined using a spectrophotometric device at 37 ^{o}C using 96 well plates. The oxidation of syringaldazine of 0.216 mM at 420 nm in absorbance mode using a 0.1 M citrate buffer (pH 5) and phosphate buffer (pH 6 and 7). The laccase TV and laccase RV were weighed and dissolved in de-ionized water of calculated volumes for the mass weighed.

ii. **Bilirubin Oxidase**: The enzyme activity was determined spectrophotometrically at 37 ^{o}C using 96 well plates. At 420 nm 0.1 M ABTS is oxidized in citrate buffer pH 4. 25 -50 units of the enzyme were used.

4.3 Synthesis and characterization of a redox polymer

This polymer was synthesized using a three-step method. Initially. the copolymer was synthesized. followed by the synthesis of the ligand combined under specific conditions. This led to the formation of the Os redox polymer. used for the analysis.

4.3.1 Synthesis of copolymer Acrylamide and Vinylimidazole (PAA-PVI)

Acrylamide was weighed (12 g. 168 mmol) and vinylimidazole (3.50 mL. 38 mmol) into a 500 mL round-bottom flask equipped with a magnetic stirrer. and dissolved in 75 mL water. as shown in Figure 4.1 (a-b). This was followed by a solution of *N. N. N. N. Tetramethylenediamine* (0.35 mL. 2 mmol) in 25 mL of water. After complete dissolution. a solution of thioglycolic acid 2 mL was added into the solution. Figure 4.1 (c) shows the polymerization reaction proceedings under argon gas in a tightly closed vessel while stirring. This reaction takes place at ambient temperature for a period of 30 minutes. The polymer that was separated by the drop-wise addition of reaction mixture into acetone is shown in Figure 4.1 (d). The precipitate was then separated and purified by the dialysis membrane of 10 kDa cut-off.

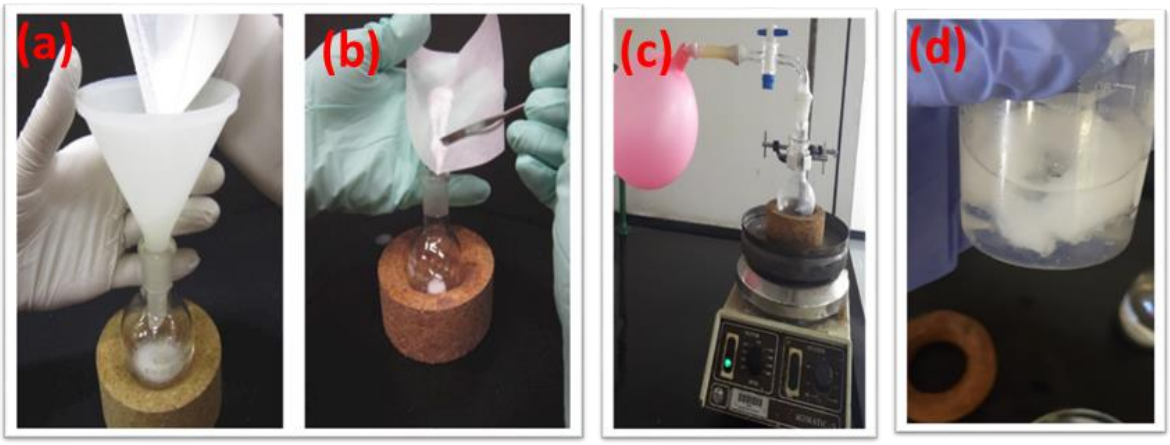

Figure 4-1; Preparation of the PAA -PVI refluxed under argon at ambient temperature.

The method of the PAA-PVI synthesis was altered from a previous report (Cadet et al.. 2013a). In this method a highly explosive chemical (2.2-azobis (2-

methylpropionitrile) was used. and one of the reagents. which could have been very hard to handle in the lab but also getting the compound to the country was very challenging. It was therefore substituted with a thioglycolic acid.

4.3.2 Synthesis of ligand Os (4.4-Dichloro-2.2-Bipyridine)$_2$Cl$_2$

A 100 mL round-bottom flask with magnetic stirrer contained 1 g of ammonium hexachloroosmiate. 25 mL ethylene glycol and 4.4-dichloro-2.2-bipyridine (1.05 g. 4.48 mmol). Figure 4.2 (a) shows the reflux system under argon gas for a period of 2 hours. Figure 4.2 (b) shows the reaction solution during filtration. with the filtrate washed with a saturated $Na_2S_2O_4$ and twice with ether. The precipitate was then allowed to dry in a vacuum. The filter paper after collection of the compound. [m = 1.154 g. yield = 70.76%]. is shown in Figure 4.2 (c).

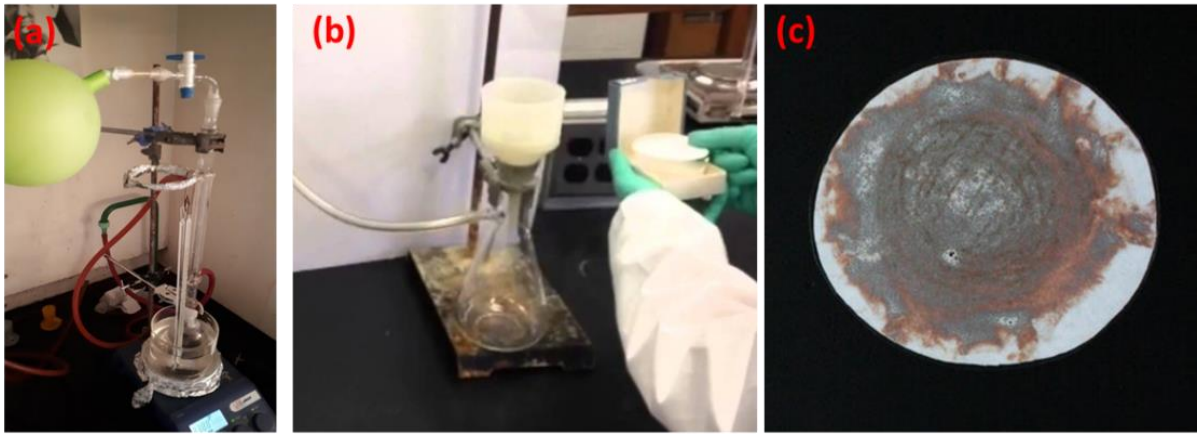

Figure 4-2: (a) reaction under árgon gas, (b) filtration of the compound, (c) filter paper after removing the ligand [Os (4.4-Dichloro-2.2-Bipyridine)$_2$Cl^2] to produce a redox polymer.

4.3.3 PAA-PVI-Os$^{/2+}$ synthesis

A 150 mg PAA-PVI. ethylene glycol (15 mL) and Os (4.4-dichloro-2.2-bipyridine)$_2$Cl$_2$ (150 mg. 0.2 mmol) was added to a 150 mL round-bottom flask with a magnetic stirrer. under argon. Figure 4.3 (a) shows the solution refluxed for 4 hours at 160 ^{o}C. The final product was then precipitated with ether and purified by ultrafiltration. using an oil bath. The dark brown solid (Figure 4.3 (b)). was then mixed with water and dialyzed using a 10 kDa membrane with ethanol as shown in Figure 4.3 (c) (Piontek et al.. 2002. Cadet et al.. 2013a).

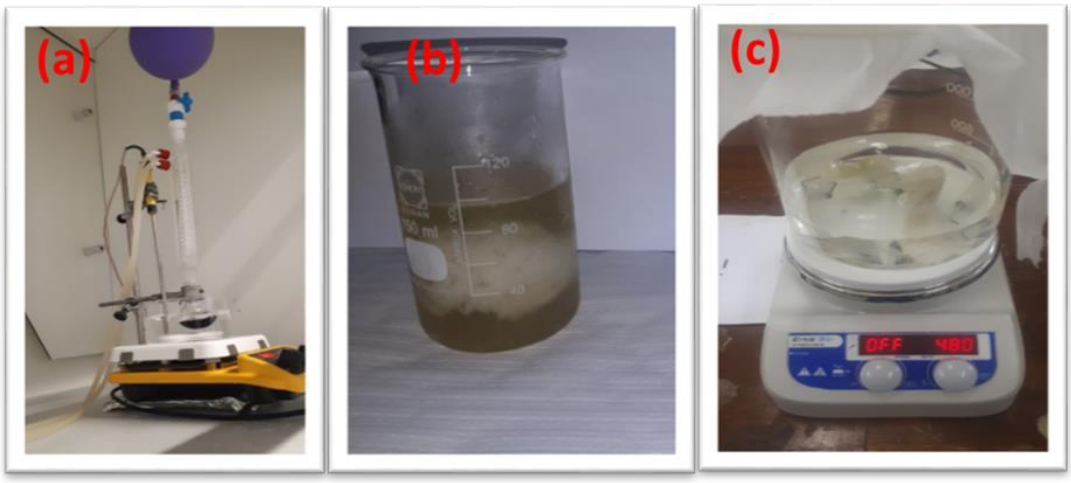

Figure 4-3; (a) reaction refluxed at 160 ^{o}C using oil bath (b) collection of polymer (c) purification of the PAA-PVI Os (4.4-dichloro-2.2-bipyridine)$_2$Cl] $^{+/2+}$ of redox polymer

4.3.3.1 Optimization of the reaction conditions

Thin Layer Chromatography (TLC) was the first step to test if the reaction was complete. This liquid-solid adsorption where the mobile phase (dichloro-methane and diethyl-ether) ascends the thin layer of the stationary phase. The separation is mostly depended on the mobile composite. solubility. affinity. and resolution. The optimum separation of compounds by TLC achieved with Rf values between 0.3 – 0.5. All the reactions were monitored by the use of TLC. to evaluate whether it is a complete reaction or not yet completed. This assisted in observing the formation of the product using the solution of the starting material and the flask containing the product. viewed under UV light.

4.3.4 Characterization of redox polymer techniques

The polymer synthesis reaction was monitored by thin-layer chromatography (TLC). and the functional group present in the redox polymer synthesis was investigated for each step of the analysis by Fourier Transform-Infrared (FTIR) at a wavelength ranging from 400-4000 cm^{-1}. The thermal stability of the polymer was evaluated using thermal gravimetric analysis (TGA). All the characterization analysis was undertaken at the Universidade do Porto in Portugal.

4.3.4.1 Thin Layer Chromatography (TLC)

This is a liquid-solid technique in which the stationary phase and mobile phase are used to partition the compounds. A thin layer coated with silica gel or alumina onto the piece of ceramic. The compound has different solubilities and adsorption onto two phases. The TLC was used to monitor the reaction. to identify if all the reagents have reacted completely to form a new product. This can be observed by the Rf value. the difference in migration distance of the starting reagent and new product. This assists to compare and monitor the entire reaction.

4.3.4.2 Thermal Gravimetric Analysis (TGA)

This study was conducted using to observe the physical and chemical properties of PAA and PAA PVI Os 4.4 dichloro2.2 pipyridine as the function of increasing temperature at a constant heating rate as the function of time at constant mass. The difference in weight between the initial and final mass is used to calculate the degradation. This is important for the thermal stability of the polymer under application conditions. A Perkin Elmer TGA system is an experiment described in this work. This is purged with 40 ml/min nitrogen. N_2 purged stream of 20 ml/min entering the system entrance.

4.3.4.3 FTIR

Fourier transform infrared spectra of acrylamide (AA) and a product polyacrylamide (PAA) are observed in the mid-infrared region 4000 – 400 cm^{-1}. The intensity of the bands is related to the frequencies of each compound. The characterization with IR was performed for each step of the polymer using a Shimadzu instrument. The ground potassium bromide (KBr) powder is used to determine the information of the sample (physical and chemical). KBr does not contain any bands in the mid-IR region of the spectrum. The preparation of sample and halide powder (KBr) is homogenously dispersed by grinding.

a. **The method used to prepare KBr disk**

Approximately 2.0 mg of the sample and 200 mg KBr powder was mixed into a mortar and pestle. KBr is of high purity and dry. A fine consistency powder is then transferred

to assemble the die with a low pellet polished faced up. This is evenly distributed across lower faced pellets. Gently insert the plunger and swiveling to achieve an even flat surface. The top pellet faced towards the mixture. Placing under die assembly into hydraulics press between the ram and piston. The assembly die must firmly hold in the press. connection a high vacuum pump. Hold the vacuum for 2 min. and then the pressure can be increased to 10 torrs. Carefully release the vacuum and remove the die from the press. The disk must be translucent. and the sample is evenly distributed in the disk. Gently mount the disk in the spectrometer. Mainly avoid touching the faces of the disk.

4.4 **Construction of PGE**

Pencil graphite electrode was constructed using accessible material that was easily available materials. simple. not harmful to nature. The double-insulated copper wires were purchased from the nearest electric workshop. Stadler 2 mm HB pencil and PVC tubing. There are some essential materials that are required too; scissors. sandpaper. soldering iron and soldering wire. The copper wire is cut open to ensure direct contact with the sharp pencil graphite. this is sealed with the PVC tubing as a sleeve

The pencil graphite was inserted and coated with the PVC tubes. The other end of the electrode was coated with soldering wire to make a conductive end. The soldering wire; is a fusible metal alloy with a low melting point. low enough to be melted with a soldering iron. It is used to bond metal workpiece together. This side of the electrode is the one used to connect crocodile clamps. which are connected to the instrument. The electrode is usually about 9 cm long and an addition of 1 cm of pencil graphite. the front end of the electrode is fined using sandpaper and smoothened using alumina slurry. This is followed by cleaning the electrode surface with deionized water. The multi-meter is then used to measure the resistance across the terminals of the electrode. The ideal is a minimal resistance as possible. and this confirms the functioning of the electrode. This can be explained using Ohm’s law (I = V/R). This relationship of I. R and V. can be used to understand the relationship between the R and I. The electrical pressure applied to charges (V). this then will release a higher number of charges at a shorter time. the movement of charges is called current (I). The current produced flow through the circuit. there is friction which opposes the

current called resistance. Hence. if there is minimal resistance between the terminal. this results into a higher current flow. All experiments were performed in a classic three-electrode electrochemical cell composed of an Ag/AgCl (KCl, 3 M) reference electrode (Metrohm. Ref. 6.0727.000). a platinum rod as a counter electrode and the PGE sensor/biosensor as a working electrode. All potentials presented throughout the test are referenced for Ag/AgCl. An equimolar 5 mM solution of potassium hexacyanoferrate. $Fe(CN)_6^{3-/4-}$ in 0.1 M of KCl (resistance of the solution R_{sol} = 180 Ω) was used for characterization experiments of the PGE sensor (without immobilized enzyme). As for the characterization of the bioelectrode. potassium phosphate buffer 0.1 M pH 7.0 was used as an electrolyte solution and was purged with N_2 or oxygenated with O_2 for 15 min. This electrode can be used in a three-electrode system connected to the electroanalytical instrument with crocodile clamps as shown in Figure 4.4.

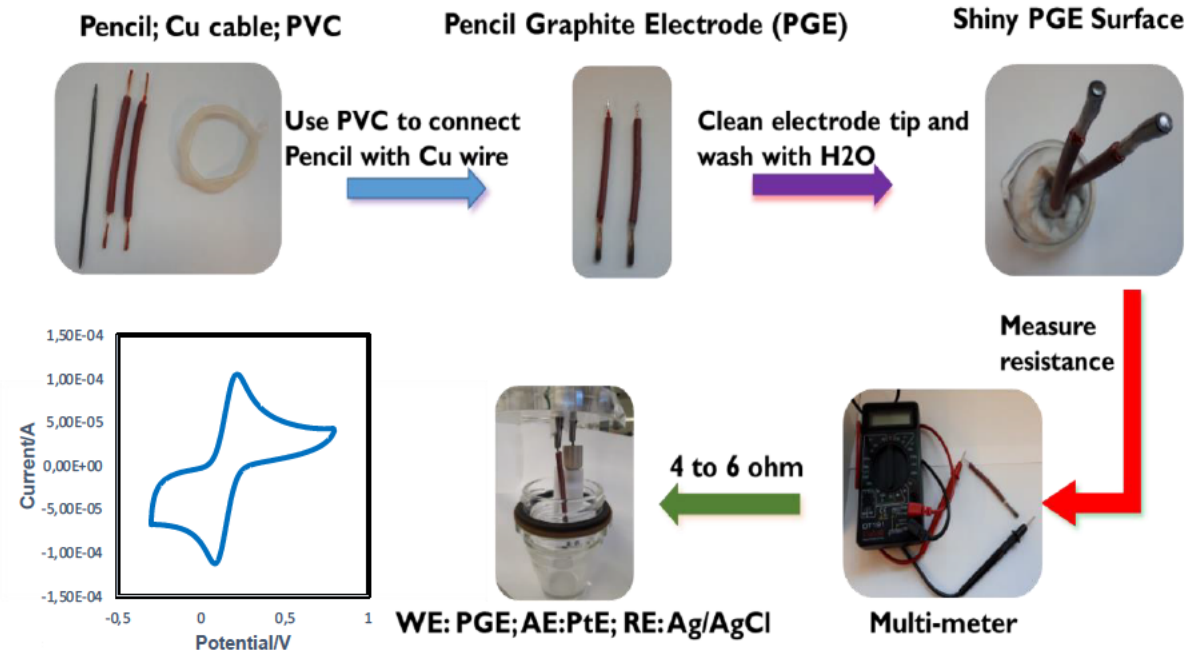

Figure 4-4;The fabrication of the PG electrode using non-expensive materials.

This can be further observed in chapter 5.1.3.. as it shows an electrochemical response of three different pencil graphite current signals. This can be expected according to the hardness of the pencil mine used as PGE. The same may be observed when varying the level of pre-treatment applied to its active surface. Thus.

PGEs with different clay/carbon ratios (hardness 4B. HB. and 4H) and type of pre-treatment were compared regarding their performance in $Fe(CN)_6^{3-/4-}$.

4.5 Fabrication of the sensors

4.5.1 Laccase enzyme activity by UV-Vis spectroscopy

In order to know and understand the enzyme kinetics being used. it is vital to analyze for its activity. This is a measure of the catalytic ability. here the decrease in substrate concentration with time is measured. The conditions selected to measure the activity of laccase enzymes are not the same as those to perform electrochemical analysis. Numerous factors affect the rate at which the enzyme behaves and the proceeding of the enzymatic reaction: temperature. pH. enzyme concentration. substrate concentration and the presence of any inhibitor or activators. as shown in Table 6.

Table 6; Mixtures used for Laccase activity analysis

Mixture	Buffer Volume	Volume Laccase 57 mg/mL in water purged 20 min with N_2	Volume of 0.216 mM Syringaldazine in 99.9 % methanol
A	220 µL buffer pH 6	50 µL enzyme	30 µL
B	220 µl buffer pH 6 (purged 20 min N_2)	50 µL enzyme	30 µL
C	220 µL buffer pH6 (with O_2 20 min)	50 µL enzyme	Nil

Table 6 shows is the detailed preparation for the analysis in the spectrophotometer. including the volumes for each reagent and composite made. The analysis was run with a spectrophotometer in absorbance mode

4.5.2 PGE/CNPs/TMOS/laccase and PGE/ GO/TMOS/ Laccase

Laccase and CNPs were immobilized onto the electrode surface in a one-step procedure-sol drop deposition. Sol-gel processed silicate was chosen as a matrix

because it provides a suitable environment for the immobilization of the protein. It was earlier used for the laccase immobilization onto a smooth electrode surface. but mediator-less bio-electrocatalytic dioxygen reduction was not observed. The catalytic activity of the enzyme encapsulated in the composite film was studied by cyclic voltammetry and chronoamperometry. The preparation of the CNPs/TMOS/laccase paste for the fabrication of the electrode was prepared. as shown in Figure 4.5.

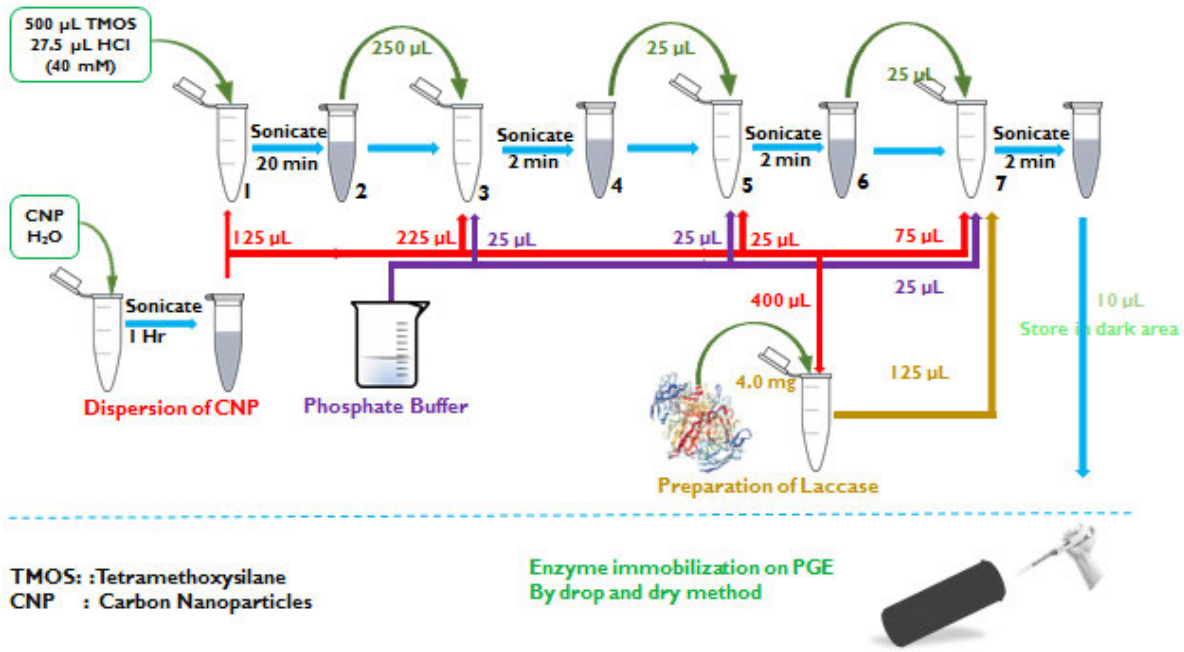

Figure 4-5;Preparation of the paste for the fabrication of electrode using TMOS as the mediator

CNP solution was prepared by adding 3.0 mg of CNPs to 1.0 mL of water. followed by 1-hour sonication. For the preparation of the film; 500 µL of tetramethoxysilane (TMOS) was mixed with 27.5 µL of 0.04 M aqueous HCl and 125 µL of CNPs solution. The next 250 µL of the sol was diluted with 225 µL of CNP solution and 25 µL of 0.1 M phosphate buffer (pH 5.8). Then a 25 µL aliquot of the diluted sol was mixed with 125 µL of laccase (145 µg of laccase dissolved in 2 mL of CNPs solution). 75 µL CNP solution and 25 µL of phosphate buffer. Finally. 25 µL of the sample obtained in the last step was diluted in the same way. Every step of solution or sol preparation was followed by sonication (Szot et al.. 2009a). PGE/GO/TMOS/Laccase was similar to the preparation of PGE/CNPs/TMOS/laccase except that CNPs were replaced with GO.

4.5.3 PGE/GO/MWCNTs/PBSE/Box

This diagram in Figure 4.6 shows the interaction of all the elements for electrode preparation to immobilize the enzyme on its surface. From a bare PGE showing the top surface made from Staedtler 2 mm diameter. smooth surface is obtained by using fine sandpaper. This is further cleaned with the alumina slurry. for removal of all the impurities from the surface. The following step is the application of GO onto the PGE surface. a micropipette was used to drop-cast 10 µL of 1 mg/mL dispersed in water. This was allowed to dry at room temperature for an hour. ensuring not to disturb the electrode surface. Once the surface was dried. an intense black color was observed on the surface. followed by an electrochemical reduction described above.

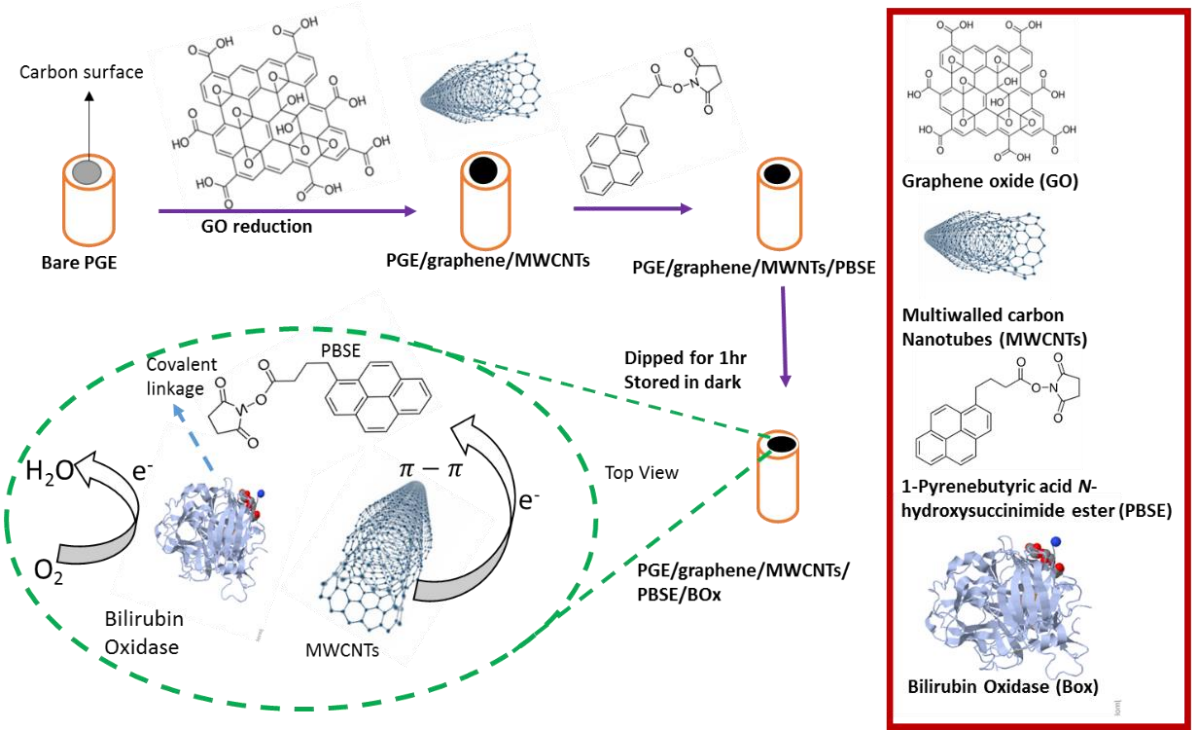

Figure 4-6;The immobilization of BOx onto the electrode surface. using carbon nanomaterials and PBSE for the electron transfer.

Another step was to apply the MWCNTs. and this step is vital for electron site and enhancement of the surface area. using a drop-casting method using a similar 10 µL micropipette. This was dried inside the oven at 45 °C. for 45 minutes. This is a safe

temperature not to temper with the material of the electrode like the electrode skin and sleeve since they are made of PVC material.

The following step involved the use of the tethering agent. PBSE bond to the MWCNTs with pie-pie stacking bonds. using the electrons around its rings. PGE/GO/MWCNTs were immersed in the PBSE 10 mg/mL dissolved in DMF. This was allowed to mix for one hour. the electrode is then rinsed very gently to remove any residues of PBSE. The last step was the immobilization of bilirubin. At this stage the method to apply a bilirubin oxidase enzyme was varied. One being the drop-casting method: where the enzyme is introduced using a pipette onto the surface of the electrode. this is further explained in chapter 5.1.8.5. Another method was to immerse the electrode into the eppondorf containing Box. The other components of the electrode were dried before immersing into the enzyme for 30 minutes. This allowed a gravitational interaction between the enzyme and the PGE/GO/MWCNTs/PBSE.

4.5.4 PGE/GO/ PAA-PVI- Os[(4. 4-dichloro-2. 2-bipyridine)$_2$ Cl]$^{+/2+}$ composite

home-made pencil graphite electrode was prepared by modifying with graphene oxide used to enhance the surface area of the electrode. Prior to electrode coating. their surface is smoothened by sandpaper followed by cleaning with aluminum slurry then thoroughly rinsed with de-ionized water. The electrode is then let too dry for 10 minutes. For electrode modification. the components are added in a particular ratio. BOx 5 Unit from *M. oryzae.* 62.6 wt. % hydrogel redox polymer poly acrylamide-poly(1-vinyl imidazole) (PAA-PVI- Os(4.4-dichloro-2.2-bipyridine)$_2$ Cl]$^{+/2+}$. 30 wt. % BOx and 7.4 wt. % polyethylene glycol (PEG) (Cadet et al.. 2013b).

4.6 Computational adsorption studies

All the structures were constructed using the drawing utilities of the Material Studio 2016 (MS. http://accelrys.com/products/collaborative-science/biovia-materials-studio/). These generated structures were placed on each other in order to construct the layer-by-layer electrode surface. Each of the layered structures was optimized using the DFT – based techniques implemented in the DMol^3 module (Delley. 2000) of the MS on the basis of the B3LYP functional theory. where possible. Using the

“Adsorption locator” module of the MS. the corresponding outputs were generated in the form of total adsorption energies.

CHAPTER 5: RESULTS AND DISCUSSION

The results and discussion of the experimental analysis. involving the fabrication of the PGE is presented here. The computational adsorption energy calculations used to assess the interaction for each of the layered electrode surfaces is also presented. as a complementary study.

5.1.1 Analysis methods

The analysis methods used for this research can be categorised into ‘electrochemical’ and ‘non-electrochemical’ methods. Three different electrochemical analysis methods were used for different parts of this research. Each electrochemical analysis (EA) method along with the parameters used are discussed below.

5.1.2 Electrode preparation

As discussed in Section 4. the choice of the electrode preparation method can influence the structure and stability of self-assembled monolayers (SAM). and therefore. affects the quality of biosensors that utilize SAM’s as a base layer (as laccase biosensor) (Pike. 2014). This sub-section therefore. reviews published electrode preparation techniques. specifically focusing upon electrodes for biosensor construction use. A distinction is made here between preparation methods employed first-time use electrodes and those utilized in regenerating electrodes upon which biosensors have been constructed (although some techniques are used for both). An additional focus for this sub-section is on the preparation methods used for the working electrodes in the form of carbon.

5.1.3 Electrochemical Optimization of PGE

The cyclic voltammetry technique was explained in detail in Section 3.7 and was used in these investigations primarily for monitoring electrode preparation techniques. and biosensor construction layers (biosensor quality). All cyclic voltammetry analysis was conducted using an Autolabs potentiostat. and scans were between potentials of -0.4 V and 1 V at a scan rate of 50 $mV.s^{-1.}$ Scans were conducted in 10 mM ferrocyanide/ferricyanide ($Fe(CN)_6^{3-/4-}$) electrolyte solution and (in 10 mM PBS at pH 7.0).The pencil graphite was selected from a range of 9H to 9B. but only three of them were used which were 4H. HB and 4B with a diameter of 2mm each and their electrochemical response is indicated in Figure 5.1 below.

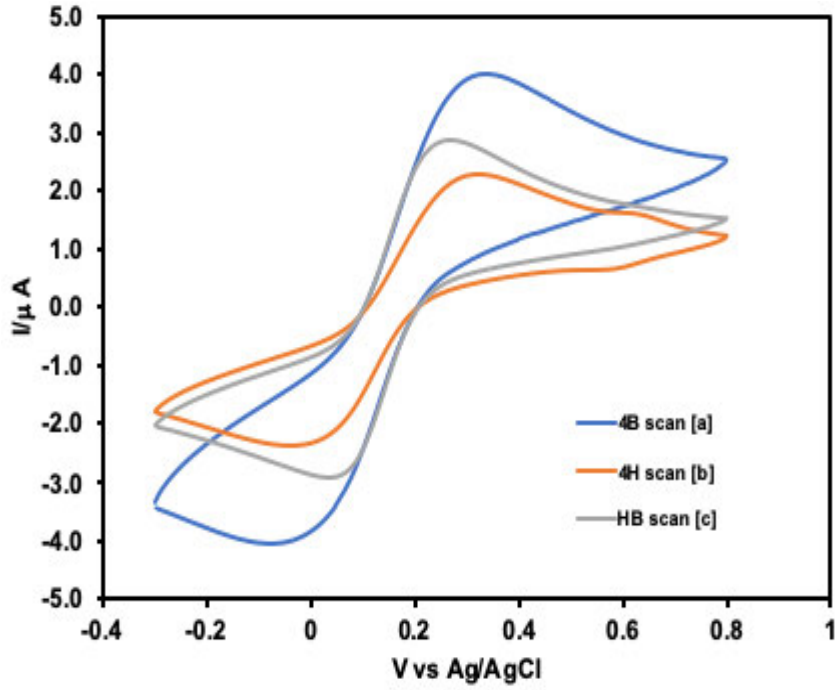

Figure 5-1; Cyclic voltammograms of different pencil mine behavior in a $Fe(CN)_6]^{3-/4-}$ redox probe. (a) the scan is the 4B. (b) 4H and (c) HB pencil graphite electrode

The H and B refer to the Hardness and Blackness. respectively. This determines the clay (silicate) to the carbon content ratio. It is observed that the peak current increases with the carbon content (blackness) present in the pencil graphite. As shown in Figure 5.1. (b) 4H showed a minimal peak followed by (c) HB and with the biggest peak current was the signal (a). The bigger signal would have been an easy pick. but there was some other aspect that was not favorable (signal noise. consistency and

background current). Hence. this can be attributed to a higher concentration of carbon. This led to a second biggest signal being the alternative pick. which proved to be vital because it was stable and consistent in most potentials. It also showed reproducibility with an appreciable signal. The HB is a normal school writing pencil that has an equal amount of clay and carbon.

The non-electrochemical methods were used to provide information relating to the surface microstructure of the PGE working electrodes. This information was then used to help in the analysis of the quality of the constructed biosensors. a thorough assessment of the influence of surface topography upon self-assembled base layer formation is presented below.

The surface analysis was examined using the Scanning Electron Microscopy (SEM). this uses the backscattering of a focussed beam of electrons directed at a surface or secondary electrons emitted as a result of interactions between the electron beam and atoms of the surface material(s). The morphology of pencil graphite shown by the SEM images confirmed the blackness of the graphite surface. Figure 5.2 illustrates the SEM images of pencil graphite 4H. HB. and 4B. and these are lower magnifications.

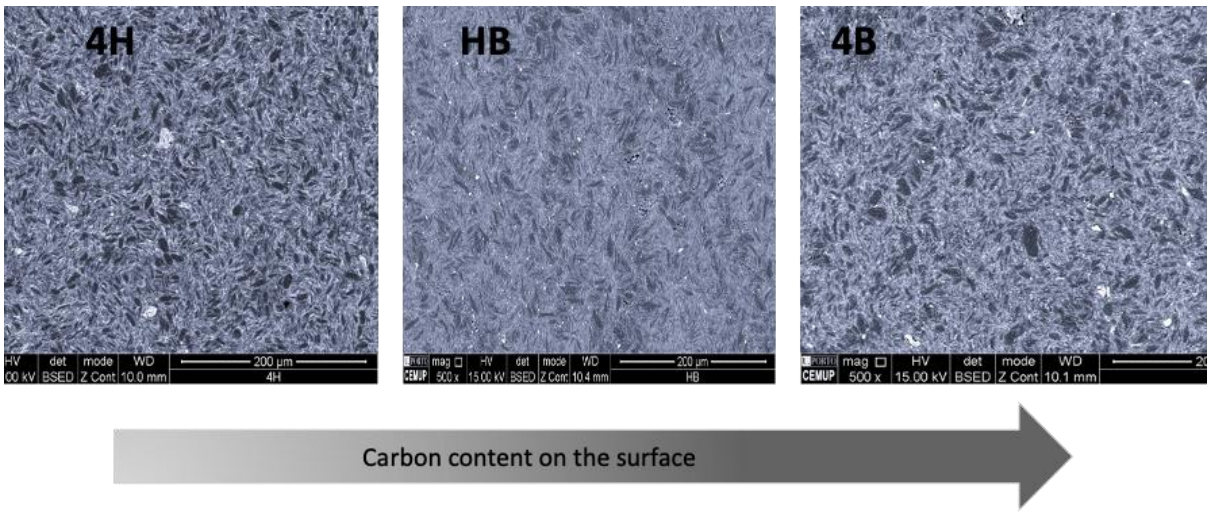

Figure 5-2; SEM morphology at 200 µm. HV 15KV in Z-CONT mode for 4H (10.0 mm); HB (10.4 mm) and 4B (10.1 mm) pencil

The scattered silicate dots are visible and defined in Figure 5.2 for the 4H pencil graphite. as for 4B there surface more blackness with regard to HB. the SEM image rather showed a mutual distribution between blackness and slight silicate dots. The

image confirmed the expected results. this was explained by the pencil graphite ranges.

5.1.3.1 Length of pencil graphite used for PGE construction

Figure 5.3 (a) shows the CV relationship between the length of the pencil graphite inserted inside the electrode and the current signal. The increase in the length of the graphite affected the resistance as well. Figure 5.3 (b) shows an increase in resistance since the current had to travel a longer path hence facing a higher number of obstacles. When the cross-sectional area increases the space electron to travel increases. and this means a smaller number of obstacles for the current. This can be defined. there is a direct relationship between the area and the resistance.

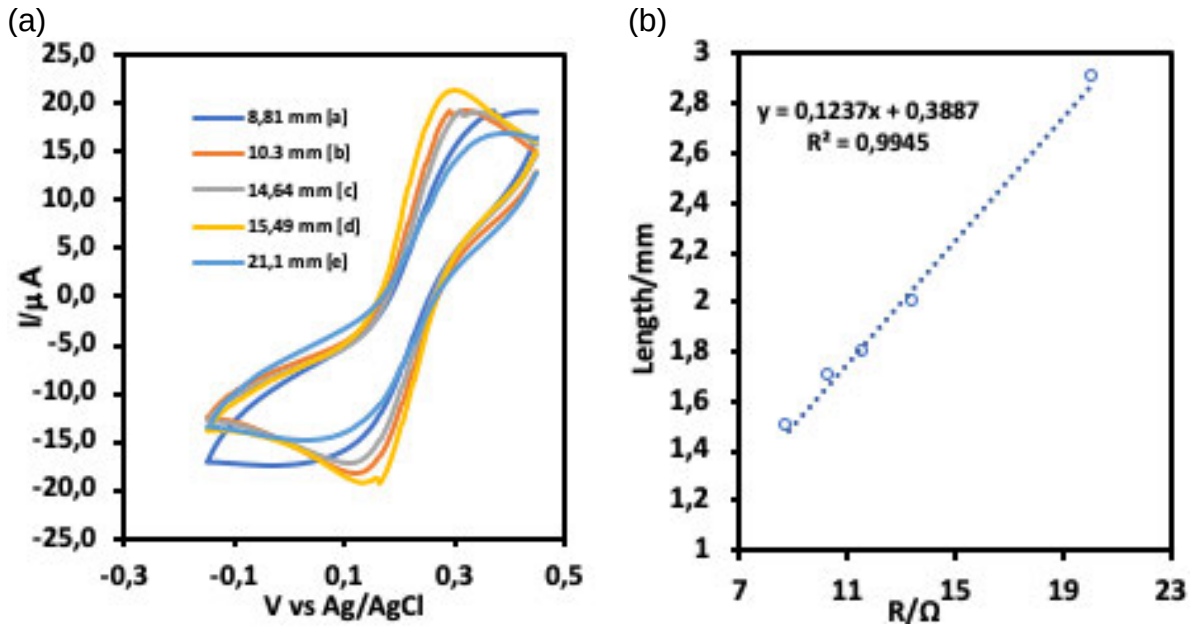

Figure 5-3; (a) Different pencil graphite length studied with Fe $^{4-/3-}$ to observe the length affect versus the current signal. (b) Linear reprentation of current response versus length of pencil graphite.

5.1.3.2 PGE comparison with other electrodes

The comparison of PGE to other electrodes that are commonly used for electrochemical analysis is vital. In this study. we report the comparison of PGE with GCE. Au electrode and SPEs. The importance of this comparison was to validate the pencil effectiveness' of the graphite electrodes. This is a new member of the carbon

electrode big family. and this electrode had to meet the standard and the range that is already set by the commercial electrodes. The development of the pencil graphite electrode was an ideal electrode. which is cost effective while offering good stability. reproducibility as well as ease of use. The electrode was constructed from readily available and cheap material. The PGE electrodes can be re-used and easily disposed of. They don't pose any harm to an environment even after use. This electrode is comparable to a commercially available electrode. and this may be due to the lower resistance values they possess. Their usual reading from a multi-meter ranged from 2-6 ohms. resulting in higher peak current. as shown by cyclic voltammogram Figure 5.4 (c) below.

The analysis was performed under similar conditions to support a higher degree of controlled variables. This study is set to determine the effect of the signal strength on changing the electrodes. The qualitative measure is useful for this element. Figure 5.4 (a) illustrates the CV for the SPE. with a very high signal response of 26.16 μA. These electrodes are single-use and have a great sensitivity for both organic and inorganic compounds. On the other hand. the gold electrode gave a signal of 8.20 μA. being the second rank. as shown in Figure 5.4 (b). The Au electrode has an inert surface and its followed by the CV scan for the glassy carbon electrode. shown in Figure 5.4 (c).

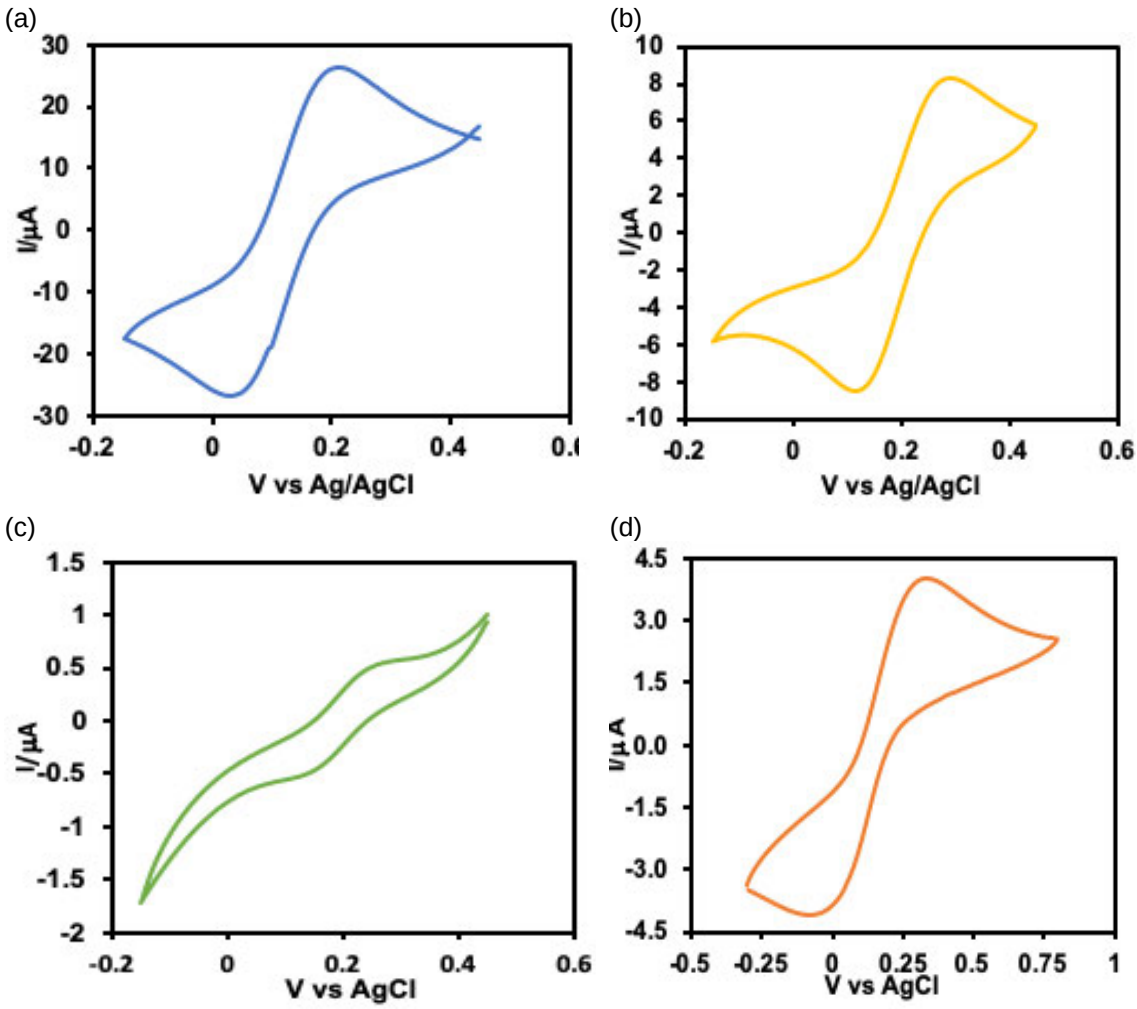

Figure 5-4;Comparison of PGE with another commercial electrode using $Fe^{4-/3-}$ 0.5 mM as an electrolyte at 50 mV/s. (a) SPE. (b) Au electrode. (c) GCE. (d) PGE.

The response and sensitivity of the $Fe^{4-/3-}$ redox probe peak is not well defined also the (0.5 μA) current signal is low. This may be due to numerous effects including the lifespan as well as cleaning the surface. GCE is mostly used in the laboratory for different analyses hence affecting the carbon surface by absorption of the analyte. This can be explained since carbon is known for its absorption abilities. Figure 5.4 (d) shows the CV signal for PGE with a maximum of 4 μA signal response. These four electrodes may have shown some distinct similarities. such as the shape of the CV. the potential values for both the anodic and cathodic peak currents. However. the GCE has different peak potentials with the shapes not consistent with the other 3 electrodes. All the electrodes were analyzed using a 0.5 mM Fe redox probe. This shows that the PGE can be used as the metal electrodes.

5.1.4 Electrochemical Optimization of PGE/GO

For the potential application of a certain kind of carbon material in electrochemistry. the basic electrochemical behaviors should be first studied to determine several important parameters of carbon electrodes: electrochemical potential window. electron transfer rate. redox potentials. etc. Based on literature reports graphene exhibits a wide electrochemical potential window of 2.5 V in 0.1 M PBS (pH 7.0). which is comparable to that of graphite. glassy carbon electrode (GCE) (Zhou et al.. 2009).

The application of carbon nanomaterial was essential for enhancing the surface area of the PGE and also enable easier electron transfer. Graphene oxide immersed in an aqueous solution is covalently bonded with the electrode surface and allowed to dry. Figure 5.5 shows the resultant effect on each graphite (H. HB. B) observed by showing a higher peak current in the 0.5 mg/mL Fe (II) and Fe (III) redox solution for the electrode with graphene. This allowed for a wider surface area. which then improved the sensitivity of the electrode.

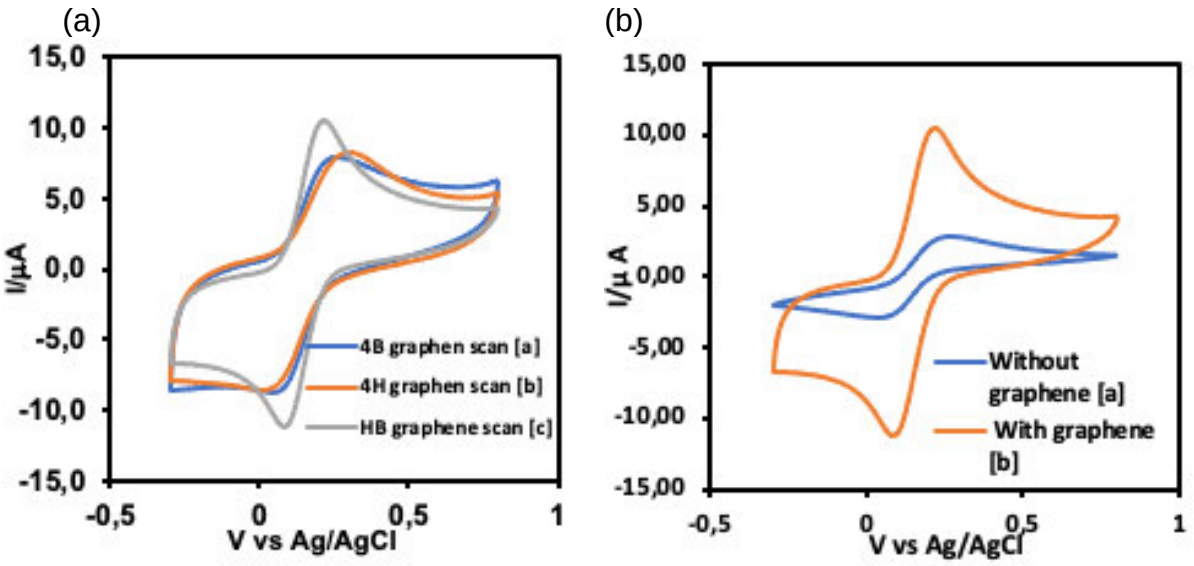

Figure 5-5; (a) $Fe(CN)_6]^{4-/3-}$ CVs of 5 mM in 0.1 M KCl with 0.1 mg/mL electrochemically reduced graphene on bare PGE (4H. HB. and B) and (b) rGO effect on the PGE electrode surface.

In Figure 5.5 (a). the variation in the peak currents was based on the different PGE used. the observed peak shift is resultant to the carbon content in each pencil graphene. However the cathodic peak has the same voltage for all the pencil

graphene's. The 4H graphene scan(b) electrode gave the smallest signal. due to the lowest clay content. Upon the addition application of graphene oxide unto the PGE surface. the signal decrease for the 4B graphene scan(a) PG electrode is observed and displayed a higher background current. the electrode was also not stable for analysis. due to a high carbon content on the electrode surface. On the other hand. a higher peak current was observed for the HB graphene scan(c) the electrode (PGE/GO). This pencil graphite has an equal amount of clay and blackness; hence the additional application of graphite gave a stable PGE/GO electrode. However. all the pencil graphite electrode examined (4H. HB and 4B) showed very distinct cathodic and anodic peak currents. Figure 5.5 (b) shows a 1 mg/mL graphene oxide entirely dissolve in water and applied to the selected pencil graphite HB. The CVs illustrates how graphene interacts with the different pencil mines' surface. PGE/rGO shows the response with two times higher current response than a bare cyclic voltammogram PGE.

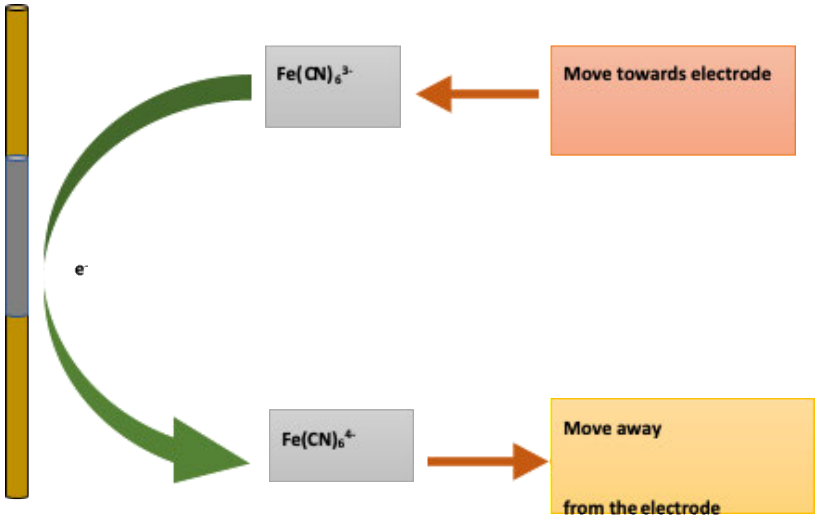

Figure 5-6 illustrations of the redox probe on the electrode surface for Fe $^{3-/4-}$. electron migration

This diagram illustrates the direction of the electron using the $Fe(CN)_6^{3-/4-}$ redox probe. Figure 5.6 shows the transportation of electron between the electrode and the redox probe. The narrowed ΔE_p of $Fe(CN)_6^{3-/4-}$ suggests the improved electron transfer kinetics by GO. which is ascribed to the reactive edge defects on graphene (Devasenathipathy et al.. 2015).

The electron transfer behavior studies of graphene using CV of redox couples. such as [Fe $(CN)_6]^{3-/4-}$ and $[Ru(NH_3)_6]^{3+/2+}$. are reported. which exhibit well-defined redox peak. Both anodic and cathodic peak currents in the CVs are linear with the square root of the scan rate. which suggests that the redox processes on graphene-based electrodes are predominantly diffusion-controlled. The observed peak-to-peak potential separations (DEp) in CVs for most one-electron-transfer redox couples were quite low. very close to the ideal value of 59 mV. for example. 61.5 – 73 mV (10 mV/s) for $[Fe(CN)_6]^{3-/4-}$ and 60 – 65 mV (100 mV/s) for $[Ru(NH_3)_6]^{3+/2+}$ (Tang et al.. 2009. Yang et al.. 2009).

In order to study the electrochemical response/activity of graphene toward different kinds of redox systems. systematically studied three representative redox couples: $[Ru(NH_3)_6]^{3+/2+}$. $[Fe(CN)_6]^{3-/4-}$. and $Fe^{3-/2-}$ (Tang et al.. 2009). The $[Ru(NH_3)_6]^{3-/2-}$ complex is a nearly ideal outer-sphere redox system that is insensitive to most surface defects or impurities on electrodes and can serve as a useful benchmark in comparing electron transfer of various carbon electrodes. The peak-to-peak potential separation is related to the electron transfer (ET) co-efficient. and a low peak potential indicates a fast electron transfer (ET) for a single-electron electrochemical reaction on graphene. This indicates that the unique electronic structure of graphene. especially the high density of the electronic states over a wide energy range. supply graphene with fast electron transfer. This indicates that the electronic structure and the surface physiochemistry of graphene are beneficial for electron transfer (Gómez-Navarro et al.. 2007).

5.1.4.1 Effect of graphene oxide concentration

Here we show that the electron transfer kinetics also correlates with the thickness of graphene film that can be easily controlled by using the electrodeposition technique. a distinct advantage over previously developed methods. The thickness of the graphene film was evaluated by the application of a higher concentration. Ideally. we looked to find if there will be a visible change on the signal. Both the 1 mg/mL and 2 mg/mL electrodes shown by Figure 5.7 (a). were electrochemically reduced in a $Na_2S_2O_4$ solution using 50 and 240 reduction cycles respectively. as exemplified in Figure 5.7 (b). to monitor change brought by the thickness of GO.

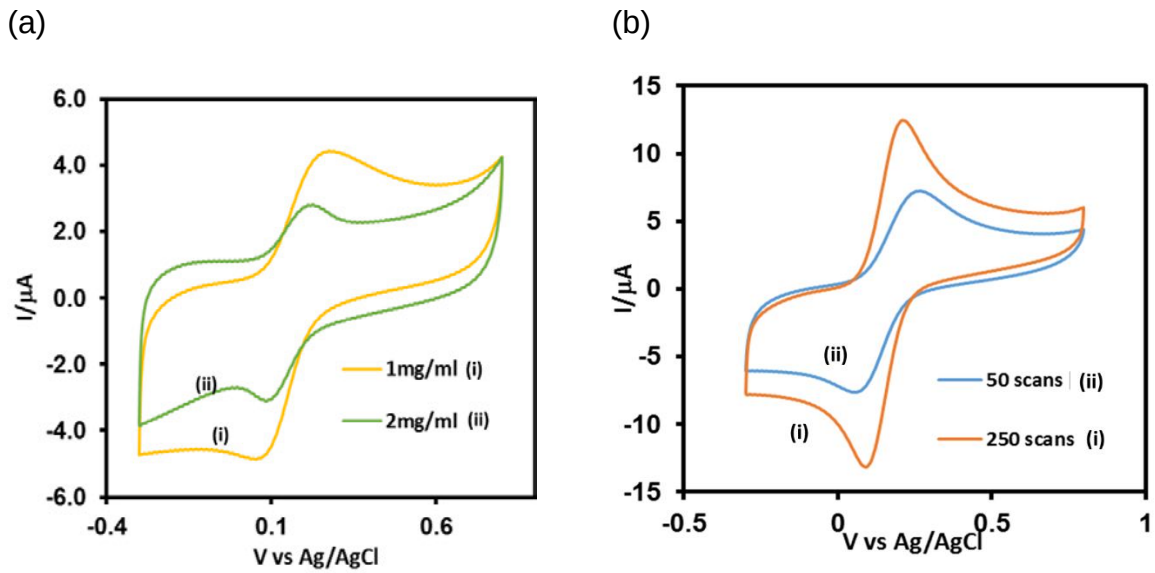

Figure 5-7: CV showing effect of (a) graphene oxide concentration to the electrode and (b) a number of reduction scans used to reduce GO to graphene. 1 mg/ml reduced with 50 CV scans and 2 mg.ml reduced with 250 CV scans using $Fe(CN)_6^{3-/4-}$.

5.1.4.2 Effect of number of reduction scans

The CV was used to determine the effect under a different number of reduction scans to electrochemically convert GO to reduced graphene (rGO) shown by Figure 5.8. Both the electrode with different concentrations were analyzed and showed similarity; the decreasing anodic peak at potential 0.15 V in a CV. However. the electrode which has a higher concentration of 2 mg/mL required an extended time. This meant that it needs more reduction in time than for 1 mg/mL. Figure 5.8 shows the CV scans of 2 mg/mL in a $Na_2S_2O_4$ (10 mM) solution with up to 240 reduction scans.

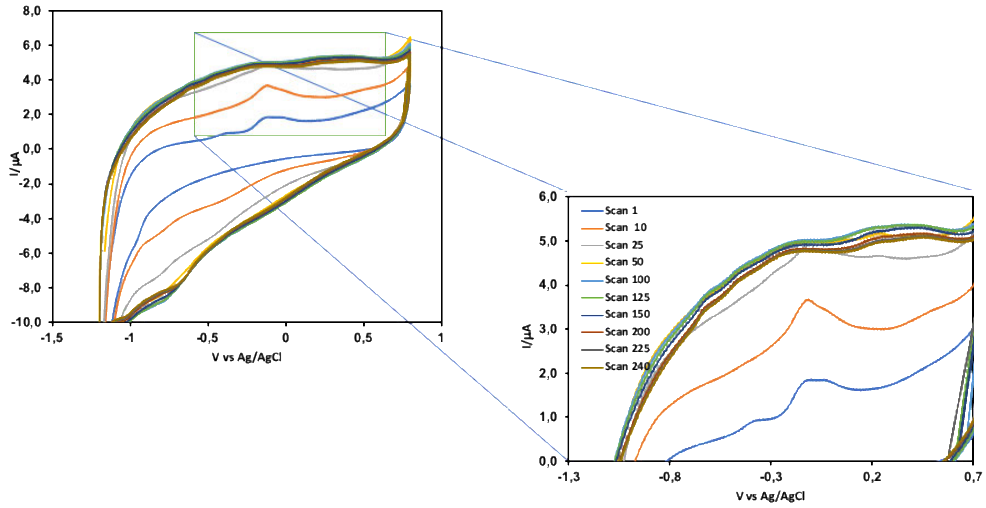

Figure 5-8; CV show. No. of graphene oxide reduction scan [2 mg/mL] to graphene. using $Na_2S_2O_4$ at a scan at 50 mV/s

Figure 5.9 shows a linear trend up to 50 scans against current response scans in Figure 5-8. The number of scans showed a direct relationship between the current signals and the increasing number of reduction linear scan. Slightly after scan 50. there is minor increase in the signal. it approaches a plateau. hence it can be concluded that the thickness of GO used does not increase the current and the surface area. hence working with lower concentration was ideal

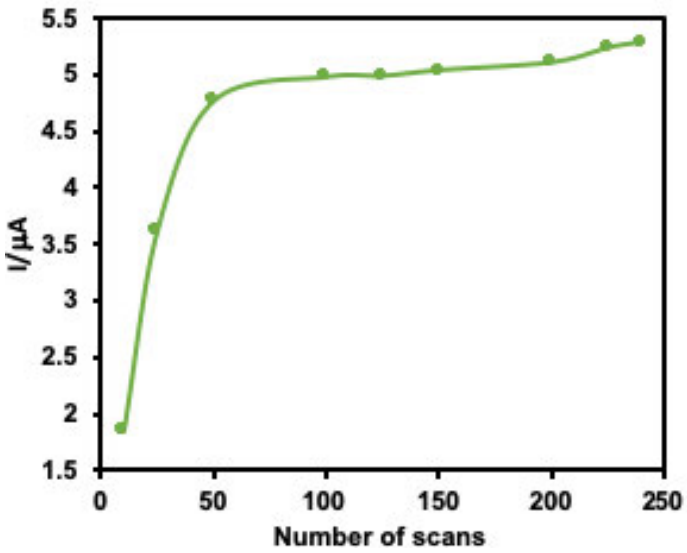

Figure 5-9; A graph showing current response and number of the scan.reach a plateau from CV reduction of graphene oxide

5.1.5 Electrochemical Optimization of PGE/CNPs/Laccase

The evaluation of the third-generation biosensor using the laccase enzyme with the PBSE as a wiring agent.

5.1.5.1 Laccase enzyme activity

The analysis was run with a spectrophotometer in absorbance mode. the color change observes from yellow to violet upon the addition of syringaldazine and the blank remains clear. This is a visual color change showing the interaction between the enzyme and the substrate. Figure 5.10 shows the laccase enzyme activity with time in the presence of syringaldazine as a substrate. A and B cells showed a trend with time. meaning the enzyme is active in the beginning and it degrades with time. for C there were no changes (color change and no enzymatic reaction) observed since the enzyme was not inside the cell.

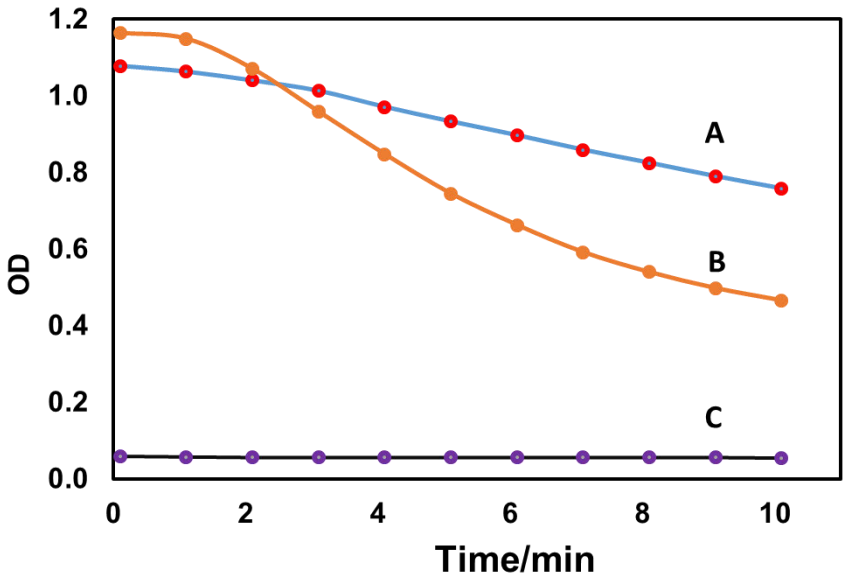

Figure 5-10: Laccase enzyme activity measured against time using a spectrophotometer. at 37 ^{o}C. pH PBS buffer. and syringaldazine. A) has the laccase enzyme, B) has Laccase and syngaldazine and C) has the blank

The incubation temperature was set at 37 ^{o}C during the kinetic measurements to mimic the biological system in the cuvette. In a 96 well plate. 1A. 2B. 3C. positions. The resultant difference in transmittance values can be correlated to the enzyme activity (Holm et al.. 1998).

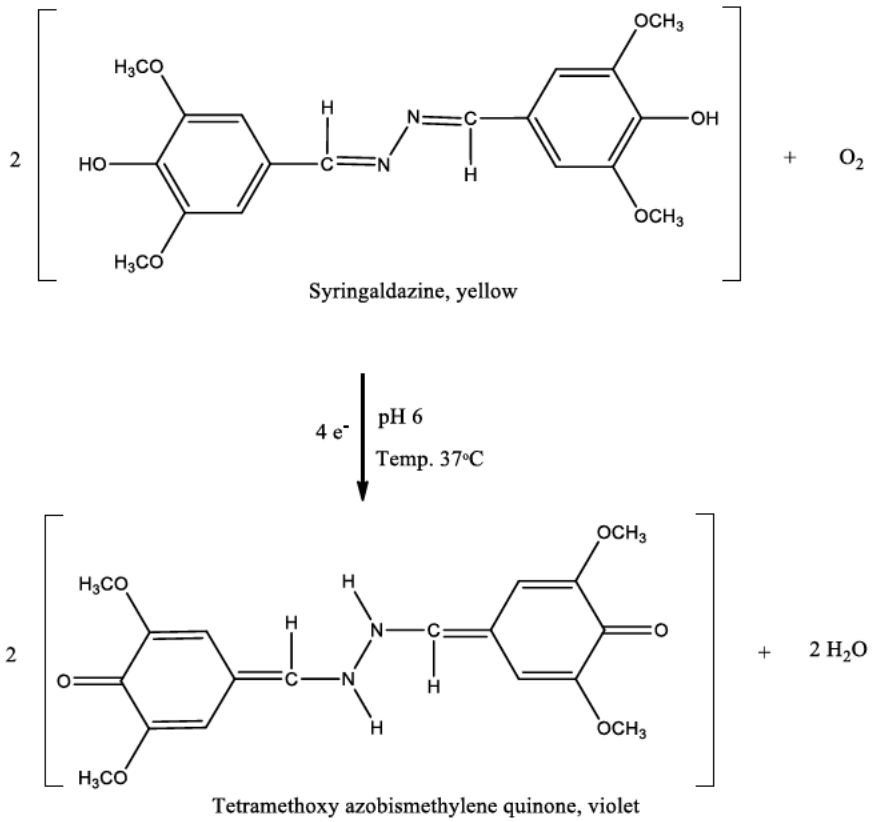

Figure 5-11; Syringaldazine reaction. confirming redox spectrophotometric behavior.

Figure 5.11 is the chemical structure of syringaldazine. showing the 4 electron exchange in the central OH of the O-methylated pyragollol ring. as a result there is a yellow to violet color change. As the oxidation takes place. OH is converted to ketone and water is produced as a byproduct.

5.6.3 Evaluation and optimization PGE/GO/MWCNTs/syringaldazine/Lac

Two electrochemical cells were used. and both contained the phosphate buffer solution. one was purged with N_2 and the other was saturated with O_2 for the period of 15 min each. Upon the addition of 1 ml syringaldazine. the N_2 purged buffer remained colourless and clear. while the O_2 saturated changed color from yellow to violet. Both solutions were electrochemically analysed at the same conditions. Figure 5.12. (a) is the cyclic voltammogram obtained? There was a cathodic peak signal at 0.25 V and a reduction peak starting at 0.30 V. which meant that the enzyme interacts with the substrate. The redox can be resultant from the formation of tetramethoxy azobismethylene quinone from syringaldazine OH- group bonding to the double-

bonded O-atoms. this experiment was run at a low scan rate of 1 mV/s. However. these two peaks had to be confirmed since the syringaldazine was dissolved in ethanol.

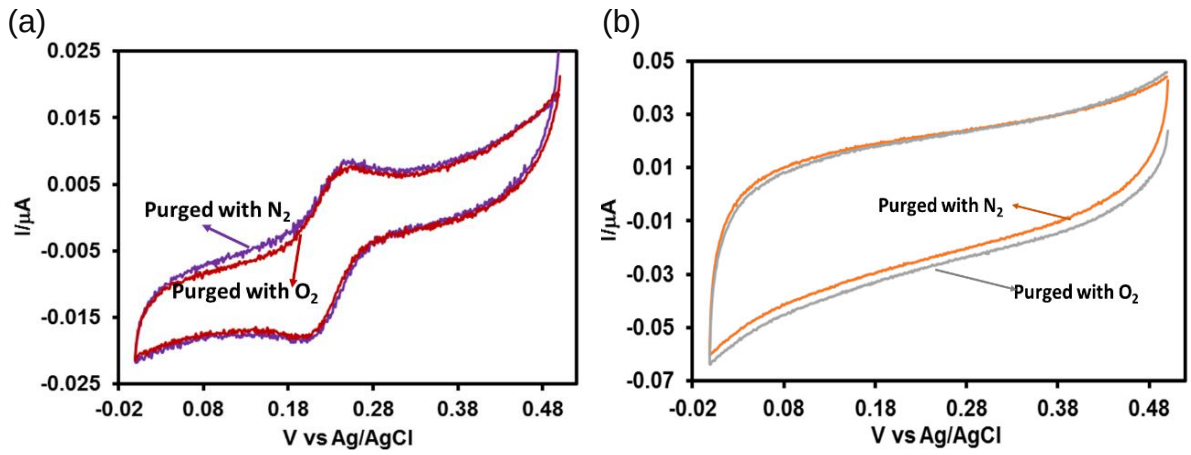

Figure 5-12; (a) cyclic voltammogram of PGE/GO/MWCNTs/syringaldazine/ Lac electrode. (b) cyclic voltammogram. the addition of methanol 30 µL. MeOH into a 10 mL Phosphate buffer pH 7.

The PGE/GO/MWCNTs/ Lac biosensor was used to evaluate the presence of the OH-group. Figure 5.12 (b) shows the cyclic voltammogram where 30 µL of the MeOH solution was injected into the cell. This was to evaluate whether the peak current observed in Figure 5.12 (a) was resultant from the OH group since the syringaldazine was dissolved into methanol. An overlay showing a distinct difference in the voltammogram for MeOH and therefore it was confirmed that the peak from Figure.5.12 is due to syringaldazine. However. the presence of O_2 only affected the spectrophotometric behaviour of the compound other than the electrochemical behaviour. The reduction peak was not resulting from oxygen reduced. looking at the reduction potential. It is lower compared to the one where oxygen will reduce around.

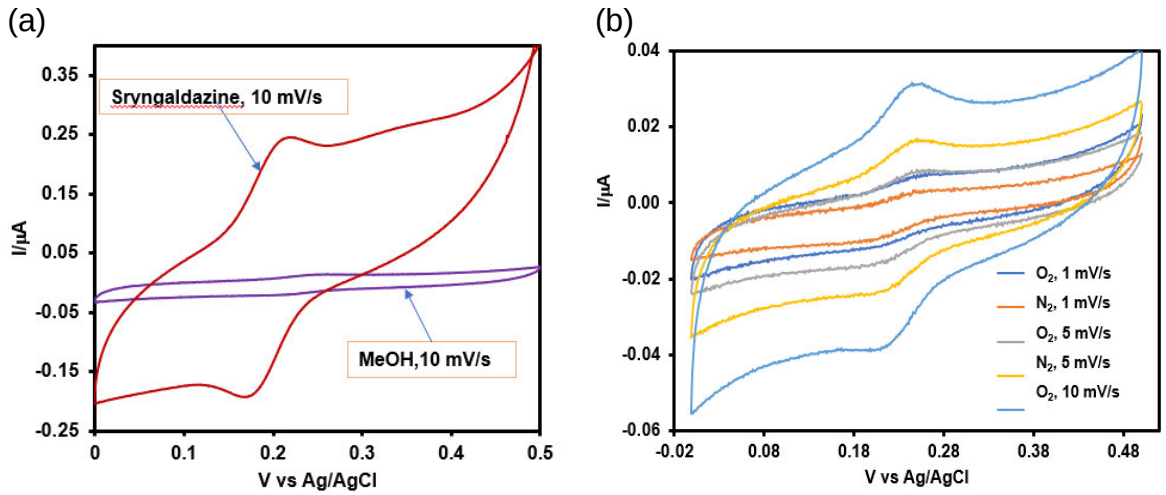

Figure 5-13; (a) The syringaldazine impact on the PGE/rGO/CNTs/Lac biosensor (b) PGE/rGO/CNTs/Lac. 4 mg of Syringaldazine dissolved in MeOH. studying the scan rates for both N_2 and O_2

Figure 5.13 (a) a cyclic voltammogram shows an enhanced surface area and redox peak which were confirmed to be syringaldazine. The scan rate for both scans was analyzed in both the oxygenated solution and nitrogen purged cell. The CV observed at 10 mV/s and 1 mV/s scan rates differed markedly. as shown in Figure 5.13(a). Thus. the lower scan rate. no cathodic signal corresponding to the reduction of syringaldazine was detected. Instead. the intensity of the peak was much greater with the increase of the scan rate. This can be observed in Figure 5.13(b) but at a lower concentration and a single addition. The reaction depended on the concentration of an electroactive species close to the surface of the electrode. in this case when the concentration of syringaldazine is higher. the reaction the reaction takes place at the electrode surface (Farneth et al.. 2005).

5.1.5.2 Evaluation of composite

The concept of adding laccase onto the PGE electrode was to create an amperometric biosensor. This makes it possible to work at very low potentials. avoiding O_2 dependence and the impact of the interfering molecules. This is further improved by substituting with electron receptors capable of carrying electrons from the redox centre of the enzyme into the electrode (Mousty et al.. 2007). The use of carbon nanomaterial is applied to improve the electron active sites. The interaction with the electrode is achieved by a covalent linkage. using carbon nanotubes (CNTs) immersed in an aqueous solution. The composite electrode PGE/GO was prepared drop-casted as

explained in section 4.5.3. The application of the GO and MWCNTS composite has enhanced the stability of interactions between nanomaterials and the enzyme. the biocatalytic lifespan of the enzyme for the immobilization is mostly limited. The analysis as can be seen in Figure 5.14 did not show any positive response signals. The initial step in the immobilization procedure was to run each component into the PGE/GO surface. There was a difference in the size of the CV but still. no visible peak changes and potential range remained the same for all composites.

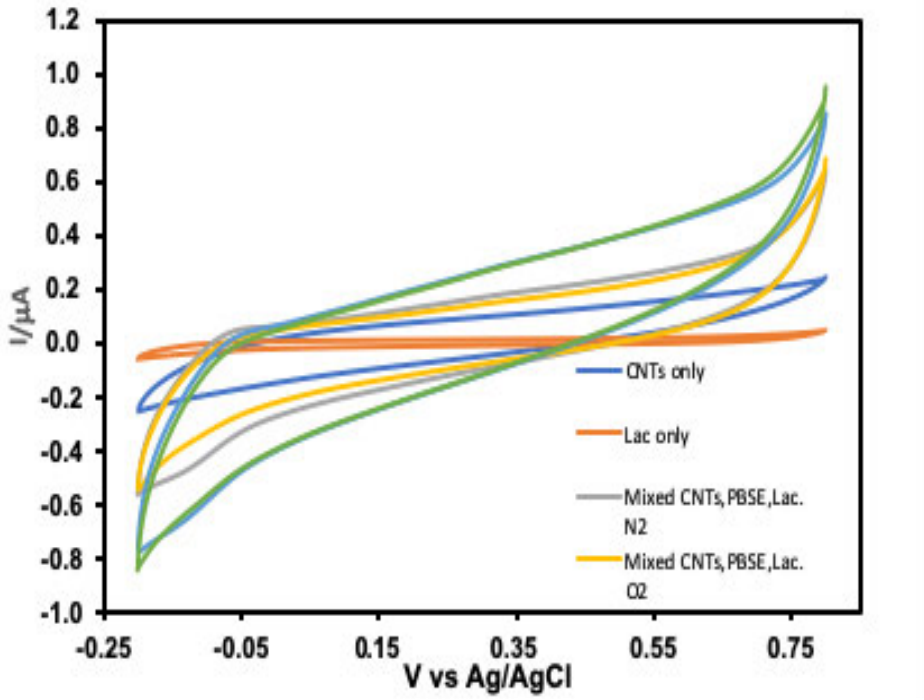

Figure 5-14: Different electrode composite. CNTs/PBSE/Laccase. evaluating each component used to fabricate a biosensor into a PGE electrode. 10 mM PBS. 10 mV/s

5.1.5.3 Evaluation of the scan rate

The impact of the scan rate with PGE/GO/CNTs/ PBSE/Lac. using a drop-cast technique as it showed greater surface area Figure 5.15 (a). There was an increase in the oxidative current signal. with an increased scan rate at around -0.02 V. The relationship can be explained if the current peak is proportional to the root square of the scan rate (linear relation) for the diffusion regime. but if the current is linear with the scan rate. then the electroactive species is confined to the electrode surface (no

diffusion mode) (Riva. 2006). Figure 5.15 (a) shows a cyclic voltammetry study conducted over the potential range of -0.3 V to 0.8 V giving an effective potential window of 0.6 V. as the scan rate was increased by increments of 10 mV/s. the curves shift towards a more oxidative potential. By analyzing the variation of the peak positions as a function of the scan rate. it is possible to gain an estimate for the electron transfer rate constants. Figure 5.15 (b). there is a proportional relation between the current signal and scan rate at 40 to 70 mV/s. This anodic peak is at -0.05 ± 0.02 V. hence it cannot be associated with the reduction of oxygen as the enzymatic reactions were slow. meaning there should be enough time for the reaction to occur in the electrode surface.

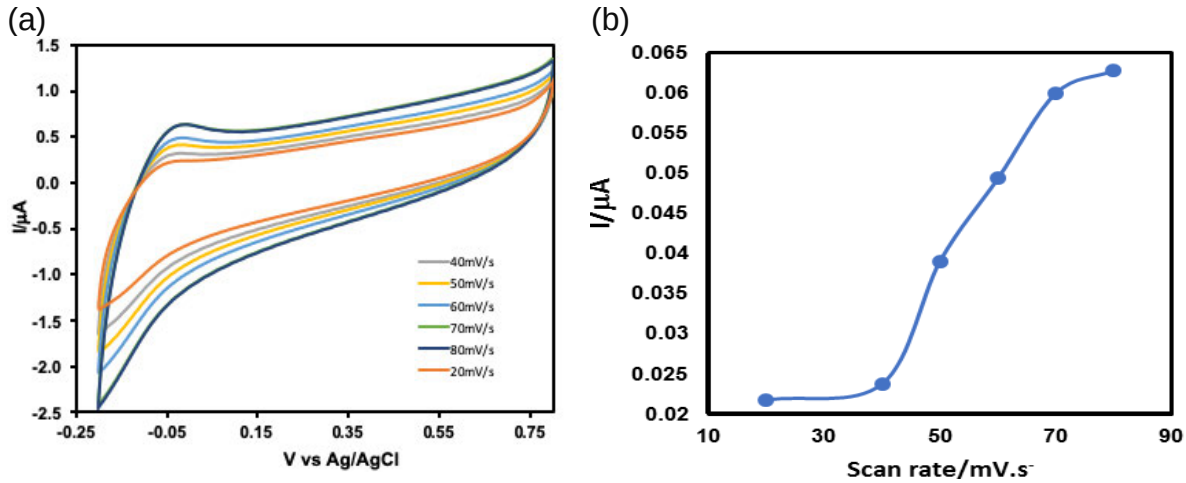

Figure 5-15; (a) PGE coated with CNTs.PBSE(1:1) + Laccase. all applied dropwise. 5 µL was drop-casted on the electrode surface. Measurements done in a Oxygenated solution of 0.01 M pH 6 phosphate buffer..(b) Linear evaluation of the cathodic peak response.

5.1.5.4 Development and optimization of oxygen alternative

The use of decomposed H_2O_2 was to find a new source of O_2. other than the O_2 cylinder. This was done by decomposition of H_2O_2 in the presence of a manganese (IV) oxide metal catalyst. This reaction in Equation 5.1 was monitored under safe precautions of H_2O_2 as a strong oxidizing agent. The use of an inorganic catalyst such as manganese (IV) oxide under monitored lighting. amount of the catalyst as well as the temperature were factors that affected the rate of decomposition.

$$2H_2O_2 \rightarrow 2H_2O + O_2 \qquad \text{(eq 5.1)}$$

The reaction was allowed to take place under the closed system. to prevent O_2 gas from escaping from the system. Using 30% H_2O_2 diluted to 1% working solution in a 10 mL beaker and addition of 0.16 MnO_2 salt. To make dilution a density of hydrogen peroxide was considered to get a correct concentration. There were small bubbles forming from the bottom of the beaker. Figure 5.16(a) shows a CV scan ran with PBS buffer purged with N_2 gas and the other one of H_2O_2 as a new source of oxygen.

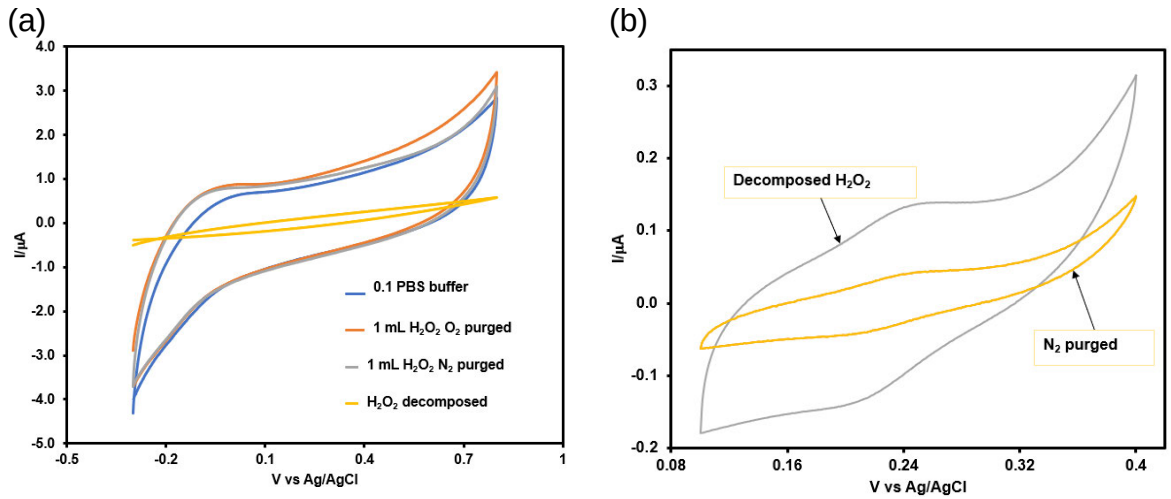

Figure 5-16; (a) CV analysis using H_2O_2 after 16 hours decomposition. analyzed 0.1 M PBS buffer pH 7 and 1 mL additions of H_2O_2 (b) Comparing CV of the analysis performed on decomposed H_2O_2 solution. N_2 purged solution in PBS pH 7.

A number of 1.0 mL additions were made to evaluate any visible change on the CV scan. There were no significant changes observed. only the buffer gave a response. H_2O_2 was then used as an electrolyte. observe any change in signal response. The overlay between PBS buffer and H_2O_2 shows a very small current was produced by hydrogen peroxide. Figure 5.16(b) shows the CV overlay between N_2 purged PBS buffer and H_2O_2. the analysis showed the Figure 5.18b a higher current response and redox peak at a potential 0.23 and 0.20 V for both cathodic and anodic peaks respectively and this can be correlated to oxygen reduction even though is very small. The nitrogen scan had a half current signal as of H_2O_2 based current response.

5.2 Development and optimization SPE/ABTS/CNPs/LAcc-T

The simple alternative electrode was used. these small and inexpensive sensors allow us to perform decentralized experiments. with small amounts of sample. These electrodes are designed for a single-use and eliminate a pre-treatment procedure. Screen printed sensors have a higher reproducibility between electrodes. A screen-printed electrode was used to substitute PGE and a 2.2′-Azino-bis (3-ethylbenzothiazoline-6-sulfonic acid) diammonium salt. used to observe the reaction kinetics of a laccase enzyme. This detects molecular affinity to each other; and is used as a substrate for a blue copper oxidase. allowing for the reaction kinetics of peroxidase to be followed. In this way. it also can be used to indirectly follow the reaction kinetics of any hydrogen peroxide-producing enzyme or to simply quantify the amount of hydrogen peroxide in a sample as shown in Figure 5-17(a). The formal reduction potential for ABTS is high enough for it to act as an electron donor for the reduction of oxo-species such as oxygen and hydrogen peroxide. At lower pH values. the sulfonate group is deprotonated fully. and the mediator exists as the dianion. This compound was chosen because the enzyme facilitates the reaction with hydrogen peroxide turning it into a soluble green end-product.

The cyclic voltammogram of 0.5 mM ABTS in 10 mM phosphate buffer with a scan rate of 10 mV/s is shown in Figure 5.17(b). The two oxidation peaks (E_{pa}) observed at a potential of 0.25 V and 0.62 V. corresponds to the oxidation of ABTS to cation radical $ABTS^{+}$ and subsequently to its dicat-ion $ABTS^{2+}$ refer to equation 2.16 and 2.17. The reverse scan showed two redox peaks (E_{pc}) at 0.52 V and 0.15 V for the reduction of the two cation radicals respectively.

(a) (b)

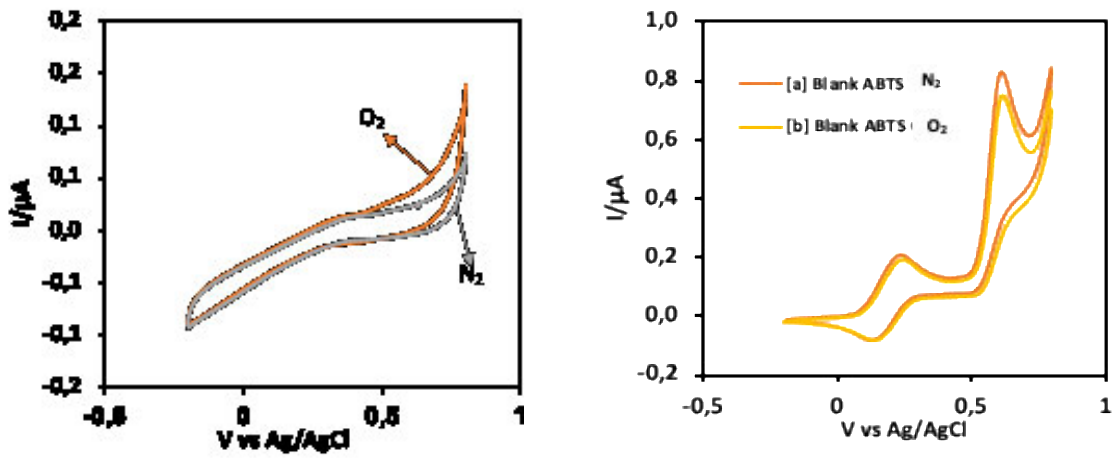

Figure 5-17;(a) SPE/Laccase analysis of O_2 and N_2. (b) using SPE/ABTS only in N_2 and O_2 PBS pH7 buffer solution

For an electrochemically-reversible reaction with a one-electron transfer process. the peak-peak potential separation ($\Delta Ep = Ep_a - Ep_c$) for each redox couple at each scan rate should be approximately 10 mV at room temperature and independent of the scan rate. However. the ΔEp for the ABTS cation radicals were significantly greater than 59 mV and increased as the scan rate increased. indicating a quasi-reversible redox process. These results might indicate slow electron transfer kinetics and may also be partly attributed to the effect of uncompensated Ohmic resistance of the electrolyte and the measuring circuit. Figure 5.17(b) is the evaluation of ABTS as a mediator for laccase biosensor detection of oxygen.

In the study reported Eshtaya and co-workers. ABTS is used to enhance the oxidation of the non-phenolic lignin model compound. vetatryl alcohol and three other types of lignin. CV was applied as a quick and efficient way to explore the impact of water in the ABTS-mediated oxidation of both organic solvent and lignosulfonate lignin. Higher catalytic efficiencies of ABTS were observed for lignosulfonate solutions either in sodium acetate buffer (Eshtaya et al.. 2016).

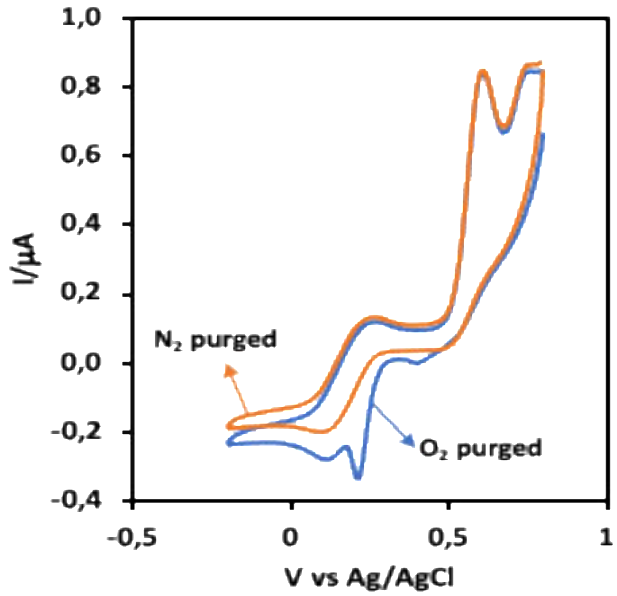

Figure 5-18;SPE analysis of N_2 and O_2 using SPE/CNTs/ABTS/Laccase

Our analysis using SPE modified on a previous day with 10 µL laccase (10 mg/ml) and 0.1 M KP pH5.8 + 0.5 mM ABTS purged with O_2 from 15 min. Figure 5. 18 shows the SPE/CNTs/ABTS/Lac biosensor behavior under each gas. Oxygen and Nitrogen purged PBS solution for 15 min. The electrode showed a visible oxygen reduction peak at 0.34 V in the anticipated potential range -0.3 to 0.9 V. The SPE/CNTs/ABTS/Lac composite was able to show variety in its CV at 0.38 V to the response of oxygenated PBS buffer solution. The electrodes were stored in -4 ^{o}C freezer for a maximum of 16 hours to elongate the interaction between enzyme and electrode components. After 16 hours the electrode was removed and left to cool at room temperature before analysis. It was kept at -4 ^{o}C. to maintain the Laccase enzyme active and eliminate any deformation to its structure. The electrode was able to show an oxidation peak at 0.28 V. this peak was available for both N_2 and O_2 electrodes in Figure 5.18.

5.3 Development and optimization of PGE/TMOS/CNPs/ABTS/Lac

In this section. the film is composed of carbon Nano-material (CNP). to offer an advantage of conductivity. adsorption site together with charged functional groups. This is a layer-by-layer electrostatic immobilization. The presence of sulfonate group increases the solubility and easy electrode preparation. For electrode preparation. CNPs have been simply attached as sol-gel processed silicate film. This allows the

electrode a higher surface area and the ability to be used for the accumulation of different redox probes. The laccase oxidase enzyme and CNPs are applied as one step sol-drop deposition (Szot et al.. 2009a).

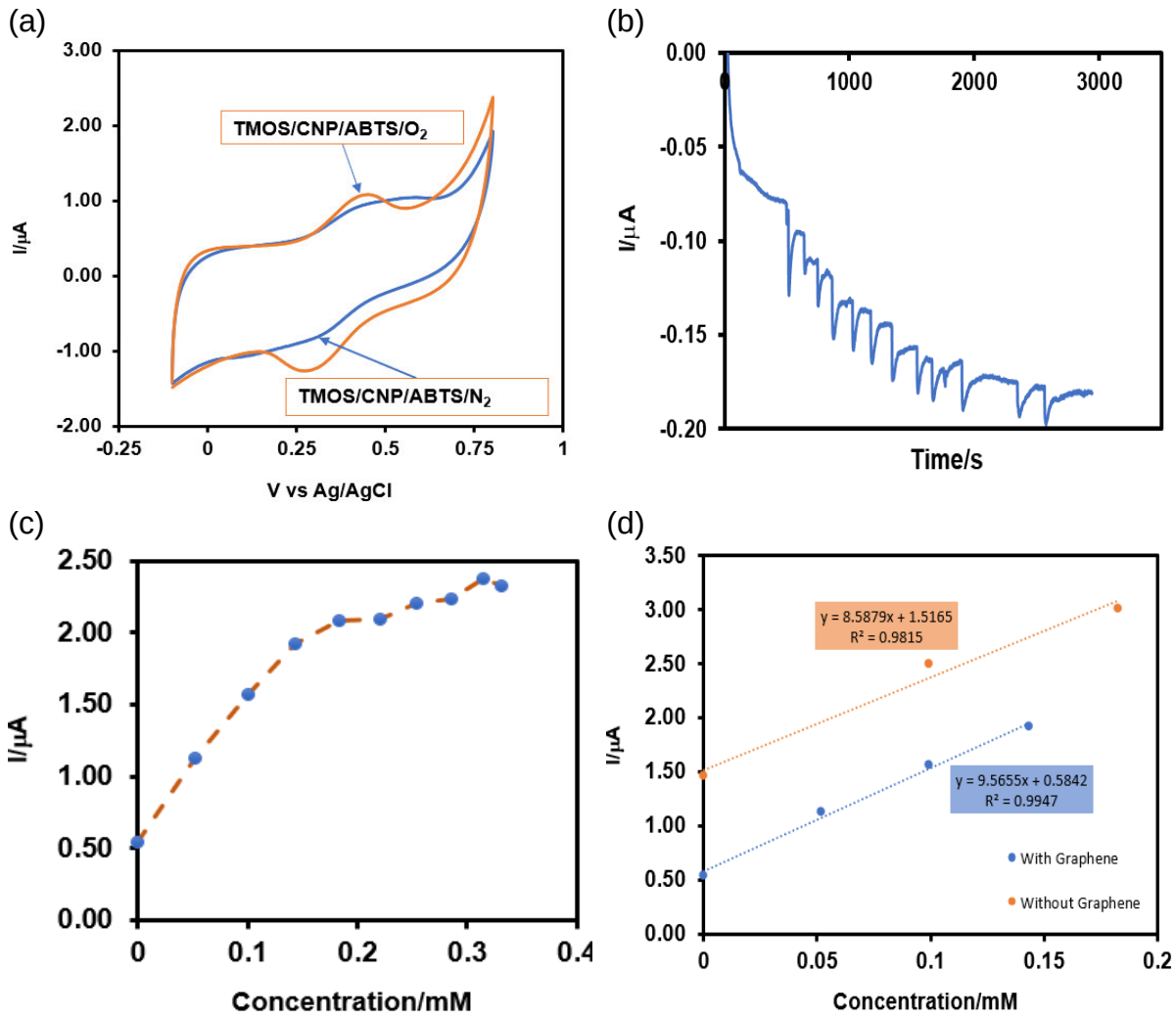

Figure 5-19;PGE/CNPs/TMOS/lac both on N_2 and O_2. (a) CV analysis in PBS at pH 7 at 50 mV/s. (b) chronoamperometric of PGE/CNPs/TMOS/lac. (c) Plot of current response and O_2 concentration (d) curve comparing a linear response of electrode coated with rGO and with no GO.

A defined difference in signal a current Figure 5.19(a) the CV shows O_2 reduction peak at 0.35 V and an increase in anodic and cathodic peak potentials. This is a result of sol-gel enzyme immobilization and adsorption of CNPs. A quantitative analysis of the sensitivity by chronoamperometric analysis. at a constant. applied reduction voltage 0.35 V. Figure 5.19 (b) the shoulders show the O_2 sensitivity with time and also the life span of the biosensor; if it gets saturated early. it is the end of the biosensor as it cannot detect O_2 further. Figure 5.19 (c) Shows the O_2 concentration using a direct relationship with the current response from chronoamperometric. Figure 5.19 (d) is the comparison between the linear function of the biosensor. The use of graphene as part of the biosensor increases the correlation coefficient and the working area.

Table 7; shows different composition layer-by-layer. and also studies the effect caused by each element of the electrode system. The sensitivity obtained for each composite can be used to determine the detection limit of that particular electrode. The linear working range was limited by the biosensor for greater sensitivity. LOD and sensitivity have a direct relationship. allowing lower concentration to be detected

Table 7;Analytical performance of PGE biosensor for O_2 detection

Type of electrode	Sensitivity ($\mu A/mM.cm^2$)	LOD (µM)	Linear range (mM)
PGE/GO/CB/TMOS	No signal	---	---
PGE/CB/TMOS/Laccase	252.7	1.26	0-0.18
PGE/GO/CB/TMOS/Laccase	281.5	1.18	0-0.14

The impact of solvent viscosity on the oxidation reaction can be related to the diffusion of the substrate. Therefore. single chronoamperometry potential step was employed in order to determine the diffusion coefficient of ABTS. Figure 5.19 (b) shows a typical chronoamperogram obtained using 10.0 mM $ABTS^{1+}$ after a potential step from a potential where no faradaic reaction occurred to a potential at which the oxidation of $ABTS^{1+}$ was diffusion controlled. The current. I. is proportional to $t^{-0.5}$ as shown by the Cottrell equation. equation (5.2).

$$\boldsymbol{i\ t = nFACD^{0.5}/\pi^{0.5}\ t^{0.5}} \qquad \text{(eq 5.2)}$$

Where *i* is the peak current. *n* is the number of electrons transferred/molecule. *A* is the electrode surface area. *C* the bulk concentration of the redox species. *D* the diffusion coefficient of the redox species and *F* the Faraday constant. Equation 5.2 shows the corresponding Cottrell profile of I (t) vs $t^{-0.5}$ and. from the gradient of the straight line best-fit to the plot. the diffusion coefficient of $ABTS^{1}/ABTS^{+2}$ [KPS] was calculated (Schröder et al.. 2003).

5.4 Development and optimization of PGE/GO/MWCNTs/PBSE/BOx (0.5M)

5.4.1 Enzyme activity of Tris HCl buffer

The buffers are needed to keep the enzymes stable at any medium acidic. basic as well as neutral. It can be in any pH value. When using tris HCl electrolyte. the Vmax and Km values were obtained from the calculated and plot diagrams. The diagram is shown below in Figure. 5.23 shows a PGE/GO/MWCNTs/PBSE/BOx sensor analysed in a tris HCl electrolyte. The observed oxygen activity corresponded to the lower sensitivity obtained. This can be related to an early saturation of the biosensor. The current increased very low. leading to a small slope. The slope is then used to calculate the sensitivity. However. the correlation coefficient was very close to the accepted value implying the direction and strength of the linear relationship between the two variables on the scatterplot. The Km value is bigger which means that the enzymes and substrate are breaking apart more than staying together. There is a low enzyme affinity for the substrate. The analysis performed in tris(hydroxymethyl) aminomethane had different responses at various pH ranges. The fitted curve plot showed adjusted R^2 of 0.99602. sum of squares of 0.0734 and Mean square of 0.0367 for 4 degrees of Freedom.

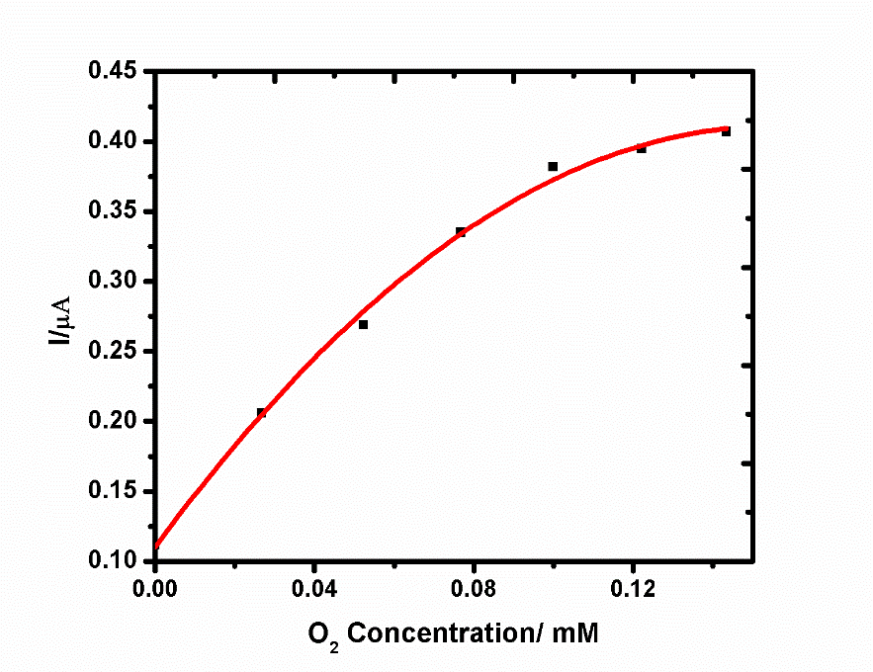

Figure 5-20;Enzyme activity examined in Tris HCl buffer at pH 7

Figure 5.20 can be explained using a hyperbolic equation. which is useful if we know Vmax and Km. we can calculate the speed at any given [S] and found to be 60.475 μmol/min and 3.447 respectively.

$$V=\frac{Vmax\ [S]}{Km+[s]} \qquad \text{eq (5.3)}$$

5.4.2 BOx performance on PBS and Tris HCl buffer solutions

Phosphate buffer is highly water-soluble and has a high buffering capacity. it dissolved in water. If dissolved in ethanol it will inhibit enzymatic activity and precipitates. The buffer is one of the most popular currently used biological. material science and cell molecular biology. A range of pH was analyzed. and the relationship is shown in Figure 5.21 (a) observing the linear response.

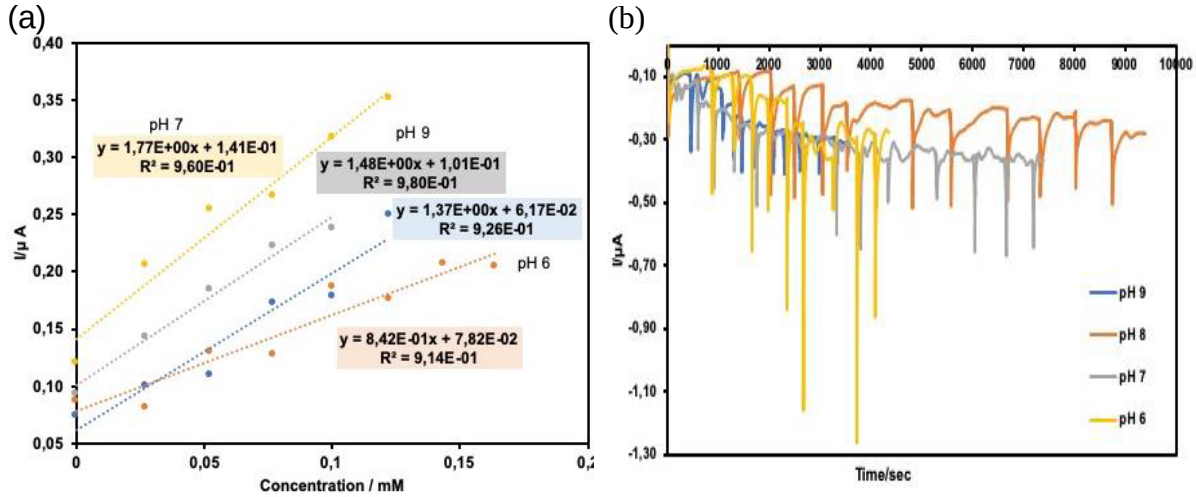

Figure 5-21: (a) PBS linear relationship for different pH range for detection of oxygen gas with PGE/rGO/MWCNTs/PBSE/BOx biosensor. (b) Chrono analysis comparing the pH of phosphate buffer pH

The linear response varies. and the correlation of the plot are different also. Figure 5.21(b) is a visual amperometric. the pH 6. 7 and 8 current signals due to oxygen and how long the life span of the electrode is. The amperometric is time-based. determining the rate of saturation. There was no particular pattern to the sensitivity of the electrode. The pH 6 to 8. pH 7. had a higher sensitivity. and working in gentle condition was ideal for the enzyme biosensor.

Table 8; O_2 sensitivity of different pH using PBS buffer

	pH	Vmax µmol/min	Km	Sensitivity µA/(mM.cm^2)
PBS buffer	6	3.007	60.5486	402.94
	7	3.1230	74.2126	520.59
	8	3.1132	76.8788	265.59

The tris HCl buffer was used to evaluate if it will give a better response. Tris (hydroxymethyl) aminomethane is a base; it can be used in conjunction with Hydrochloric acid to make a buffer for the desired pH. The pH range of the buffer solution was considered since the reaction was aimed to occur at a noncorrosive pH range. Tris HCl. pH was the maximum alkaline pH solution. The analysis conditions and parameters were kept constant. The different signals would have been the result of the electrolyte.

(a) (b)

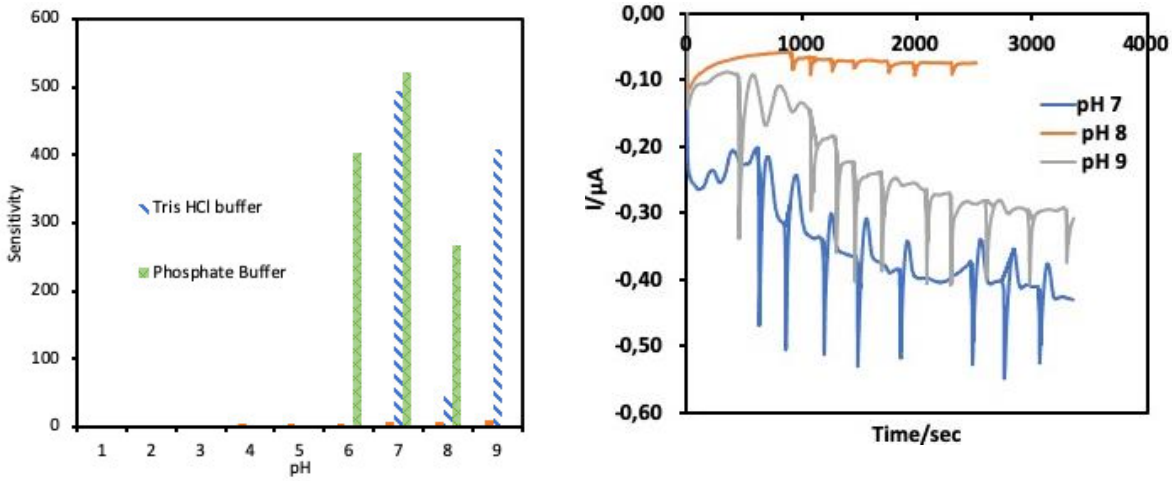

Figure 5-22; Shows (a) Bar graph comparing the electrolyte used for PGE/GO/MWCNTs/PBSE/Box (b) Chronoamperometric analysis using a tris HCl buffer solution

This electrolyte gave some optimum values regarding the sensitivity of O_2. pH 7 gave the maximum signal as can be seen in Figure 5.22 (a). However. it was not greater than of phosphate buffer. This electrolyte can be used as a good alternative in the case where the PBS buffer is not available. There was a good agreement between results obtained from the enzyme activity. looking at the Vmax and the Km. The ends of basic gave the value had a wide gap from 49 and 409 between pH 8 and 9. At a neutral pH 7. the sensitivity is the highest sensitivity. but also with the great interaction between enzyme and electrode at 34.36. Figure 5.22 (b) is amperometric of all three pH values of Tris HCl. showing pH 7 being more favorable since it gives the lower current signal.

Table 9; O_2 sensitivity in in different pH using Tris HCl buffer

	pH	Vmax µmol/min	Km	Sensitivity µA/(mM.cm^2)
Tris HCl	7	3.007	60.55	494.12
	8	3.123	74.21	49.12
	9	3.1132	76.88	408.82

There was a noticeable pattern in the Km values and the Tris HCl buffer. The increment in the pH value increased the Km value. but the maximum sensitivity was obtained at a neutral pH.

5.4.3 Temperature effect

Temperature and pH are extremely important factors when considering the design of biofuel cells because they allow various cell designs and various reactions at the anode. MCOs receive electrons at the T1 Cu site from electron-donating substrates. The electrons are then transferred to the T2–T3 cluster. composed of one T2 Cu and two T3 Cu ions. where O_2 is reduced directly to water in a four-electron reduction process. shown by Figure 5.23.

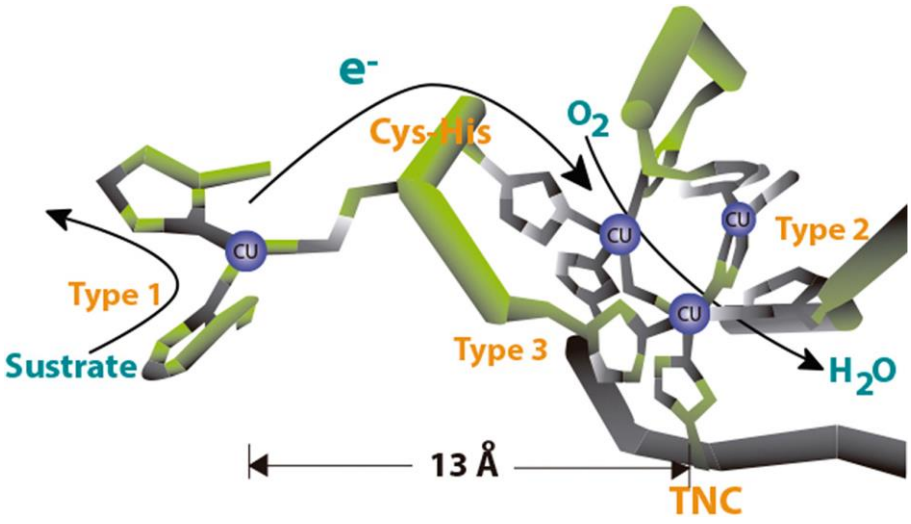

Figure 5-23;MCO illustrating the active and marking the electron flow from T1 to trinuclear site.

The chronoamperogram in Figure.5.24 shows the oxygen reduction. the PGE/GO/MWCNTs/PBSE/BOx electrode has a shorter saturated time at a biological temperature. The oxygen activity can be related directly with the chronoamperometric response. The time and current relation showed a quicker saturation period. The sensitivity of the PGE/GO/MWCNTs/PBSE/BOx at 37^0C decreased compared to the same electrode analyzed at ambient temperature. There was a significant difference between the two electrodes. favoring the ambient temperature. This can be further explained using the enzyme kinetics. The V_{max} of the enzyme was observed to be lower. which means that the biocatalytic reaction is very slow hence the distribution on the electrode surface is affected leading to lower electrode sensitivity.

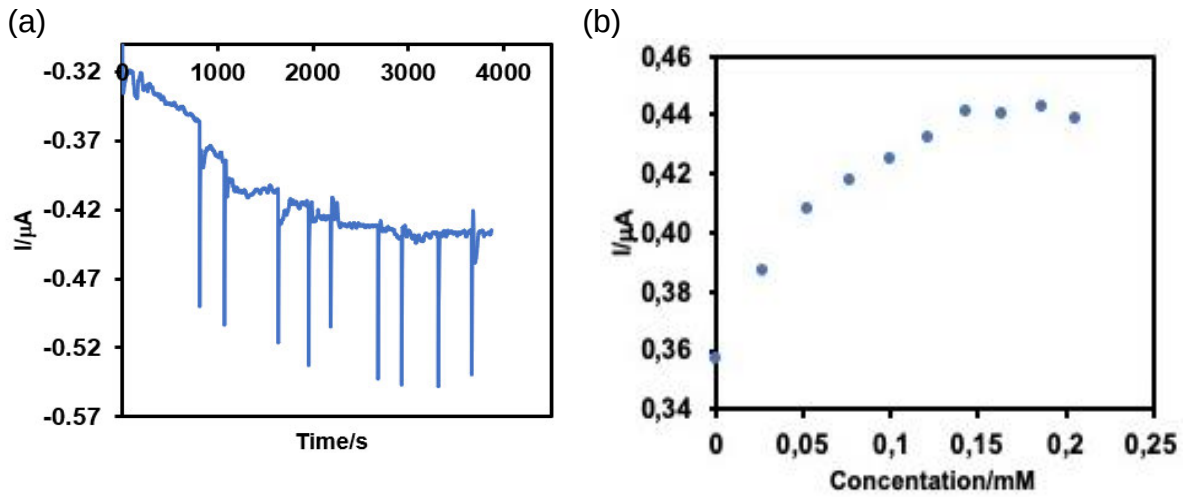

Figure 5-24;(a) Amperometric analysis performed at 37ºC. (b) concentration curve at 37ºC

The two established thermal properties of enzymes are their activation energy and their thermal stability. Arising from careful measurements of the thermal behavior of enzymes. In this study. the kinetic model of Figure.5.24 (b) is used and can be supported by statistically different kinetic parameters. The temperature of the reaction was raised to 37 ℃. the buffer solution was heated to a biological temperature. This was to monitor the behavior of the enzyme bilirubin oxidase. Once the electrochemical was at an ideal temperature 37 ºC. the addition of oxygenated PBS buffer solution was also at the same temperature.Using the gradient of the curve 3.67 $x10^{-6}$ A/mM then

converted to 3.67 µA/mM it is then multiplied by the area of the electrode of 0.034. the value obtain is sensitivity 107.94 µA/ mM.cm^2.

5.4.4 Qualitative analysis

The immobilization procedure consisted of tethering BOx enzyme to multi-walled carbon nanotubes (MWCNT) via pyrene-based succinimidyl ester compound (PBSE). similarly as performed by others (Atalah et al.. 2018), (Ramaraja P.Ramasamy et al.. 2010). Hence. the positive features of PGE are in this work assessed through the implementation of a bioelectrode containing immobilized BOx with DET feature. in order to be used as O_2 biosensor or biocathode with high electrocatalytic performance on O_2 reduction with a direct electron transfer process (Tasca et al.. 2015).

Figure 5.25 (a) is the PGE/rGO/MWCNTs/PBSE/BOx CV biosensor. the enzyme was drop cast onto the electrode surface using a micropipette. Drop casting means that the bilirubin enzyme was introduced on top of the PGE electrode in the form of a drop. Before using the biosensor. it was allowed to dry in a darker place (inside the clean cupboard). This was done to avoid direct fluorescence and natural light in the laboratory to avoid any structural deformation. Current peak values reduced from ±0.025 µA for N_2 and < 0.05 µA for O_2 detection. The most noticeable feature of the cyclic voltammogram was the distinct difference in response to the construction of the full biosensor upon the electrode surface between the two gases.

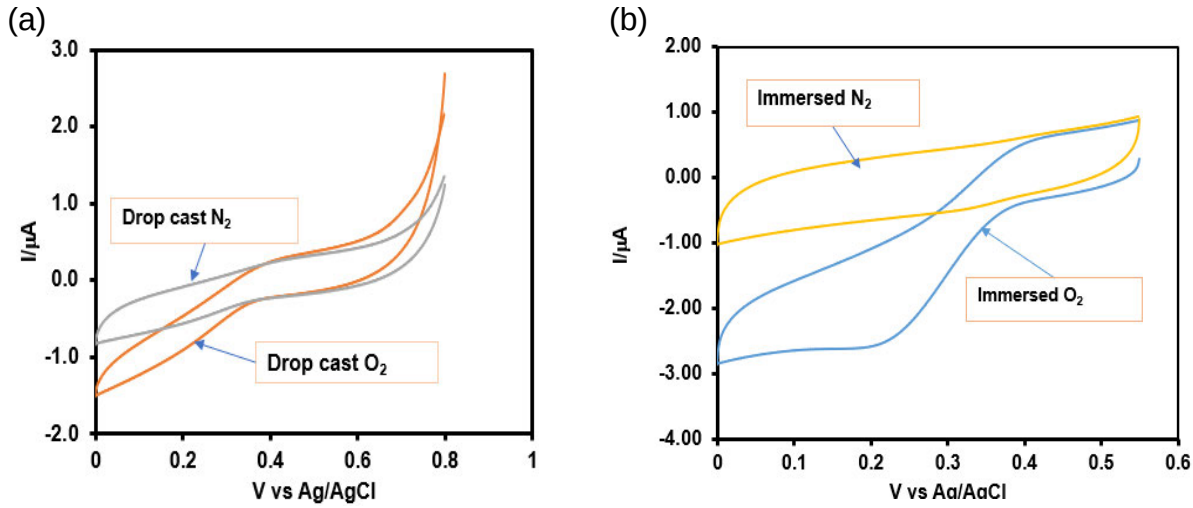

Figure 5-25;CV of PGE/GO/MWCNTs/PBSE/BOx modified electrode (a) with N_2 purged and with O_2. PBS buffer 0.1 M. pH = 7 as the electrolyte. (b) PGE/rGO/MWCNTs/PBSE/Box. electrode immersed for 60 minutes into bilirubin oxidase enzyme

The results are shown in Figure 5.25 (b) corresponds to the PGE/rGO/MWCNTs/PBSE/BOx. that was prepared by immersing method explained in section 4.5.3. The visible onset reduction peak at 0.35 V of oxygen the initial reduction current at -0.04 µA to 0.026 µA while N_2 maintained a constant signal of -0.07 µA at a range of 0 to 0.6 V potential window. There is a covalent bonding between the enzyme (amino acids) and the tethering agent PBSE. this makes an easy electron communication between the electrode and the components of the fabrication. This was an insight to a biocathode of bilirubin oxidase (BOx) as a promising development. in nature. this enzyme oxidizes bilirubin with simultaneous reduction of oxygen. Once attached to an electrode surface. BOx is also capable of fast and unmediated electron exchange with an electrode via a redox center naturally employed for bilirubin oxidation (Cadet et al.. 2013b. Sergey Shleeve et al.. 2005).

5.4.5 Quantitative Analysis

Chronoamperometry is used to study the kinetics of chemical reactions. diffusion processes. and adsorption. In this technique. a potential step is applied to the electrode and the resulting current vs. time is observed. The chronoamperometry experiment can be used to monitor or detect events. The Faradaic current - which is due to electron transfer events and is most often the current component of interest. Zero time is defined as the time at which the potential step is initiated. For reactions that are under diffusion control. the current decays with a $t^{1/2}$ decay as shown in equation 5.3 below. and obeys the Cottrell equation 2:

The solution is usually. but not necessarily. unstirred and contains an excess of a supporting electrolyte so that diffusion is the principal mechanism of mass transport. The functional relationship between the current response and time was measured after applying a single potential step to the working electrode of the electrochemical system. The type of chronoamperometry used in this study is the controlled potential chronoamperometry. Before running this type. cyclic voltammetry was run to determine the reduction potential of the analyte (BOx).

Several calibration curves with the same and different electrodes were used to evaluate the figures of merit. To establish the accuracy. reliability. and reproducibility of the collected data. all tests were recorded in triplicate and only average values are reported. Blank tests were run in parallel. All the labware used in the study was previously cleaned with soap. rinsed with distilled water. and finally with ultrapure water and allowed to dry at room temperature.

To develop the ORR biosensor. initially. two enzymes were used. laccase from *Trametes Versicolor* and bilirubin from *Myrothecium verrucaria* because they are part of the MCO (Pita et al.. 2013). Based on the different experiments. we decided to work with bilirubin oxidase which had been tested with phosphate buffer in both acidic and alkaline medium. To the best literature. the determination of oxygen using biosensor based on the inhibitory effect of the element on the solution has not been reported up to now. The ORR biosensor is based on the following reaction. depending on the medium;

Acidic; O_2 (g) + 4 H^+(aq) + 4e → 2 H_2O(l) E^0 = + 1.229 (eq 5.4)

Alkaline; O_2(g) + H_2O (aq) + 2e→ HO_2^- (l) + OH^- E^0 = -0.065 V (eq 5.5)

There are two ways of reductions that can take place. Oxygen can reduce to water by direct 4-electron pathway (Equation 5.4) or to peroxide by two-electron pathways (Equation 5.5). The most desirable one is the 4-electron pathway as it results in twice the number of electron transfer occurrences per ORR and. therefore. higher current generation. It is well-known that chronoamperometric measurements are influenced by different factors such as pH of the medium. the applied potential. the substrate concentration. and also ionic strength among others. depending on the studied system. Based on the optimization process to obtain the best current signals. the optimized parameters are summarized in Table 8 which were used in oxygen determination: supporting electrolyte pH 7.00. working potential of +0.0 V vs. Ag/AgCl PGE. a buffer concentration of 0.1 M and PO_3^- concentration of 0.1 M. Easily quantifiable chronoamperometric signals are registered under these optimized conditions for oxygen

Table 10;Values used to optimize experimental conditions for oxygen detection.

Parameter	**Low value**	**High value**	**Optimum value**
pH supporting electrolyte	6.0	9.0	7.0
Substrate additional volume	10 μL	50 μL	10 μL
Ionic strength	0.01 M	0.1 M	0.01 M
Applied reduction potential vs Ag/AgCl	+ 0.29 V	+ 0.35 V	+ 0.3 V

The optimal values from the table showed a higher oxygen sensitivity at an average applied potential. 0.3 V was the best potential for all the experiments. To analyze the signal with the immobilized enzyme. control experiments were carried out under the optimum conditions using bare PGE/GO and PGE/GO/MWCNTs but without the enzyme. No analytical signal was obtained; hence the inhibition response registered after the addition of the substrate is only related to oxygen concentration.

Consequently. oxygen can be determined by its inhibitory effect on the response of BOx. by calibration.

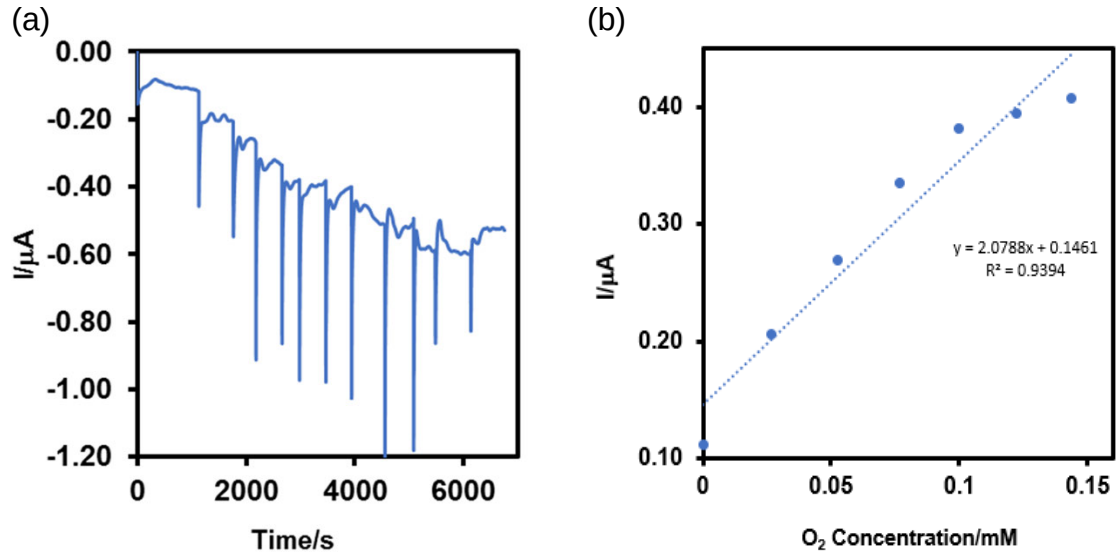

Figure 5-26;(a) Chronoamperogram an PGE applied potential. +0.30 V vs. Ag/AgCl PGE; pH 7.00 (PBS buffer. 0.01 M) concentration range. Inset figure (b). a calibration curve optimum conditions

Some important characteristics of the amperometric oxygen sensor are examined in detail with particular emphasis on the influence of electrode polarization on sensor behavior. Figure 5.26 (a) represents a chronoamperogram obtained for alkaline oxygen biosensor. a baseline represents the current of the buffer signal. the first current step is due to substrate addition. and the rest. 1 to 12. resembles consecutive additions of aliquots of W(VI) standard. The onset calibration curve of this chronoamperogram is shown in Figure 5.26.(b). with the experimental conditions indicated on the graph.the slope of $2.08x10^{-5}$ A/mM was converted to µA/mM then multiplied by the electrode area of 0.034 cm^2. The resultant value of 611.76 µA/ mM.cm2 is used as determined O_2 sensitivity.

The ionic compounds dissociate into ions when dissolved in water. the ionic strength of the solution can then be measured with the concentration of ions. For potentiometric analysis. this is important since it measures the activity of the analyte other than its concentration. HCl was used as the ionic strength adjuster for tris buffer. to increase the ionic strength of the solution to a higher stable level. making a linear correlation between the logarithm of the concentration of the oxygen and the measured voltage.

$$E_{cell} = E^0 - (RT/nF)\ ln\ Q \qquad \text{(eq 5.6)}$$

Equation 5.6; where *E* is measured voltage. *R* is the gas constant. *T* the temperature measured in kelvins. F is the Faraday constant and n the charge of the analyte and c is the concentration of the analyte.

The goal was to ensure that the activity coefficient is constant across the solution and assuming that there no other ion present in the solution. Their significant errors were eliminated by using a sample with a negligible difference between the activity of the analytes in both the dilute solution and concentrated samples.

5.4.6 Characterization of BOx biosensor

To characterize an analytical method. it is important to establish its precision in terms of reproducibility and repeatability. The first one was calculated considering calibration curves registered using different biosensors (inter-biosensors). and the second one with one single biosensor (intra-biosensor). In this way. several calibration curves were performed in the range of concentration from numerous additions at optimum conditions of the experimental variables. Both figures of merit were calculated by the relative standard deviation (RSD) of the slopes from different calibration curves. The reproducibility associated with slopes of these calibration curves in terms of RSD was 4.2% (n = 3). Determination of the repeatability was performed similarly using a single BOx based PGE. which kept 83% of its initial sensibility after the third calibration curve. obtaining a value of 9.4% (n = 3) in terms of RSD. Table 10 shows the validated parameters of the calibration curves registered using different biosensors and one biosensor respectively.

The detection of O_2 through the inhibition of the BOx reaction was determined. In this way. the limit of detection based on the standard deviation (3 S/m) in triplicate of the calibration curve was 8.24 ± 0.091 µM. and the limit of quantification was 0.58 ± 0.15 µM.

Table 11; Precision parameters obtained through ordinary least square (OLS) regression for O_2 using one or different PGE/rGO/MWCNTs/PBSE/BOx under optimum conditions

Reproducibility			Repeatability	
Electrode	**Slope (µA/mM)**	**R^2**	**Electrode 2 Slope**	**R^2**
1	17.73	0.960	7.94	0.973
2	8.42	0.914	8.36	0.962
3	13.90	0.980	8.42	0.914
Media	13.35		8.24	
Std. Dev.	4.67		0.26	
RSD %	3.82		0.21	

5.4.7 Inhibitory effect of Oxygen over the BOx enzyme

The inhibitory effect of O_2 in the enzymatic activity. when using bilirubin oxidase was studied by means of kinetic parameters of the Lineweaver-Bulk plot. The y-intercept of this graph is equivalent to the inverse of Vmax. the x-intercept of the graph represents −1/Km (Km is the Michaelis–Menten constant and Vmax is the maximum reaction velocity). It also gives a quick. visual impression of the different forms of enzyme inhibition. both in the absence and presence of oxygen. This study was performed under different ionic strength. according to values of Km and slopes. suggesting a mixed inhibition (Dias et al.. 2014). In fact. the inhibitory effect of oxygen on the bilirubin oxidase reaction was confirmed through the higher affinity of BOx for the substrate in the absence of this element. As can be seen from Table 10. slopes and Km increases directly with the concentration of O_2 as an inhibitor. In addition. Table 11. shows the variation of Km with pH.

Table 12;Michaelis-Menten apparent constant values at different pH with PBS buffer.

O_2 conc	Correct µmol/min O_2	Km
0	0.00	0.00
26.76	0.112	$4.66x10^{-5}$
52.31	0.206	$7.93x10^{-5}$
76.68	0.269	$9.33x10^{-5}$
99.93	0.335	$1.06x10^{-4}$
122.12	0.382	$1.17x10^{-4}$

Table 13; Showing PBS buffer at different pH and resultant sensitivity

PBS pH 7	Slope =	$1.77x10^{-5}$	A/mM
		17.7	µA/mM
	Area =	0.034	cm^2
	Sensitivity	520.59	µA/mM.cm^2
PBS pH 8	Slope	$8.42x10^{-6}$	A/mM
		8.42	µA/mM
	Area	0.034	cm^2
	Sensitivity	247.65	µA/ mM.cm^2
PBS pH 9	Slope	$1.39x10^{-05}$	A/mM
		13.90	µA/mM
	Area	0.034	cm^2
	Sensitivity	408.82	µA/ mM.cm^2

5.4.8 Electrochemical Impedance Spectroscopy (EIS)

EIS is one of the most generally used electrochemical techniques to monitor electrode surface properties. The Randles equivalent circuit is consists of solution resistance (Rs). charge-transfer resistance (Rct). constant-phase element (CPE) and Warburg impedance (Zw). Rs represents the effect of the concentration and the type of electrolyte solution on the ionic conductivity. CPE is a general frequency-dependent element. which is often associated with non-ideal capacitive behavior resulting from electrode roughness and inhomogeneous conductivity. Zw depends both on the rate of diffusion in the electrode and on the frequency used to probe the impedance. A

nonlinear least-squares method was used to fit and determine the parameters of the elements in an equivalent circuit (EIS Nyquist plots and equivalent circuit. Figure 3.4).

From Section 3.4. it was clear that different equivalent circuit components are represented by electrochemical impedance spectroscopy measurements taken at different frequencies. Specifically. the solution resistance is determined at high frequencies (i.e. left-hand side of Nyquist plot). and charge-transfer resistance at lower frequencies (i.e. right-hand side of Nyquist plot) (Pike. 2014). It is useful therefore for any impedimetric analysis to form the relationship between the biosensor-analyte impedance response and the frequency at which the impedance measurements are taken. Figure 3.4 presents the impedance response (both the real component and imaginary component to a range of analyte concentrations for three selected measurement frequencies.

Figure 5-27;Nyquist plots and frequency simulation with time for both PGE (a) 4B and (b) HB

Rsol =	140	Ω
Rct =	4000	Ω
Cdl =	150	nF
tau =	6.0×10^{-4}	s

Rsol =	100	Ω
Rct =	4000	Ω
val_n=	0.80	
val_q=	9.5×10^{-7}	$\Omega^{-1}s^{n}$

(a)

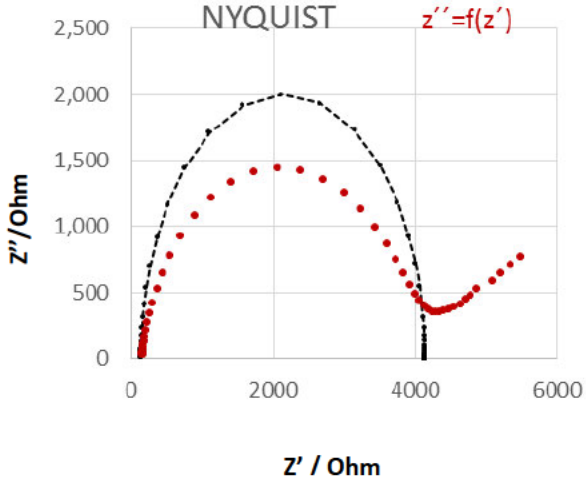

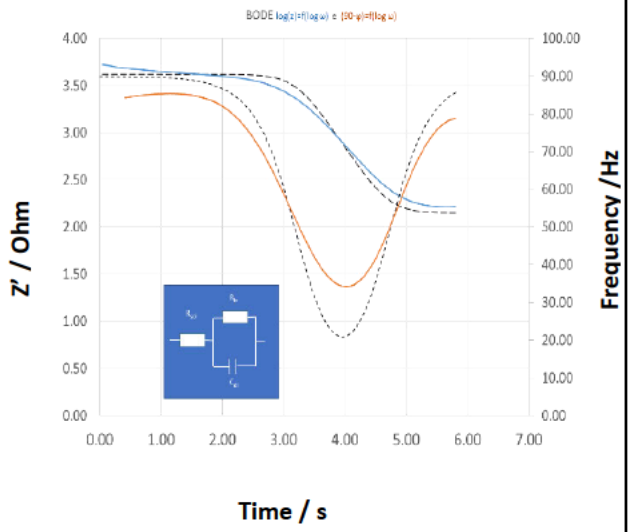

(b)

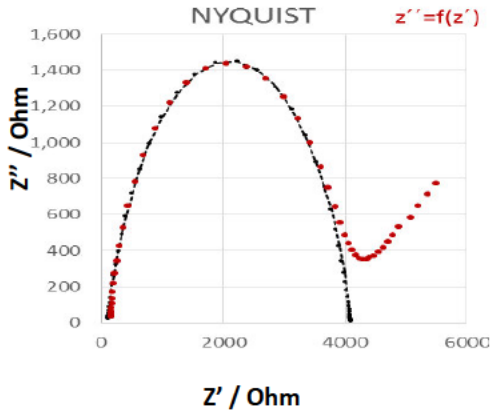

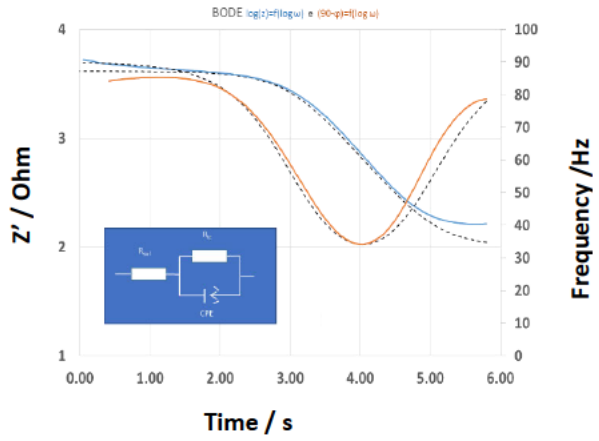

Rsol =	180	Ω
Rct =	3500	Ω
Cdl =	1.3×10^{-7}	nF
val_n=	0.26	
val_q=	5.7×10^{-4}	

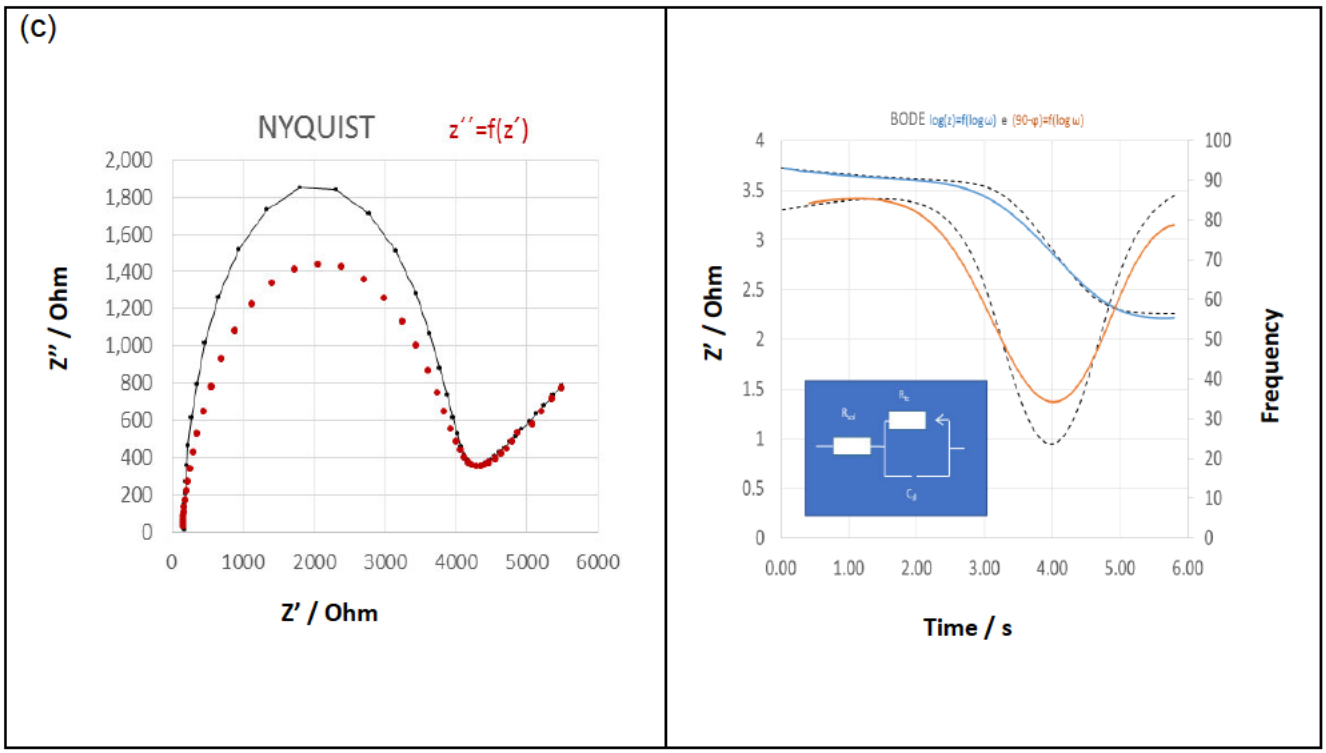

Figure 5-28; (c) Nyquist plots and frequency simulation of the PGE 4H

All the simulations were the response of an electrochemical system of different pencil graphite (HB. 4B. 4H). to an applied potential. The resultant ratio of voltage to current can be used to describe the impedance. The frequency dependence of this impedance can reveal the underlying chemical process. The response of the electrochemical system is very nonlinear. and it is possible to interrogate the impedance involving the deviation of a system. Small amplitude (10 mV) AC ripple over the controlled DC polarization potential. This response of the system is usually displayed in Nyquist format. with the reactants inverted. These systems are permanent capacitive. The system response as the function of perturbation frequency can reveal internal dynamics as seen in figure 5.32

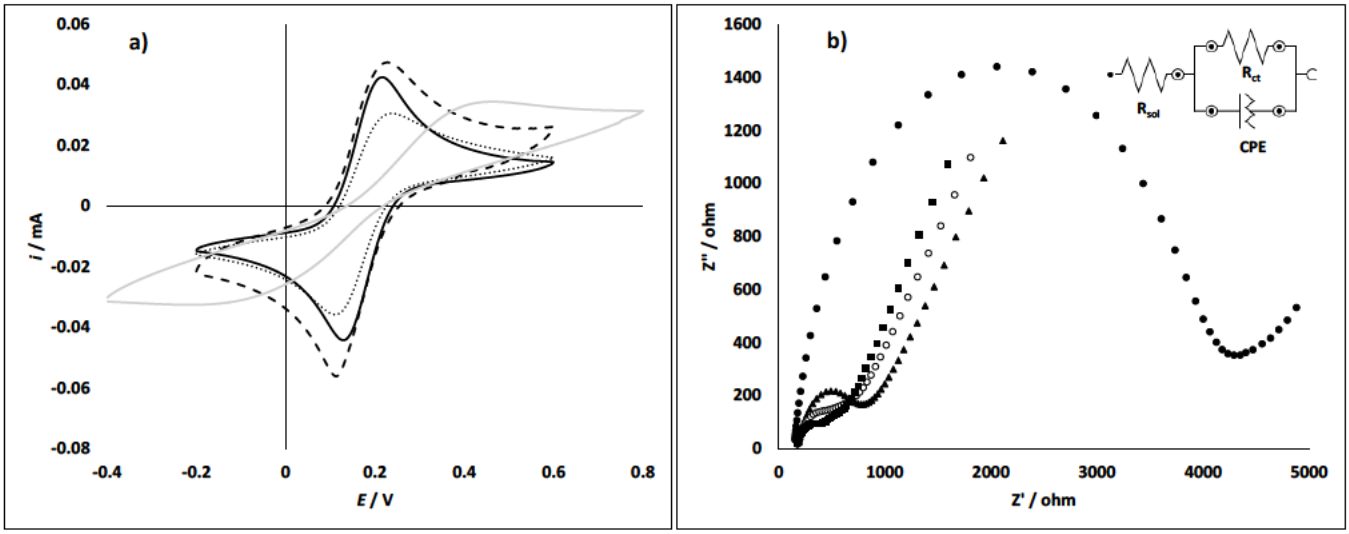

Figure 5-29;(a) Cv scans for 4B, HB, HB and HB without alumina polishing. (b) Nyquist plots of the PGE 4B (squares). HB (open circle). 4H (triangle) and for PGE HB without pre-treatment by polishing with alumina (full circle).

5.4.9 Enzyme kinetics

Enzyme kinetics is concerned with the influence of enzymes on chemical reaction rates. Enzymes are biological catalysts that speed up chemical reactions. They occur naturally in biological systems. although in modern biotechnology they are also used in isolation to facilitate reactions of organic chemistry or to participate in the detection of analytes.

(a) Enzymes Inhibitors

The Michaelis-Menten equations can be used to describe the different types of inhibitory. Table 12 is a model type along with the equation used to calculate. to make it easy to start the simulation with the simpler model.

Table 14; Enzyme inhibitory models eqautions

Model	Michaelis-Menten equation
Without inhibition	$$v_{inic} = \frac{V_{máx}(S)}{K_m + (S)}$$
Competitive inhibition	$$v_{inic} = \frac{V_{máx}(S)}{K_m(1 + \frac{\|I\|}{K_{ic}}) + (S)}$$
Non-competitive inhibition	$$v_{inic} = \frac{V_{máx}(S)}{K_m(1 + \frac{\|I\|}{K_{.}}) + (S)(1 + \frac{\|I\|}{K_{.}})}$$
Uncompetitive inhibition	$$v_{inic} = \frac{V_{máx}(S)}{K_m + (S)(1 + \frac{\|I\|}{K_{iu}})}$$
Mixed inhibition	$$v_{inic} = \frac{V_{máx}(S)}{K_m(1 + \frac{\|I\|}{K_{ic}}) + (S)(1 + \frac{\|I\|}{K_{iu}})}$$

Table 15; calculated Km and Vmax values using different Michealis Menten equations

S_Inib		I_Comp		I_Ncomp		I_Acomp		I_Mist	
$w_i.(y_{exp} - y_{cal})^2$	Ycalc	$w_i.(y_{exp} - y_{cal})^2$	Ycalc	$w_i.(y_{exp} - y_{cal})^2$	Ycalc	$w_i.(y_{exp} - y_{cal})^2$	Ycalc	$w_i.(y_{exp} - y_{cal})^2$	Ycalc
0.0000	0.0000	0.0000	0.0000	0.0000	0.0000	0.0000	0.0000	0.0000	0.0000
0.0000	0.0001	0.8494	0.9217	0.6850	0.8277	0.6461	0.8038	0.8431	0.9182
0.0000	0.0001	1.9423	1.3938	1.6670	1.2912	1.5889	1.2606	1.9347	1.3910
0.0000	0.0001	2.8229	1.6803	2.5185	1.5871	2.4165	1.5546	2.8179	1.6787
0.0000	0.0001	3.5058	1.8725	3.2114	1.7921	3.0956	1.7595	3.5045	1.8721
0.0000	0.0001	4.0408	2.0103	3.7731	1.9426	3.6495	1.9105	4.0435	2.0110
0.0000	0.0001	4.4701	2.1144	4.2352	2.0581	4.1073	2.0268	4.4764	2.1159
0.0000	0.0001	4.8191	2.1954	4.6183	2.1492	4.4881	2.1187	4.8288	2.1976
0.0000	0.0001	5.1615	2.2720	5.0007	2.2363	4.8694	2.2068	5.1749	2.2750
0.0000	Sum	298223.6872	Sum	277672.9588	Sum	268517.2466	Sum	298352.4904	Sum
V max =	0.00018306	V max =	3.0070271	V max =	3.12305654	V max =	3.11321849	V max =	3.01916424
K m =	65.5936039	K m =	60.5486428	K m =	74.2126389	K m =	76.8788702	K m =	61.2263024
		K ic =	16.2051047	K iu= K ic=	104.470908	K iu =	110.898587	K ic =	16.950959
								K iu =	1059.31376

The kinetic parameters of the Lineweaver Burk plot were studied for the O_2 inhibitory effect in the enzymatic reaction when using the PBSE as the wiring agent for a third-generation biosensor. The y-intercept of this graph is equivalent to the inverse of Vmax. the x-intercept of the graph represents −1/Km (Km is the Michaelis–Menten constant and Vmax is the maximum reaction velocity). It also gives a quick. visual impression of the different forms of enzyme inhibition. both in the absence and presence of oxygen. The analysis parameters were varied from ionic strength. pH and buffer. according to Km values and slopes. The WI inhibitory effect of O_2 on the PBSE was observed (Elgrishi et al.. 2017).

(b) Temperature dependence of reaction rates

The reaction rate increases with increasing temperature; as a rule of thumb raising the temperature by 10 K doubles the reaction rate. The temperature dependence of a rate constant is described by the Arrhenius equation:

$$k = Ae^{\frac{-Ea}{RT}} \qquad \text{eq (5.7)}$$

With k: rate constant. A: pre-exponential factor (in the units of the rate constant). EA: activation energy (in J mol-1). R = 8.314 J K-1 mol-1 and T: temperature in Kelvin. The pre-exponential factor A is related to the collision between molecules and to internal motions (in a bimolecular reaction) or to internal motions of the molecule only (in a unimolecular reaction) (Leenson. 1999). While there are theories that allow calculation of A from molecular properties. it is usually determined through experiments. When the ratio of two rate constants at two different temperatures T1 and T2 is considered. A cancels out

$$\frac{K_2}{K_1} = 1^{\frac{Ea}{R\left[\frac{1}{T_1}-\frac{1}{T_2}\right]}} \qquad \text{eq (5.8)}$$

The activation energy can be interpreted as an energy barrier that must be overcome before the reaction proceeds to products. The point at the top of this energy barrier is called the transition state (Leenson. 1999).

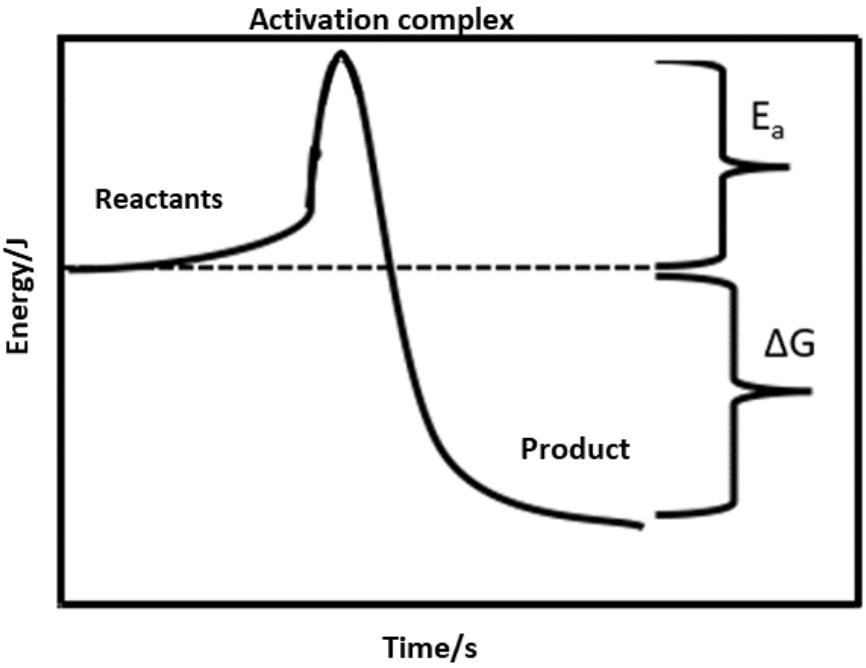

Figure 5-30; A ---- B. a energy profile for the reaction. Ea is the activation energy and ΔG is the free enthalpy change of the reaction.

As a reaction proceeds the reactants must overcome this energy barrier. With increasing temperature. the thermal energy of the reactants increases. which makes it more likely for them to overcome the energy barrier. This temperature dependence is described by the Arrhenius equation (Leenson. 1999). The height of the activation barrier is related to the rate constant as EA = (ln A/k)/RT. i.e. the lower the rate constant. the higher the activation barrier as seen in Figure 5.29.

The speed of an enzyme on this increased temperature was very fast and was able to mimic the biological system and the Km values were lower compared to the Tris HCl enzyme kinetics behavior. The lower Km implies a good affinity with the substrate hence the enzyme and the substrate stay together more other than breaking apart.

(c) Interpretation of the Michaelis-Menten equation

The Michaelis-Menten equation provides the dependence of the initial reaction rate v_0 on substrate concentration. The hyperbolic plot or saturation plot of v_0 against substrate concentration and shown in Figure 5.30. The typical feature of the saturation plot is the initial steep rise of v_0 with increasing substrate concentrations followed by a gradual flattening of the curve. The maximum initial reaction rate V_{max} is approached asymptotically.

In the limit of infinite substrate concentration. the V_{max} of 1.0 concentration/time is reached. The targeted aim of enzyme kinetic data analysis was to determine KM and V_{max}. If we know the concentration of active enzyme sites. we can use V_{max} to calculate the turnover number that was the number of reactions the enzyme performs per unit time. Which is also known as k_{cat}: $k_{cat} = V_{max} / [E]T$. Note that for multimeric enzymes. the concentration of active sites [E]T was a multiple of the enzyme concentration. while for enzymes with one active site [E]T was equal to the concentration of active enzyme. Furthermore. the concentration of active enzyme was often not equal to the total protein concentration. as proteins are sensitive biological materials (Leenson 1999).

5.5 Development and optimization of PGE/PEG/PAA-PVI-Os[4.4-dichloro-(2.2-Bipyridine)$_2$ Cl]$^{-2+}$/ BOx

5.5.1 Evaluation of the redox polymer

Chemical polymerization of acrylamide at ambient temperature was evaluated by the three-step synthesis in an aqueous medium shown in Figure. 5.34. It is familiar when proton-conducting polymer electrolytes can be obtained by doping polymers carrying ether. alcohol. imines. and amide and imides acidic groups. The formation of proton defects is required for proton conduction. The heterocycles like imidazole have their nitrogen site act as a strong proton acceptor to form protonic charge carriers. The protonation of PVI through doping with PVA is proposed in the direction shown in scheme 5.1

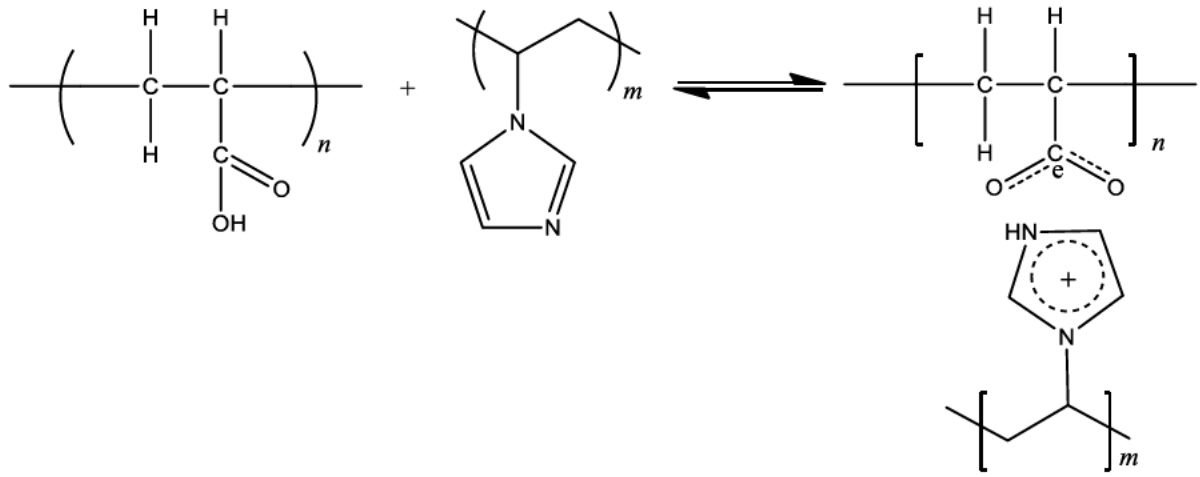

Figure 5-31;Proposed protonation of PVI with PAA

From the work reported by cadet (Cadet et al.. 2013a). the 2.2 azobis(2-methylpropionitrile) is a white columnar crystal. it is insoluble in water. Possesses explosive hazardous characteristics. decomposes drastically at 100 -107^{o}C and flammable. This 2.2 Azobis (2-methylpropionitrile was substituted with thioglycolic acid. An electron transfer from thioglycolic acid to Os (IV) leads to the formation of free radicals and the following proposed reaction occurs.

$$HS - CH_2 - COOH + Os\ (IV) \xrightarrow{I} HOOC - CH_2 - S\bullet + Os\ (III) + H^+$$

$$\xrightarrow{II} HS - \bullet CH - COOH + Os\ (III) + H^+$$

$$\xrightarrow{III} HS - CH_2 - COO\bullet + Os\ (III) + H^+$$

$$\Downarrow$$

$$HS - \bullet CH_2 + CO_2$$

Scheme 5.1; Os (IV) and thioglycolic acid radical formation reaction

Since the S-H bond has low bonding energy. the formation of radicals in reaction I is most likely to occur in order to start the polymerization of acrylamide and the oxidative

termination of polymer radicals by osmium ions. This leads to polymerization reaction. water-soluble polyacrylamides proposed structure represented in the scheme

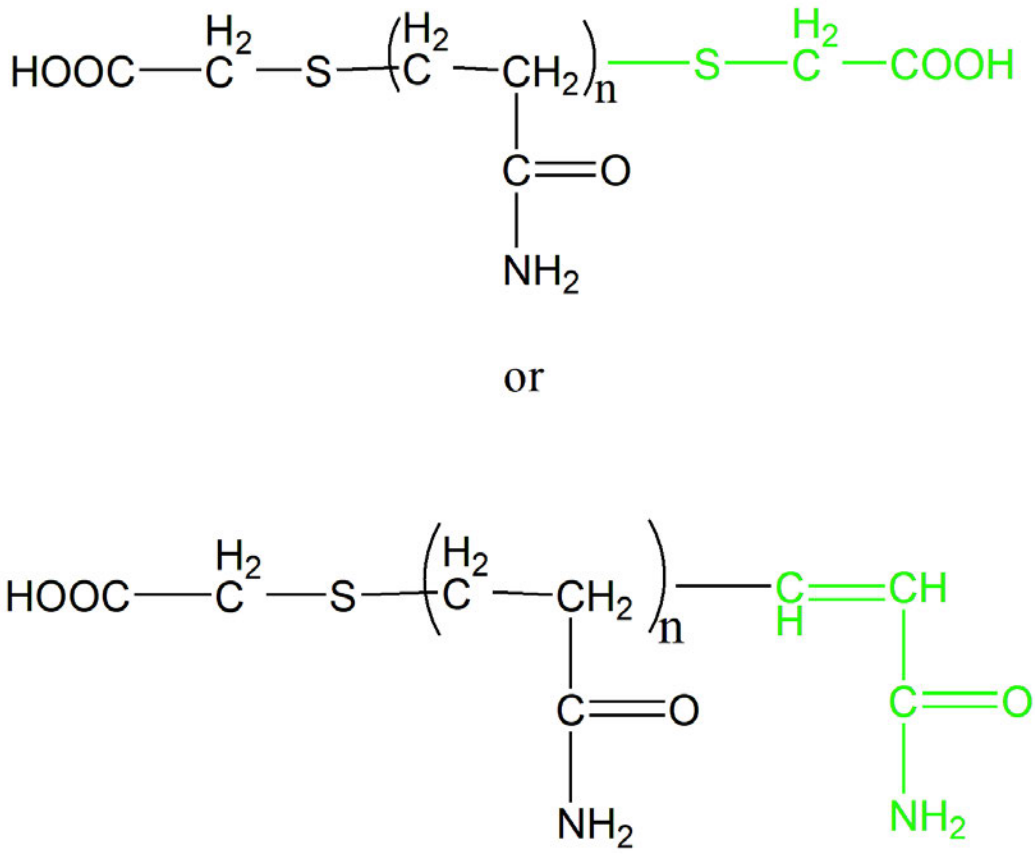

Figure 32; The possible structure of polymer synthesized.

The molecular ratio of acrylamide to thioglycolic acid at different temperatures and time could lead to an increase in molecular weight. The effect of polymerization temperature. the acid concentration and the mole ratio of Os(4.4-dichloro-2.2 bipyridine) Cl_2 under reflux at 160 ^oC for 4 hours. Significant changes in the yield and molecular weight of the polymer were not observed.

In this study. two commonly used thermal analysis is used for this polymer. differential scanning calorimetry (DSC). thermogravimetric analysis (TGA). In TGA analysis. the polymer is held isothermally in a defined atmosphere. it is heated. cooled and its mass is weighed in TGA. DSC is most versatile in analyzing various properties such as heat capacity. melting point. vaporization. crystallization. temperature stability. elasticity and glass transition.

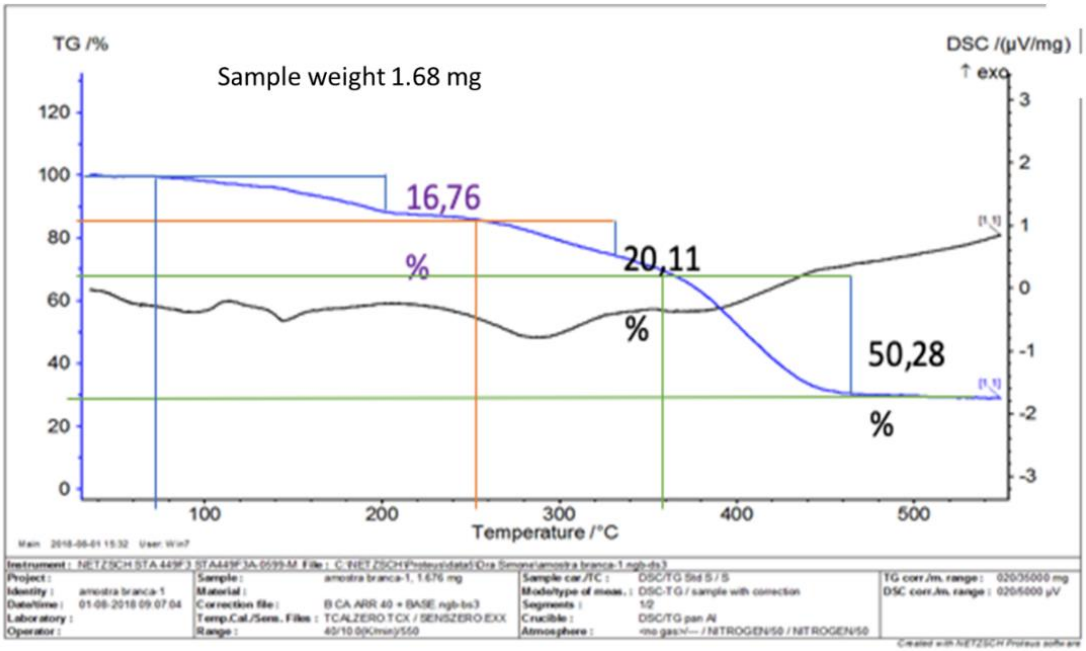

Figure 5-33;Thermal analysis of PAA-PVI polymer. N_2 gas carrier. Al pan.

This polymer was characterized by STA 449F3. the black DSC thermal curve and the blue TGA mass loss curve is displayed in Figure. 5.35. The 1.676 mg sample was used for analysis. Thermoset mass loss is observed starting from 75 – 200 ^oC resulting in 16.76% sample loss. The slight changes can mean polymer deformation. Changing its original form. The DSC curve indicates that the crystalline melt defined peak temperature at 300 ^oC. After a melt transition. the baseline returns into a slightly lower position than the pre-melt. These changes indicate a liquid phase which has lower heat capacity than of crystalline phase. The decomposition of the sample is initiated by a post-melt baseline at 450 ^oC. the DSC decomposition peak at 450 ^oC corresponds to the TGA extrapolated onset temperature of 45 ^oC as this sample starts to decompose. The entire analysis was continuously monitored by inert nitrogen gas and very high temperature.

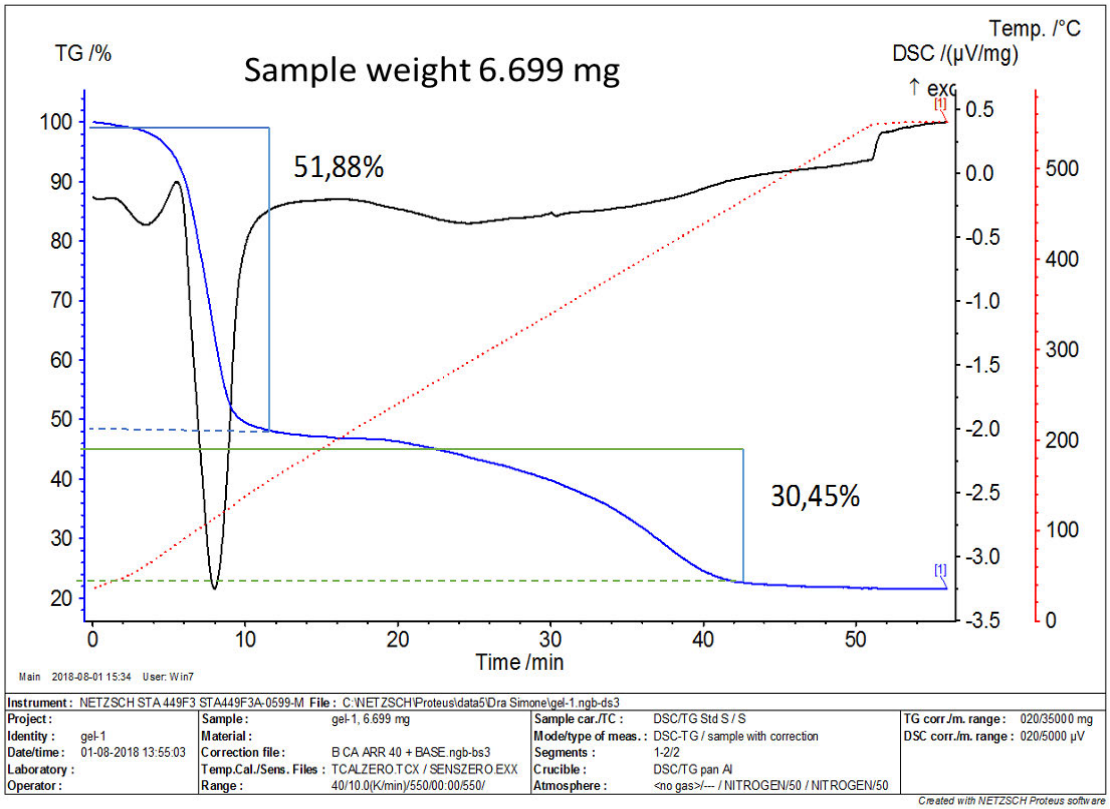

Figure 5-34;Dialyzed PAA-PVI polymer

Above in Figure 5.36 is a dialyzed PAA-PVI. this was very vital. This was to eliminate any type of inferences in the molecules by size. The membrane is selectively permeable with the microscopic pore. The black curve is DSC heat flow (1st derivative). the blue curve is the mass loss. the sample is run in static from 0 ^{o}C to 600 ^{o}C. The difference in temperature for up to 60 ^{o}C for dialyzed samples. The polymer has fewer volatiles and no moisture compound absorbed inside the polymer. However. there is a big weight loss of 51.88% during the glass transitioning stage. The other is observe post-melting with a 30.45% mass loss and the remains of 18 % on the surface.

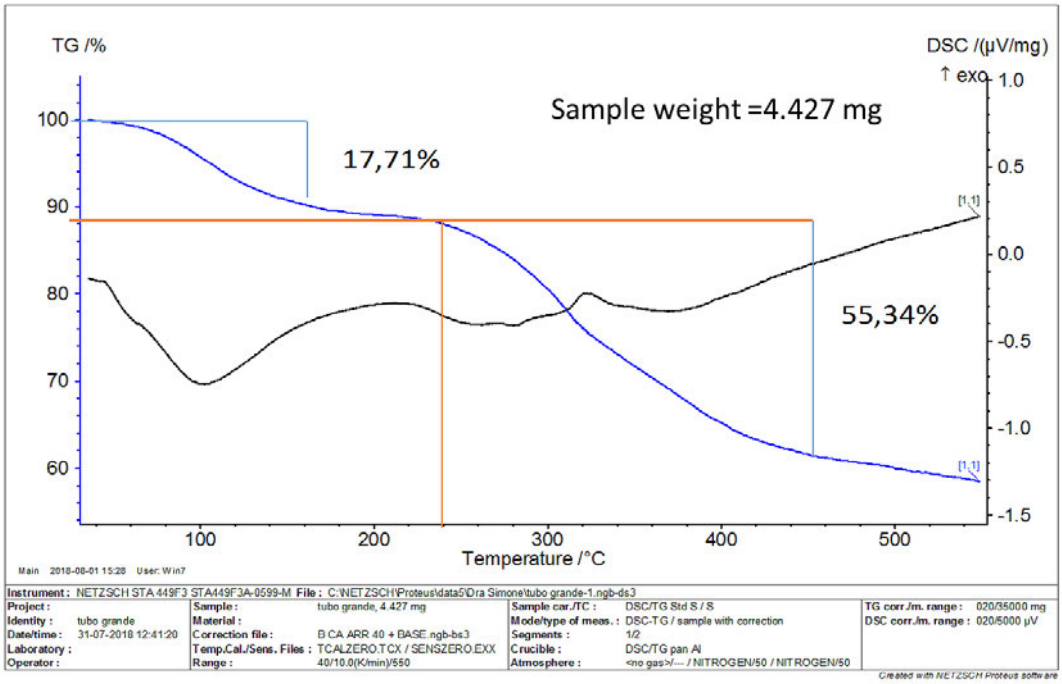

Figure 5-35;Primary redox polymer thermal analysis.

Figure 5.34 shows that there is a very slow progressive loss of 17.71% of volatile components. absorbed moisture and residual solvents from 100 ^{o}C to 200 ^{o}C. The blue curve is mass loss. shows a redox polymer to be stable. there are few physical changes observed in the whole polymer structure. At 130 ^{o}C there is a glass transition stage. this slowly spreads to 300 ^{o}C where it crystallizes. The melting point of the polymer starts at 450 ^{o}C. In most TGA analysis. most metal oxides start to form at a temperature above 500 ^{o}C but in this case. our metal oxide is at 40.25 ^{o}C.

5.5.2 FTIR analysis of the Os PAA-PVI

In order to confirm the characteristics of polymer assumed structure [-CH_2-$CH(CONH_2)$ -] $_n$. the standard infrared (IR) spectrum of acrylamide (AA) and observe for any noticeable variation from a monomer. The NH_2 asymmetric mode is assigned at 3404 cm^{-1}. showing strong intensity and shape on the spectrum. On the other side. the AA bands correlating to the C - H stretching are greater than 3000 cm^{-1} which is likely for olefinic hydrogens and shows the presence of sp^2 hybrid carbon in CH. In the product properties. these bands vanish and appear new ones at 2954.28. CH stretch for asymmetric and symmetric respectively. Table 14 shows the IR extrapolated result.

Table 16; FTIR spectrum analysis

KEY; § - deformation. tw – twisting. wa – wagging. ro- rocking. s – stretching. as – antisymmetric.

The IR spectrum of the amide functional group is resultant to several characteristics of amide vibration (C = O stretching [i] and wagging [ii]. NH_2 deformation [iii] and wagging

Acrylamide		**Product - polyacrylamide**	
Frequency	Property	Frequency	Property
3404	NH_2 as	3356	NH_2 as
2813	C – H s	2954	CH_2 as
1921	2 X 962	2813	CH s
1674	C = O s	1670	C = O s
1619	NH_2 §	1612	NH_2 §
1430	$=CH_2$ §	1428	C -N s
1353	C – N s	1352	CH_2
1136	NH_2 ro	1230	NH_2 ro
1049	$=CH_2$ ro	1136	C - C
987	$=CH_2$ wa	989	NH_2 tw
962	$=CH_2$ wa		
814	C = O wa. CH =CH wa		
618	C = O wa. CH = CH wa		
507	CCN §		

[iv]. C – N stretching [v]. In the spectra amide. i and iii appear as strong bands in (1674 ± 40) cm^{-1} and (1912 ± 30) cm^{-1} respectively. Henceforth. at AA spectra the deformation of NH2 at 1619 cm^{-1} and C=O stretch at 1674 cm^{-1} are very clear.

The product spectrum in this region does not differ from the AA spectrum pinpointing both amide functional modes remain unchanged on the product. The observed frequency up-shift of C – N stretching mode at 1619 cm^{-1} (amide v) and $=CH_2$ deformation at 1430 cm^{-1} can be used to confirm polymerization. The vinyl group

changes can be evaluated through the three-wagging mode involving all three hydrogens in – CH = CH_2 substituent. the hydrogen atom in *cis* and *trans* position participate. They are observed in a narrow 962 ± 45 cm^{-1} and wide-range 618 cm^{-1} and are known to as CH = CH cis and trans wagging. The α-bonded atom C = O appeared 814 cm^{-1}. Hence. the absorption 987 cm^{-1} are the most essential bands to explain -CH = CH_2 structure. In the IR spectra of AA. at 987 and 962 cm^{-1} = CH_2 wagging and overtone at 1049 cm^{-1}. The absence of these bands on the IR spectrum of the polymer product shows the transformation of a vinyl group into a saturated carbon chain the same as one mentioned above scheme 5.1 and 2 (Roeges and Baas. 1994).

In this redox polymer. a copolymer of polyacrylamide and ligand which is derivatized Osmium redox center were covalently bonded. Polyacrylamide gel is advantageously utilized in biochemistry to eliminate matrices in macromolecules as they weakly bind the protein.

The polymer and BOx were cross-linked with PEG to fabricate the electrode film. This redox-hydrogel film has a sufficient electron diffusion coefficient (no rate limit) as well as permeability to water-soluble substrate and product of the enzymatic reaction. For this electrode type. MCO enzyme-containing layers communicate with the electrode. When a cross-linked redox polymer substituents transfer electrons (wire) an enzyme that is covalently bonded to it. the gel and the ligand form the enzyme electrode. A single way to realize such communication is through networks that’s connects to the enzyme center to the electrode. The electron communication between the redox center of the enzyme and metal electrode is of the essence in an amperometric biosensor. Such electrodes are in applications where the release of the diffusional mediators from the electrode id to be avoided and where miniaturized is vital.

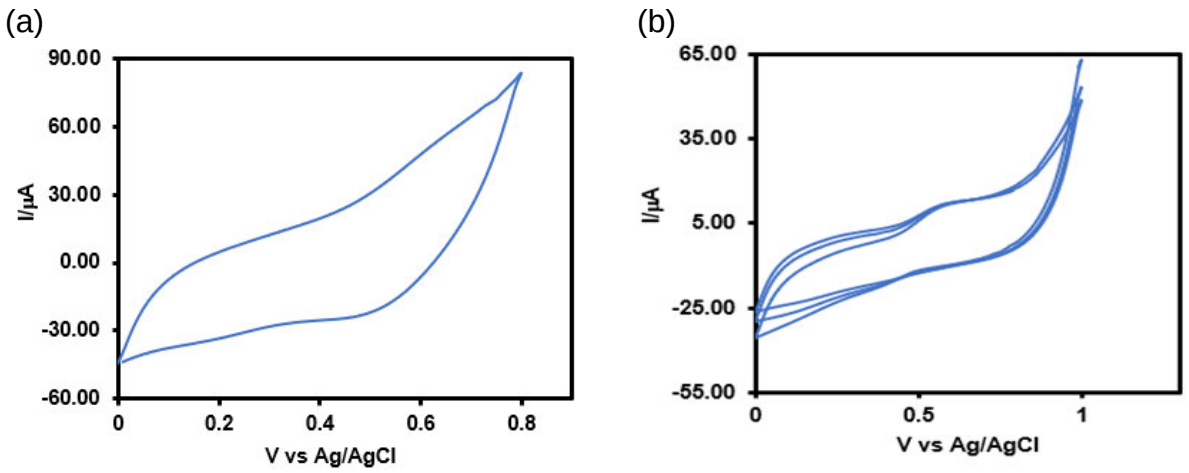

Figure 5-36;The CV of PAA-PVI Os complex (a) N_2 purged (b) O_2 PBS buffer pH 7

The electrochemical analysis was prepared on the polished PGE surface. Before the coating. the electrode was let too dry for 10 minutes. The modification consists of ratio: 60 % PAA-PVI Os polymer. 7 % PEG. and 33 % BOx *M. oryzae*. This was the optimum ratio. keeping the PAA-PVI Os complex redox mediator constant.

The cyclic voltammograms are shown in Figure. 5.38 are analyzed under phosphate buffer at pH 7 0.1 M. (a) represents a N_2 purged solution there are no visible anodic or reduction peaks. (b) this shows a CV at a similar potential as of (a) other than the at 0.6 V and a 0.5 V anodic peak and cathodic peak respectively. The cathodic peak is the confirmation of the reduction of oxygen. Oxygen was introduced using a cylinder. the buffer was oxygenated for 15 minutes. to saturate the buffer. The reduction potential is then used for chronoamperometric. to detect the sensitivity of O_2 inside the cell.

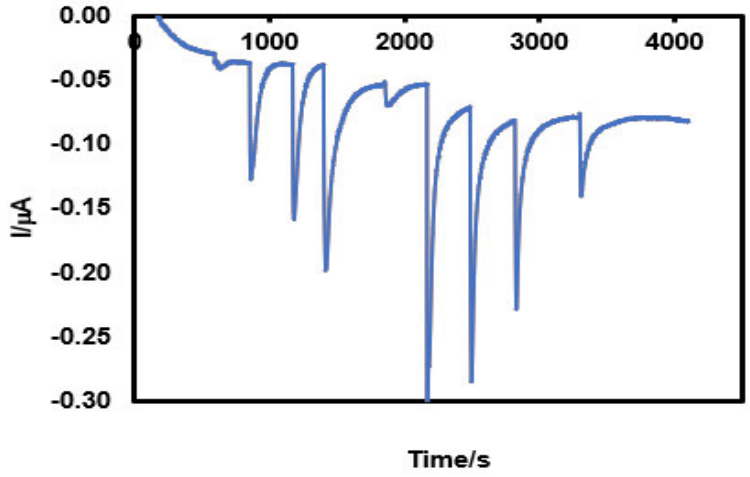

Figure 5-37;The amperometric PGE/ PAA-PVI(Os) redox/ PEG/Box Observing O_2 sensitivity

The quantitative analysis using PAA-PVI(Os) complex is to measure the sensitivity of the PGE/PAA-PVI(Os)/ PEG/BOx. to oxygen. The reduction potential is set to 0.55 V. this was per the reduction peak observed at the cyclic voltammogram in Figure. 5.39

The electrode was saturated just before 4000 sec. this is enough time for analysis using a biosensor. The linearity of the electrode was fair. considering the fact that this was the synthesized. The correlation coefficient was 0.92. the range of detection for this type of electrode is very fair. The calculated value was determined to be 294 using the sphere radius.

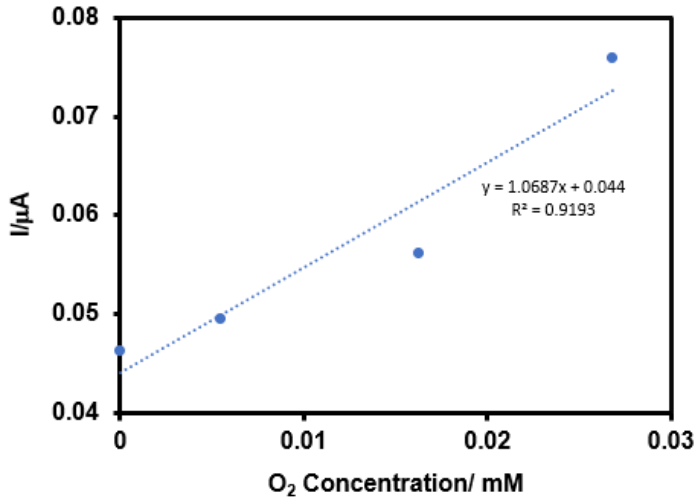

Figure 5-38;PGE/PAA-PVI-BOx. pH7 PBS sensitivty curve

The stable suspension of the PGE/PAA-PVI (Os) complex was obtained by dispersing in polyethylene glycol (PEG). The electron transfer of BOx which is immobilized in the PGE was enhanced by the PAA-PVI (Os) redox polymer. The electrochemical parameters such as the value of midpoint potential ($E_{1/2}$) were estimated and dependence on pH indicated electron transfer coupled with a two-electron transfer reaction process. The current response of the polymer was not uniform. giving a potential working range of 0 to 0.3 V. although the correlation coefficient was 0.9 as seen in Figure 5.37 The sensitivity of this electrode was 294 µA/mM.cm^2. numerous aspects affect this result as the polymer was synthesized in the laboratory. The slope obtained in figure 5.38 of 1.0x10^{-5} A/mM was converted to 1.0x10^1 µA/mM and multiplied by the electrode area 0.034 cm^2 the resultant value is O_2 sensivity 294.12 µA/mM.cm^2.

5.6 Development and optimization of PGE-rGO-MWCNTS-BOx

The direct electron transfer of enzymes with electrodes is applied in this study of enzyme-catalysed reaction in the biological system. The enzyme-modified electrode provides a basis for the construction of biosensor. This enzyme is capable of DET and keeping the its bioactivity. The electrochemical response is promoted by the accessibility of the redox centre. usually the large three-dimensional structure of an enzyme. The ability of rGO/MWCNTs electrode to promote electrode transfer reaction has been documented in connection with biomolecules (Cracknell et al.. 2011).(Di Bari et al.. 2016).

5.6.1 CV analysis

The voltammetric results indicate that the direct electron transfer between the active site of bilirubin and the surface of the PGE surface occurred. The BOx immobilized on the MWCNTs was able to retain its biocatalytic activity for the reduced oxygen with good stability. The goal of fabricating a DET and applying r-GO/MWCNTs. In Figure. 5.41 (a) is the cv of PGE/rGO/MWCNTs/BOx in a phosphate electrolyte pH 7.1 purge with nitrogen (N_2). in the same electrochemical parameters. Figure 5.41 (b) was

oxygenated for a period of 15 minutes. From the cyclic voltammetric response obtained. there are visible changes. which confirm the reduction of oxygen. The broad shoulder of a cathodic peak at potential 0.53 V. The midpoint potential ($E_{1/2}$). which defines the average of anodic and cathodic peak 0.46 V. The anodic and cathodic peak potentials of direct electron transfer of BOx are scan rate dependent (Figure.5.45). The anodic and cathodic peak potential shifts slightly too positive and negative directions. respectively. and consequently. the ΔE_p increases with increasing scan rate. However. the value of $E_{1/2}$ is independent of the scan rates ($E_{1/2}$=−0.466±0.001 V in the scan rate range of 20–140 mV/s).

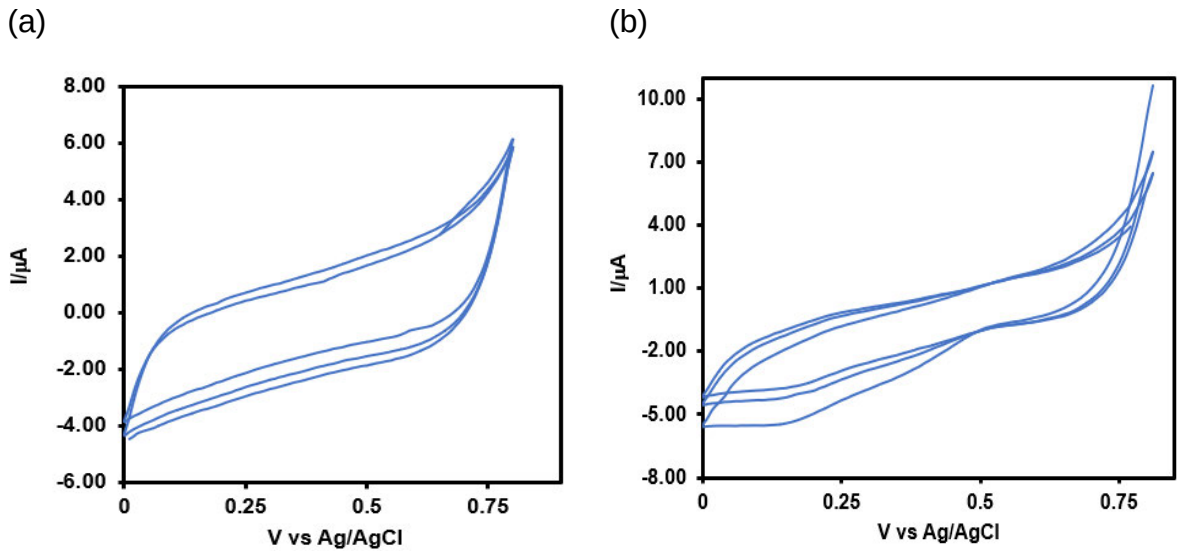

Figure 5-39;CV of (a) N_2 and (b) O_2 0.1 M PBS (pH 7.1)

5.6.2 Determination of O_2 analysis

The amperometric measurement of oxygen at the PGE/r-GO/MWCNTs/BOx electrode has been investigated. and the calibration curve of the current response current of the enzyme electrode. The onset plot shows the successive current response addition of 250 µL of 0.1 mM PBS buffer saturated with O_2. From the linear range correlation and coefficient (R^2) of 0.83.

(a) (b)

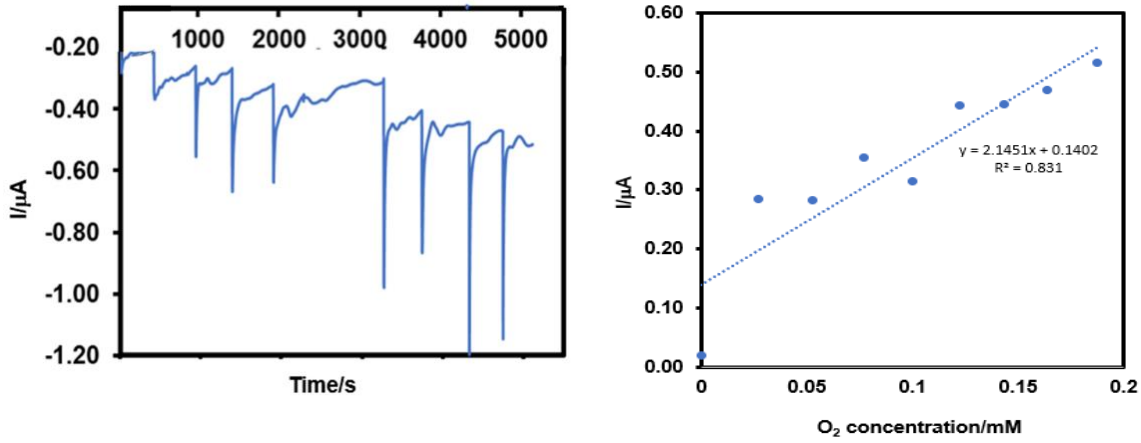

Figure 5-40; PGE/GO/MWCNTs/BOx.(a) Amperometric responses of enzyme electrode at an applied potential +0.35 V. 010 mM PBS pH 7.1.(b) electrode O_2 sensitivity detection

PGE/rGO/MWCNTs/BOx was analyzed and the intercept for the plot of the reciprocal of the cathodic current with oxygen concentration. Figure 5.42 (a) shows the amperometric detection of PGE/GO/MWCNTs/Box. the use of only carbon nanomaterial produce the calculated sensitivity robe 632.4 µA/mM.cm$^{2.}$ The current signal spread seen in Figure 5.42 (b) at a potential range of 0 to 0.2 V. The sensitivity of O_2 632.35 µA/ mM.cm^2 was determined using the curve slope 21.50 µA/mM with the electrode area 0.034.

5.7 Computational Adsorption energy calculations

The 3-dimensional low energy conformations for each of the layered structures is presented in Figure 5.43 below. along with the corresponding adsorption energies are depicted in Table 15 below.

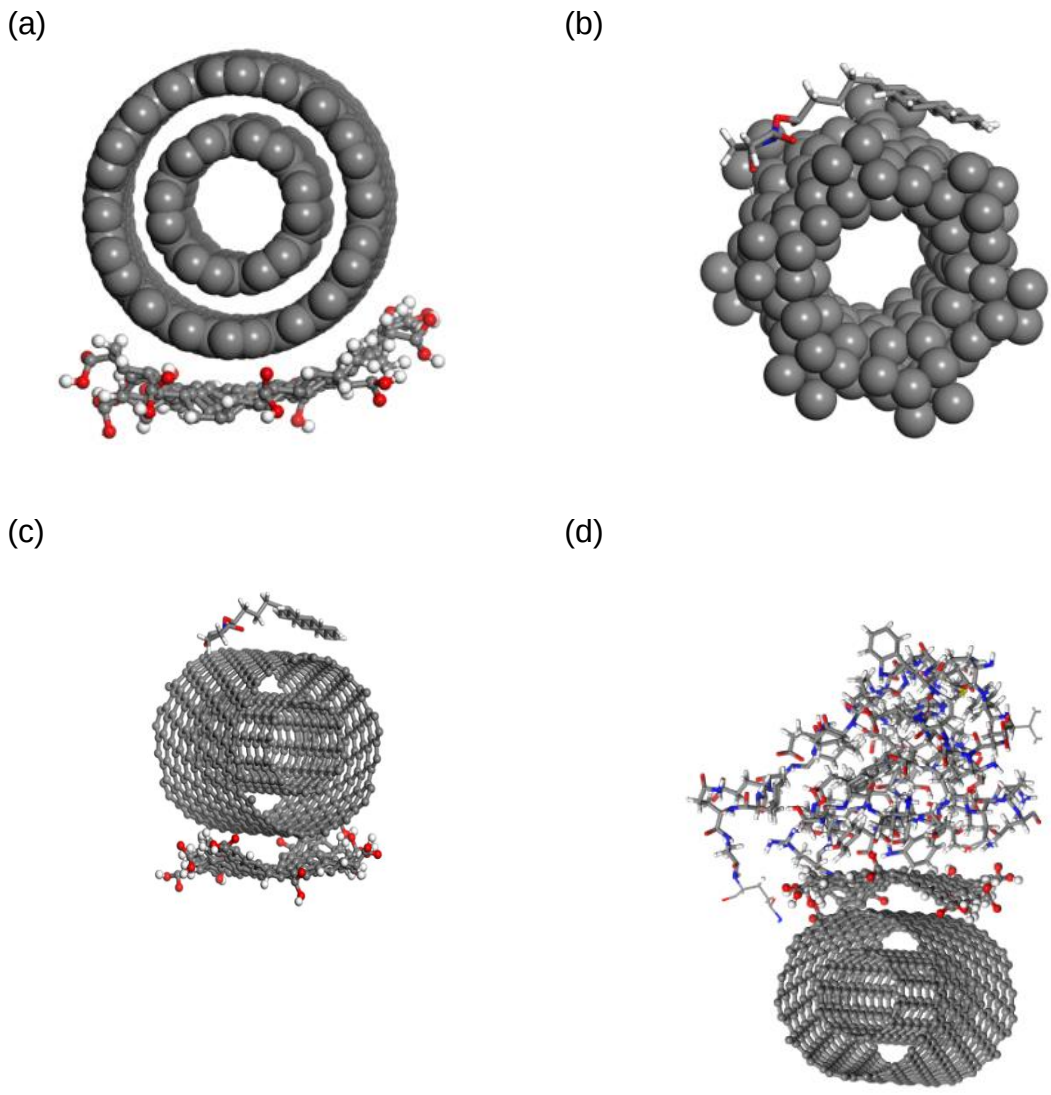

Figure 5-41; showing (a) GO/MWCNTs nanocomposite. (b) MWCNTs/PBSE nanocomposite. (c) GO/MWCNTs/PBSE nanocomposite. and (d) GO/MWCNTs/PBSE/Box nanocomposite

Table 17 Calculated adsorption energy for the electrode layer-by-layer system

Systems	Adsorption energy kcal/mol
GO/MWCNTs	-170.447
MWCNTs/PBSE	-265.783
GO/MWCNTs/PBSE	-560.519
GO/MWCNTs/PBSE/BOx	-573.193

Table 15 demonstrates the dEads/dNi. which explains the energy in kcal/mol. of substrate-adsorbate configurations for each electrode layer. The trends of adsorption energy distribution are consistent with the average total energy. The lowest adsorption energy is generated by addition of the BOx onto the electrode surface containing the nanocomposite GO/MWCNTs/PBSE (-573.193 kcal/mol) (Table 15). This trend emphasizes that the addition of each absorbate molecule. provide a direct influence upon its adsorption capability onto the electrode surface. in accordance with an increase in the signal amplification obtained experimentally.

CHAPTER 6: CONCLUSION

The results obtained in this study. revealed that PGEs are a good working electrode in high-potential electrochemical detection systems. The PGEs can be easily modified directly with carbon nanostructures. polymers. or a combination of both. similar to the commercially available metal electrodes. such as gold or platinum. An increasing amount of the nanostructures at the PGE surfaces. not only enhanced the surface area of the electrodes. but also provides an excellent platform for the immobilization of biomolecules. thus enabling their use as biosensors. The PGEs are applicable to pharmaceutical analysis and are equally useful in the clinical. agricultural. and food industries. The high popularities of PGE arise from its cost-effectiveness. simplicity. and low background noise.

Our results revealed that a favourable orientation of the bilirubin oxidase (BOx) on a MWCNT matrix was achieved through the cathode modification with an ABTS cross-linker and the natural substrate bilirubin as orientating agents. subsequently. an increase in electrocatalytic activity was observed. Among the orientating agents tested. Box was shown to have a more polarization curves were performed by chronoamperometric measurements of 5000 s. starting from the open circuit potential (OCP) of the electrode and decreasing to 0.00 V at 50 mV intervals. For the determination of the orientation efficiency. chronoamperometry was performed at 0.35 V for 4000 s in the aforementioned electrochemical cell. before and after the addition of 0.1 mm ABTS.

The bio-conjugates formed using PBSE effectively linked MCO with MWCNT to facilitate a direct electron transfer (DET) and bio-electrocatalytic oxygen reduction. The catalytic efficiency was significantly greater than previous reports for MCO electrodes. The process provided a porous. potentially scalable. architecture that can advance bio-electrocatalytic applications. Future research will provide a deeper understanding of the attachment mechanism that directs enzyme orientation and provides guidance to optimize the interaction further. The applicability to alternative catalysts was demonstrated with the two MCOs but could be extended to a wider range of biomolecules and applications.

Bearing in mind the potential applications of laccase-modified electrodes in energy source the stability of TMOS /CNP/Lacc film electrode was tested by chronoamperometry. It is probable that the proper enzyme orientation towards nanoparticles allow for an efficient electron exchange between the CNP and the active sites of the enzyme. This can only be achieved if laccase is first mixed with the CNP solution. possibly allowing for the adsorption of the enzyme onto the CNP surface. The procedure involving the addition of the enzyme solution directly to the sol. results in an electrode exhibiting only a minor mediator with less electrocatalysis.

PAA-PVI (Os) redox complex. as a polymeric redox mediator. has been revealed as an attractive material for the immobilization of the BOx to construct the oxygen biosensor. Immobilized BOx on the PAA-PVI (Os) films maintained its activity. A reliable. low-cost and sensitive biosensor for oxygen detection is thus developed. possessing a variety of excellent characteristics. including high sensitivity. good repeatability and reproducibility. rapid response and long-term stability.

Practical application of enzyme-based electronics and fuel cells requires that the biocatalysts with-stand environmental fluctuations and continually catalyze redox reactions. To render self-powered bioelectronic devices fit for sustained built-in information processing under continuous flow. the present work uses a bilirubin oxidase functionalized architecture that responds directly to a continuous input chemical signal (i.e.. dissolved O_2) and generates an amperometric output response.

However. the modification of PGE surfaces using nanomaterials or nanomaterial polymer composites significantly improved the redox capacity. sensitivity. and selectivity of the working electrode. Such development suggests that the coupling of nanomaterial-modified PGE with other technological advances such as lab on chip. lateral-flow. test-strip. and electronics will result in a powerful. simple. hand-held. prototype device for fast. selective. sensitive and low-cost sensor for practical applications. Therefore. PGEs modified using advanced technologies would possess a good prospect in the electrochemical detection techniques. However. the major challenges using the nanostructured-modified PGEs for wide application in electro analysis are the mass production of nanomaterial-modified PGEs. and the reliable. simultaneous detection of analyte in complex sample like biological fluids and waste water.

6.1 Recommendations for further research

The future work will be directed in the design of a miniaturized biosensor device for the real time monitoring of oxygen in a sample of a biological structure that mimics a specific function of a real organ. The collection and analysis of data in real time will offer richer insights into the oxygenated blood levels.

A particular focus of the future research with PGEs will include the following:

(i) mass production of advanced nanomaterial-modified PGEs with suitable method. (ii) exploring the development of novel nanostructured. which are not explored yet. for modification of PGE. and (iii) detection of explored or unexplored analyte such as pathogenic virus in complex sample.

APPENDIX A

REFERENCES

AKANDA. M. R.. SOHAIL. M.. AZIZ. M. A. & KAWDE. A. N. 2016. Recent Advances in Nanomaterial-Modified Pencil Graphite Electrodes for Electroanalysis. *Electroanalysis.* 28**.** 408-424.

AKINWANDE. D.. TAO. L.. YU. Q.. LOU. X.. PENG. P. & KUZUM. D. 2015. Large-Area Graphene Electrodes: Using CVD to facilitate applications in commercial touchscreens. flexible nanoelectronics. and neural interfaces. *IEEE Nanotechnology Magazine.* 9**.** 6-14.

ALIPOUR. E. & GASEMLOU. S. 2012. Easy modification of pencil graphite electrode for discrimination and determination of morphine in biological and street samples. *Analytical Methods.* 4**.** 2962-2969.

ATALAH. J.. ZHOU. Y.. ESPINA. G.. BLAMEY. J. M. & RAMASAMY. R. P. 2018. Improved stability of multicopper oxidase–carbon nanotube conjugates using a thermophilic laccase. *Catalysis Science & Technology.* 8**.** 1272-1276.

BALGOBIND. K.. KANCHI. S.. SHARMA. D.. BISETTY. K. & SABELA. M. I. 2016. Hybrid of ZnONPs/MWCNTs for electrochemical detection of aspartame in food and beverage samples. *Journal of Electroanalytical Chemistry.* 774**.** 51-57.

BARD. A. J.. FAULKNER. L. R.. LEDDY. J. & ZOSKI. C. G. 1980. *Electrochemical methods: fundamentals and applications*. wiley New York.

BONANNI. A.. LOO. A. H. & PUMERA. M. 2012. Graphene for impedimetric biosensing. *TrAC Trends in Analytical Chemistry.* 37**.** 12-21.

BRIONES. M.. CASERO. E.. VÁZQUEZ. L.. PARIENTE. F.. LORENZO. E. & PETIT-DOMÍNGUEZ. M. 2016. Diamond nanoparticles as a way to improve electron transfer in sol–gel l-lactate biosensing platforms. *Analytica Chimica acta.* 908**.** 141-149.

CADET. M.. BRILLAND. X.. GOUNEL. S.. LOUERAT. F. & MANO. N. 2013a. Design of a highly efficient O_2 cathode based on bilirubin oxidase from Magnaporthe oryzae. *ChemPhysChem.* 14**.** 2097-2100.

CADET. M.. BRILLAND. X.. GOUNEL. S.. LOUERAT. F. & MANO. N. 2013b. Design of a highly efficient O_2 cathode based on bilirubin oxidase from Magnaporthe oryzae. *Chemphyschem.* 14**.** 2097-100.

CARLSSON. J. M. 2007. Graphene: buckle or break. *Nature Materials.* 6**.** 801.

CHAUBEY. A. & MALHOTRA. B. 2002. Mediated biosensors. *Biosensors and bioelectronics.* 17**.** 441-456.

CHEHREH CHELGANI. S.. RUDOLPH. M.. KRATZSCH. R.. SANDMANN. D. & GUTZMER. J. 2016. A review of graphite beneficiation techniques. *Mineral Processing and Extractive Metallurgy Review.* 37**.** 58-68.

CLAUS. H. 2003. Laccases and their occurrence in prokaryotes. *Archives of microbiology.* 179**.** 145-150.

CONROY. D. J.. MILLNER. P. A.. STEWART. D. I. & POLLMANN. K. 2010. Biosensing for the environment and defence: Aqueous uranyl detection using bacterial surface layer proteins. *Sensors.* 10**.** 4739-4755.

COOPER. D. R.. D'ANJOU. B.. GHATTAMANENI. N.. HARACK. B.. HILKE. M.. HORTH. A.. MAJLIS. N.. MASSICOTTE. M.. VANDSBURGER. L. & WHITEWAY. E. 2012. Experimental review of graphene. *ISRN Condensed Matter Physics.* 2012.

CORNISH-BOWDEN. A. 2013. *Fundamentals of enzyme kinetics*. John Wiley & Sons.

CRACKNELL. J. A.. MCNAMARA. T. P.. LOWE. E. D. & BLANFORD. C. F. 2011. Bilirubin oxidase from Myrothecium verrucaria: X-ray determination of the complete crystal structure and a rational surface modification for enhanced electrocatalytic O_2 reduction. *Dalton Transactions.* 40**.** 6668-6675.

CRISTINA GUTIERREZ-SANCHEZ. SERGEY SHLEEV. LACEY. A. L. D. & PITA. M. 2015. Third-generation oxygen amperometric biosensor based on. *Chemical Papers.* 69**.** 237-240.

DELLEY. B. 2000. From molecules to solids with the DMol3 approach. *The Journal of Chemical Physics.* 113**.** 7756-7764.

DENG. D.. POPOVICH. N.. HUNTER. T.. SLOMSKI. D. & BELL. D. 2006. Biosensors comprising semiconducting electrodes or ruthenium containing mediators and method of using the same. Google Patents.

DEVASENATHIPATHY. R.. MANI. V.. CHEN. S.-M.. HUANG. S.-T.. HUANG. T.-T.. LIN. C.-M.. HWA. K.-Y.. CHEN. T.-Y. & CHEN. B.-J. 2015. Glucose biosensor based on glucose oxidase immobilized at gold nanoparticles decorated graphene-carbon nanotubes. *Enzyme and Microbial Technology.* 78**.** 40-45.

DI BARI. C.. SHLEEV. S.. DE LACEY. A. L. & PITA. M. 2016. Laccase-modified gold nanorods for electrocatalytic reduction of oxygen. *Bioelectrochemistry.* 107**.** 30-6.

DIAS. A. A.. PINTO. P. A.. FRAGA. I. & BEZERRA. R. M. 2014. Diagnosis of enzyme inhibition using excel solver: A combined dry and wet laboratory exercise. *Journal of Chemical Education.* 91**.** 1017-1021.

DREYER. D. R. 2010. Sungjin. Park. Christopher W. Bielawski. Rodney S. Ruoff. The chemistry of graphene oxide. *Chemical Society Reviews.* 39**.** 228-240.

DURAND. F.. KJAERGAARD. C. H.. SURANITI. E.. GOUNEL. S.. HADT. R. G.. SOLOMON. E. I. & MANO. N. 2012. Bilirubin oxidase from Bacillus pumilus: A promising enzyme for the elaboration of efficient cathodes in biofuel cells. *Biosensors & Bioelectronics.* 35**.** 140-146.

ELGRISHI. N.. ROUNTREE. K. J.. MCCARTHY. B. D.. ROUNTREE. E. S.. EISENHART. T. T. & DEMPSEY. J. L. 2017. A Practical Beginner's Guide to Cyclic Voltammetry. *Journal of Chemical Education.* 95**.** 197-206.

ESHTAYA. M.. EJIGU. A.. STEPHENS. G.. WALSH. D. A.. CHEN. G. Z. & CROFT. A. K. 2016. Developing energy efficient lignin biomass processing–towards understanding mediator behaviour in ionic liquids. *Faraday discussions.* 190**.** 127-145.

FARNETH. W. E.. BRUCE A. DINER. TIMOTHY D. GIERKE & AMORE. M. B. D. 2005. Current densities from electrocatalytic oxygen reduction in laccase/ABTS solutions. *Journal of Electroanalytical Chemistry.* 581**.** 190–196.

FILIP. J. & TKAC. J. 2014. Effective bioelectrocatalysis of bilirubin oxidase on electrochemically reduced graphene oxide. *Electrochemistry Communications.* 49**.** 70–74.

GALLAGHER. A. J.. FRICK. L. H.. BUSHNELL. P. G.. BRILL. R. W. & MANDELMAN. J. W. 2010. Blood gas. oxygen saturation. pH. and lactate values in elasmobranch blood measured with a commercially available portable clinical analyzer and standard laboratory instruments. *Journal of Aquatic Animal Health.* 22**.** 229-234.

GONZALEZ-RIVERA. J. C. & OSMA. J. F. 2015. Fabrication of an amperometric flow-injection microfluidic biosensor based on laccase for in situ determination of phenolic compounds. *BioMed Research International.* 2015.

GOURLEY. G. R. 1997. Bilirubin metabolism and kernicterus. *Advances in Pediatrics.* 44**.** 173-229.

GOYAL. R. N.. GUPTA. V. K. & CHATTERJEE. S. 2010. Voltammetric biosensors for the determination of paracetamol at carbon nanotube modified pyrolytic graphite electrode. *Sensors and Actuators B: Chemical.* 149**.** 252-258.

GUAN. J.-G.. MIAO. Y.-Q. & ZHANG. Q.-J. 2004. Impedimetric biosensors. *Journal of bioscience and bioengineering.* 97**.** 219-226.

GÓMEZ-ANQUELA. C.. GARCÍA-MENDIOLA. T.. ABAD. J. M.. PITA. M.. PARIENTE. F. & LORENZO. E. 2015. Scaffold electrodes based on thioctic acid-capped gold nanoparticles coordinated Alcohol Dehydrogenase and Azure A films for high performance biosensor. *Bioelectrochemistry.* 106**.** 335-342.

GÓMEZ-NAVARRO. C.. WEITZ. R. T.. BITTNER. A. M.. SCOLARI. M.. MEWS. A.. BURGHARD. M. & KERN. K. 2007. Electronic transport properties of individual chemically reduced graphene oxide sheets. *Nano letters.* 7**.** 3499-3503.

HABERMÜLLER. K.. MOSBACH. M. & SCHUHMANN. W. 2000. Electron-transfer mechanisms in amperometric biosensors. *Fresenius' Journal of Analytical Chemistry.* 366**.** 560-568.

HARPER. A. & ANDERSON. M. R. 2010. Electrochemical glucose sensors—developments using electrostatic assembly and carbon nanotubes for biosensor construction. *Sensors.* 10**.** 8248-8274.

HERNÁNDEZ-IBÁÑEZ. N.. GARCÍA-CRUZ. L.. MONTIEL. V.. FOSTER. C. W.. BANKS. C. E. & INIESTA. J. 2016. Electrochemical lactate biosensor based upon chitosan/carbon nanotubes modified screen-printed graphite electrodes for the determination of lactate in embryonic cell cultures. *Biosensors and bioelectronics.* 77**.** 1168-1174.

HILDER. M.. WINTHER-JENSEN. B.. LI. D.. FORSYTH. M. & MACFARLANE. D. R. 2011. Direct electro-deposition of graphene from aqueous suspensions. *Physical Chemistry Chemical Physics.* 13**.** 9187-9193.

HOEGGER. P. J.. KILARU. S.. JAMES. T. Y.. THACKER. J. R. & KÜES. U. 2006. Phylogenetic comparison and classification of laccase and related multicopper oxidase protein sequences. *The FEBS journal.* 273**.** 2308-2326.

HOLM. K.. NIELSEN. D. & ERIKSEN. J. 1998. Automated colorimetric determination of recombinant fungal laccase activity in fermentation sarples using syringaldazine as chromogenic substrate. *Journal of Analytical Methods in Chemistry.* 20**.** 199-203.

HUANG. V. M.. WU. S.-L.. ORAZEM. M. E.. PÉBÈRE. N.. TRIBOLLET. B. & VIVIER. V. 2011. Local electrochemical impedance spectroscopy: A review and some recent developments. *Electrochimica Acta.* 56**.** 8048-8057.

JENIE. S. A.. PRIETO-SIMON. B. & VOELCKER. N. H. 2015. Development of L-lactate dehydrogenase biosensor based on porous silicon resonant microcavities as fluorescence enhancers. *Biosensors and Bioelectronics.* 74**.** 637-643.

JOHNSON. L. H.. BHUTANI. V. K. & BROWN. A. K. 2002. System-based approach to management of neonatal jaundice and prevention of kernicterus. *The Journal of Pediatrics.* 140**.** 396.

JOKERST. J. V.. COLE. A. J.. VAN DE SOMPEL. D. & GAMBHIR. S. S. 2012. Gold nanorods for ovarian cancer detection with photoacoustic imaging and resection guidance via Raman imaging in living mice. *ACS nano.* 6**.** 10366-10377.

KASHYAP. S.. MISHRA. S. & BEHERA. S. K. 2014. Aqueous colloidal stability of graphene oxide and chemically converted graphene. *Journal of Nanoparticles.* 2014.

KIM. D.-M.. KIM. M.-Y.. REDDY. S. S.. CHO. J.. CHO. C.-H.. JUNG. S. & SHIM. Y.-B. 2013. Electron-transfer mediator for a NAD-glucose dehydrogenase-based glucose sensor. *Analytical Chemistry.* 85**.** 11643-11649.

KIRCHER. M. F.. DE LA ZERDA. A.. JOKERST. J. V.. ZAVALETA. C. L.. KEMPEN. P. J.. MITTRA. E.. PITTER. K.. HUANG. R.. CAMPOS. C. & HABTE. F. 2012.

A brain tumor molecular imaging strategy using a new triple-modality MRI-photoacoustic-Raman nanoparticle. *Nature Medicine.* 18**.** 829.

KISSINGER. P. T. 1983. Cyclic Voltametry. *Chemical Education.* 60**.** 702–706.

KONCKI. R. 2007. Recent developments in potentiometric biosensors for biomedical analysis. *Analytica Chimica Acta.* 599**.** 7-15.

KUNENE. K. W. 2018. *Fabrication of electrochemical biosensors for the determination of phenolic compounds by experimental and computational methods.*

LASA. I. & BERENGUER. J. 1993. Thermophilic enzymes and their biotechnological potential. *Microbiologia.* 9**.** 77-89.

LASIA. A. 2002. Electrochemical impedance spectroscopy and its applications. *Modern aspects of electrochemistry.* Springer.

LAU. C.. MOEHLENBROCK. M. J.. ARECHEDERRA. R. L.. FALASE. A.. GARCIA. K.. RINCON. R.. MINTEER. S. D.. BANTA. S.. GUPTA. G. & BABANOVA. S. 2015. Paper based biofuel cells: Incorporating enzymatic cascades for ethanol and methanol oxidation. *International Journal of Hydrogen Energy.* 40**.** 14661-14666.

LEENSON. I. A. 1999. Old rule of thumb and the Arrhenius equation. *Journal of chemical education.* 76**.** 1459.

LEVENT. A.. YARDIM. Y. & SENTURK. Z. 2009. Voltammetric behavior of nicotine at pencil graphite electrode and its enhancement determination in the presence of anionic surfactant. *Electrochimica Acta.* 55**.** 190-195.

LIANG. B.. LI. L.. TANG. X.. LANG. Q.. WANG. H.. LI. F.. SHI. J.. SHEN. W.. PALCHETTI. I. & MASCINI. M. 2013. Microbial surface display of glucose dehydrogenase for amperometric glucose biosensor. *Biosensors and Bioelectronics.* 45**.** 19-24.

LIANG. B.. ZHANG. S.. LANG. Q.. SONG. J.. HAN. L. & LIU. A. 2015. Amperometric L-glutamate biosensor based on bacterial cell-surface displayed glutamate dehydrogenase. *Analytica chimica acta.* 884**.** 83-89.

LOPEZ. R. J. & ATANASSOV. P. 2014a. Improved interfacial electron transfer in modified Bilirubin oxidase biocathodes. *Chem. Electro. Chem..* 1**.** 241–218.

LOPEZ. R. J. & ATANASSOV. P. 2014b. Improved interfacial electron transfer in modified Bilirubin oxidase biocathodes. *ChemElectroChem.* 1**.** 241–218.

MACDONALD. J. R. 1992. Impedance spectroscopy. *Annals of biomedical engineering.* 20**.** 289-305.

MILLNER. P.. CAYGILL. R.. CONROY. D. & SHAHIDAN. M. 2012. Impedance interrogated affinity biosensors for medical applications: novel targets and mechanistic studies. *Biosensors for medical applications.* Elsevier.

MOTULSKY. H. J. & RANSNAS. L. A. 1987. Fitting curves to data using nonlinear regression: a practical and nonmathematical review. *The FASEB journal.* 1**.** 365-374.

MOUSTY. C.. VIEILLE. L. & COSNIER. S. 2007. Laccase immobilization in redox active layered double hydroxides: A reagentless amperometric biosensor. *Biosensors and Bioelectronics.* 22**.** 1733–1738.

PERSON. R. V.. PETERSON. B. R. & LIGHTNER. D. A. 1994. Bilirubin conformational analysis and circular dichroism. *Journal of the American Chemical Society.* 116**.** 42-59.

PIKE. D. J. 2014. *Innovative system for deploying novel biosensors for water contaminant monitoring.* Doctrate. University of Leeds.

PINGARRÓN. J. M.. YÁÑEZ-SEDEÑO. P. & GONZÁLEZ-CORTÉS. A. 2008. Gold nanoparticle-based electrochemical biosensors. *Electrochimica Acta.* 53**.** 5848-5866.

PIONTEK. K.. ANTORINI. M. & CHOINOWSKI. T. 2002. Crystal structure of a laccase from the fungusTrametes versicolor at 1.90-Å resolution containing a full complement of coppers. *Journal of Biological Chemistry.* 277**.** 37663-37669.

PITA. M.. GUTIERREZ-SANCHEZ. C.. TOSCANO. M. D.. SHLEEV. S. & DE LACEY. A. L. 2013. Oxygen biosensor based on bilirubin oxidase immobilized on a nanostructured gold electrode. *Bioelectrochemistry.* 94**.** 69-74.

PRASAD. B. B.. MADHURI. R.. TIWARI. M. P. & SHARMA. P. S. 2010. Electrochemical sensor for folic acid based on a hyperbranched molecularly imprinted polymer-immobilized sol–gel-modified pencil graphite electrode. *Sensors and Actuators B: Chemical.* 146**.** 321-330.

PUMERA. M.. AMBROSI. A.. BONANNI. A.. CHNG. E. L. K. & POH. H. L. 2010. Graphene for electrochemical sensing and biosensing. *TrAC Trends in Analytical Chemistry.* 29**.** 954-965.

RAMARAJA P.RAMASAMY. HEATHER R. LUCKARIFT. DMITRI M.IVNITSKI. ATANASSOV. P. B. & .JOHNSON. G. R. 2010. High elelctrocatalytic activity oftethered multicopper oxidase–carbon nantubes conjugates. *ChemComm.* 46**.** 6045–6047.

RAMASAMY. R. P.. LUCKARIFT. H. R.. IVNITSKI. D. M.. ATANASSOV. P. B. & JOHNSON. G. R. 2010. High electrocatalytic activity of tethered multicopper oxidase-carbon nanotube conjugates. *Chem Commun (Camb).* 46**.** 6045-7.

RAO. C.. SOOD. A.. VOGGU. R. & SUBRAHMANYAM. K. 2010. Some novel attributes of graphene. *The Journal of Physical Chemistry Letters.* 1**.** 572-580.

REETZ. M. T.. ZONTA. A. & SIMPELKAMP. J. 1996. Efficient immobilization of lipases by entrapment in hydrophobic sol-gel materials. *Biotechnology and Bioengineering.* 49**.** 527-534.

RENEDO. O. D.. ALONSO-LOMILLO. M. & MARTÍNEZ. M. A. 2007. Recent developments in the field of screen-printed electrodes and their related applications. *Talanta.* 73**.** 202-219.

RIVA. S. 2006. Laccases: blue enzymes for green chemistry. *TRENDS in Biotechnology.* 24**.** 219-226.

RIVERA. K. R.. POZDIN. V. A.. YOUNG. A. T.. ERB. P. D.. WISNIEWSKI. N. A.. MAGNESS. S. T. & DANIELE. M. 2019. Integrated phosphorescence-based photonic biosensor (iPOB) for monitoring oxygen levels in 3D cell culture systems. *Biosensors and Bioelectronics.* 123**.** 131-140.

ROCCHITTA. G.. SPANU. A.. BABUDIERI. S.. LATTE. G.. MADEDDU. G.. GALLERI. G.. NUVOLI. S.. BAGELLA. P.. DEMARTIS. M. & FIORE. V. 2016. Enzyme biosensors for biomedical applications: Strategies for safeguarding analytical performances in biological fluids. *Sensors.* 16**.** 780.

ROEGES. N. P. & BAAS. J. 1994. *A guide to the complete interpretation of infrared spectra of organic structures*. Wiley Chichester etc.

ROTH. B. & ROTABAKK. B. T. 2012. Stress associated with commercial longlining and recreational fishing of saithe (Pollachius virens) and the subsequent effect on blood gases and chemistry. *Fisheries Research.* 115**.** 110-114.

ROY. S. & GAO. Z. 2009. Nanostructure-based electrical biosensors. *Nano Today.* 4**.** 318-334.

RUSHWORTH. J. V.. AHMED. A.. GRIFFITHS. H. H.. POLLOCK. N. M.. HOOPER. N. M. & MILLNER. P. A. 2014. A label-free electrical impedimetric biosensor for the specific detection of Alzheimer's amyloid-beta oligomers. *Biosensors and bioelectronics.* 56**.** 83-90.

RUSHWORTH. J. V. & HIRST. N. A. 2013. *Impedimetric biosensors for medical applications: current progress and challenges*. Momentum Press.

SABELA. M. I.. KUNENE. K.. KANCHI. S.. XHAKAZA. N. M.. BATHINAPATLA. A.. MDLULI. P.. SHARMA. D. & BISETTY. K. 2016. Removal of copper (II) from wastewater using green vegetable waste derived activated carbon: An approach to equilibrium and kinetic study. *Arabian Journal of Chemistry*.

SAKAČ. N.. HERENDA. S.. KORAĆ. F.. OSTOJIĆ. J. & BEŠIĆ. Z. A Novel. Low-cost. Disposable Wooden Pencil Graphite Electrode for Peroxide Determination. 2nd International Congress of Chemists and Chemical Engineers of Bosnia and Herzegovina. 2016.

SAKURAI. T. & KATAOKA. K. 2007. Basic and applied features of multicopper oxidases. CueO. bilirubin oxidase. and laccase. *The Chemical Record.* 7**.** 220-229.

SALAJ-KOSLA. U.. PÖLLER. S.. BEYL. Y.. SCANLON. M. D.. SERGEY BELOSHAPKIN. SHLEEV. S.. SCHUHMANN. W. & MAGNER. E. 2012. Direct

electron transfer of bilirubin oxidase (Myrothecium verrucaria) at an unmodified nanoporous gold biocathode. *Electrochemistry Communications.* 16**.** 92–95.

SAY. J.. TOMASCO. M. F.. HELLER. A.. GAL. Y.. ARIA. B.. HELLER. E.. PLANTE. P. J. & VREEKE. M. S. 2000. Process for producing an electrochemical biosensor. Google Patents.

SCHALLER. U.. BAKKER. E.. SPICHIGER. U. E. & PRETSCH. E. 1994. Ionic additives for ion-selective electrodes based on electrically charged carriers. *Analytical Chemistry.* 66**.** 391-398.

SCHRÖDER. I.. STECKHAN. E. & LIESE. A. 2003. In situ NAD+ regeneration using 2. 2′-azinobis (3-ethylbenzothiazoline-6-sulfonate) as an electron transfer mediator. *Journal of Electroanalytical Chemistry.* 541**.** 109-115.

SERGEY SHLEEVE. ANNA JAROSZ–WILKOLAZKA. ANNA KHALUNINA. OLGA MOROZOVA. ALEXANDER YAROPOLOV. RUZGAS. T. & GORTON. L. 2005. Direct electron transfere reactions of laccase from different origins on carbom electrode. *Bioelectrochemistry.* 67**.** 115–124.

SHOHAM. B.. MIGRON. Y.. RIKLIN. A.. WILLNER. I. & TARTAKOVSKY. B. 1995. A bilirubin biosensor based on a multilayer network enzyme electrode. *Biosensors and Bioelectronics.* 10**.** 341-352.

SHUKLA. S. K.. TURNER. A. P. & TIWARI. A. 2015. Cholesterol oxidase functionalised polyaniline/carbon nanotube hybrids for an amperometric biosensor. *Journal of Nanoscience and Nanotechnology.* 15**.** 3373-3377.

SO. K.. ONIZUKA. M.. KOMUKAI. T.. KITAZUMI. Y.. SHIRAI. O. & KENJI KANOA 2016. Binder/surfactant-free biocathode with bilirubin oxidase for gas-diffusion-type system. *Electrochemistry Communications.* 66**.** 58–61.

SURANITI. E.. TSUJIMURA. S.. DURAND. F. & MANO. N. 2013. Thermophilic biocathode with bilirubin oxidase from Bacillus pumilus. *Electrochemistry Communications.* 26**.** 41-44.

SZOT. K.. NOGALA. W.. NIEDZIOLKA-JÖNSSON. J.. JÖNSSON-NIEDZIOLKA. M.. MARKEN. F.. ROGALSKI. J.. KIRCHNER. C. N.. WITTSTOCK. G. & OPALLO. M. 2009a. Hydrophilic carbon nanoparticle-laccase thin film electrode for mediatorless dioxygen reduction: SECM activity mapping and application in zinc-dioxygen battery. *Electrochimica Acta.* 54**.** 4620-4625.

SZOT. K.. NOGALA. W.. NIEDZIOLKA-JÖNSSONA. J.. MARTIN JÖNSSON-NIEDZIOLKA. MARKEN. F.. ROGALSKI. J.. KIRCHNERD. C. N.. WITTSTOCK. G. & OPALLOA. M. 2009b. Hydrophilic carbon nanoparticle-laccase thin film electrode for mediatorless dioxygen reduction SECM activity mapping and application in zinc-ioxygen battery. *Electrochimica.* 54**.** 4620–4625.

TANG. L.. WANG. Y.. LI. Y.. FENG. H.. LU. J. & LI. J. 2009. Preparation. structure. and electrochemical properties of reduced graphene sheet films. *Advanced Functional Materials.* 19**.** 2782-2789.

TANIMOTO. S. & ICHIMURA. A. 2013. Discrimination of inner-and outer-sphere electrode reactions by cyclic voltammetry experiments. *Journal of Chemical Education.* 90**.** 778-781.

TASCA. F.. FARIAS. D.. CASTRO. C.. ACUNA-ROUGIER. C. & ANTIOCHIA. R. 2015. Bilirubin oxidase from Myrothecium verrucaria physically absorbed on graphite electrodes. Insights into the alternative resting form and the sources of activity loss. *PloS one.* 10**.** e0132181.

TOMBELLI. S. 2012. Piezoelectric biosensors for medical applications. *Biosensors for Medical Applications.* Elsevier.

VARFOLOMEEV. S. D.. N.. I. & YAROPOLOV. A. I. 1996. Direct electron transfer effect blosensors. *Biosensors & Bioelectronics.* 11**.** 863-871.

VASYLIEVA. N.. BARNYCH. B.. MEILLER. A.. MAUCLER. C.. POLLEGIONI. L.. LIN. J.-S.. BARBIER. D. & MARINESCO. S. 2011. Covalent enzyme immobilization by poly(ethylene glycol) diglycidyl ether (PEGDE) for microelectrode biosensor preparation. *Biosensors and Bioelectronics.* 26**.** 3993-4000.

WANG. B. 2005a. Recent development of non-platinum catalysts for oxygen reduction reaction. *Journal of Power Sources.* 152**.** 1-15.

WANG. J. 2005b. Carbon-nanotube based electrochemical biosensors: A review. *Electroanalysis: An International Journal Devoted to Fundamental and Practical Aspects of Electroanalysis.* 17**.** 7-14.

WANG. J. & KAWDE. A.-N. 2001. Pencil-based renewable biosensor for label-free electrochemical detection of DNA hybridization. *Analytica Chimica Acta.* 431**.** 219-224.

WISNIEWSKI. N. & REICHERT. M. 2000. Methods for reducing biosensor membrane biofouling. *Colloids and Surfaces B: Biointerfaces.* 18**.** 197-219.

XIA. H.-Q.. KITAZUMI. Y.. SHIRAI. O. & KANO. K. 2016. Enhanced direct electron transfer-type bioelectrocatalysis of bilirubin oxidase on negatively charged aromatic compound-modified carbon electrode. *Journal of Electroanalytical Chemistry.* 763**.** 104-109.

YANG. C.. JACOBS. C. B.. NGUYEN. M. D.. GANESANA. M.. ZESTOS. A. G.. IVANOV. I. N.. PURETZKY. A. A.. ROULEAU. C. M.. GEOHEGAN. D. B. & VENTON. B. J. 2015. Carbon nanotubes grown on metal microelectrodes for the detection of dopamine. *Analytical chemistry.* 88**.** 645-652.

YANG. S.. GUO. D.. SU. L.. YU. P.. LI. D.. YE. J. & MAO. L. 2009. A facile method for preparation of graphene film electrodes with tailor-made dimensions with Vaseline as the insulating binder. *Electrochemistry Communications.* 11**.** 1912-1915.

YILDIRIM. N.. AKÇAY. F.. OKUR. H. & YILDIRIM. D. 2003. Parameter estimation of nonlinear models in biochemistry: a comparative study on optimization methods. *Applied Mathematics and Computation.* 140**.** 29-36.

YING LIU. L. H.. SHAOJUN DONG 2007. Electrochemical catalysis and thermal stability characterization of laccase–carbon nanotubes-ionic liquid nanocomposite modified graphite electrode. *Biosensors and Bioelectronics.* 23**.** 35–41.

ZHONG. M.. XU. D.. YU. X.. HUANG. K.. LIU. X.. QU. Y.. XU. Y. & YANG. D. 2016. Interface coupling in graphene/fluorographene heterostructure for high-performance graphene/silicon solar cells. *Nano Energy.* 28**.** 12-18.

ZHOU. M.. ZHAI. Y. & DONG. S. 2009. Electrochemical sensing and biosensing platform based on chemically reduced graphene oxide. *Analytical chemistry.* 81**.** 5603-5613.

ZHOU. Y.. MARAR. A.. KNER. P. & RAMASAMY. R. P. 2017. Charge-directed immobilization of bacteriophage on nanostructured electrode for whole-cell electrochemical biosensors. *Analytical chemistry.* 89**.** 5734-5741.

ÖZCAN. A. & ŞAHIN. Y. 2010. Preparation of selective and sensitive electrochemically treated pencil graphite electrodes for the determination of uric acid in urine and blood serum. *Biosensors and Bioelectronics.* 25**.** 2497-2502.

ŞENEL. M.. ÇEVIK. E. & ABASIYANIK. M. F. 2010. Amperometric hydrogen peroxide biosensor based on covalent immobilization of horseradish peroxidase on ferrocene containing polymeric mediator. *Sensors and Actuators B: Chemical.* 145**.** 444-450.